

and *Eurytrema* spp., and the purified native and recombinant OV28GST proteins were blotted onto a nitrocellulose membrane and probed with the anti-recOV28GST polyclonal antiserum. The antiserum detected the 28 kDa OV28GST in the crude worm protein extract of *O. viverrini* and the purified native and recombinant OV28GST proteins while no signals were obtained at 28 kDa in crude worm protein extracts of *S. mansoni*, *S. japonicum*, *S. mekongi*, *F. gigantica* and *Eurytrema* spp. (Fig. 4).

Immunolocalization of OV28GST

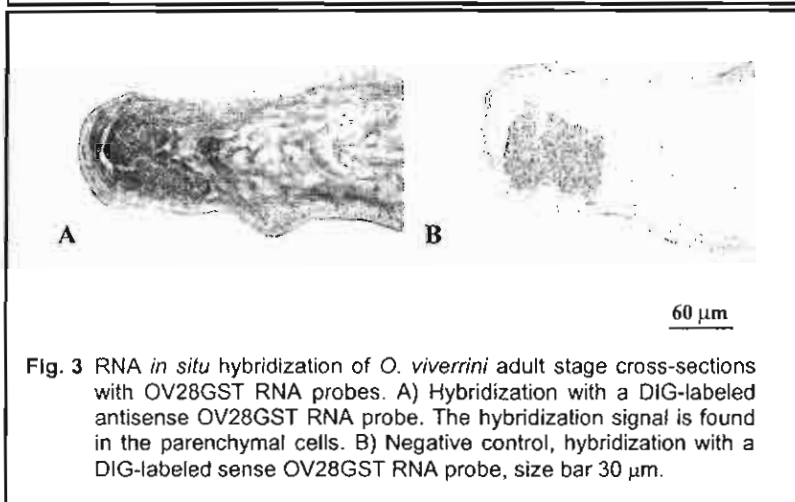
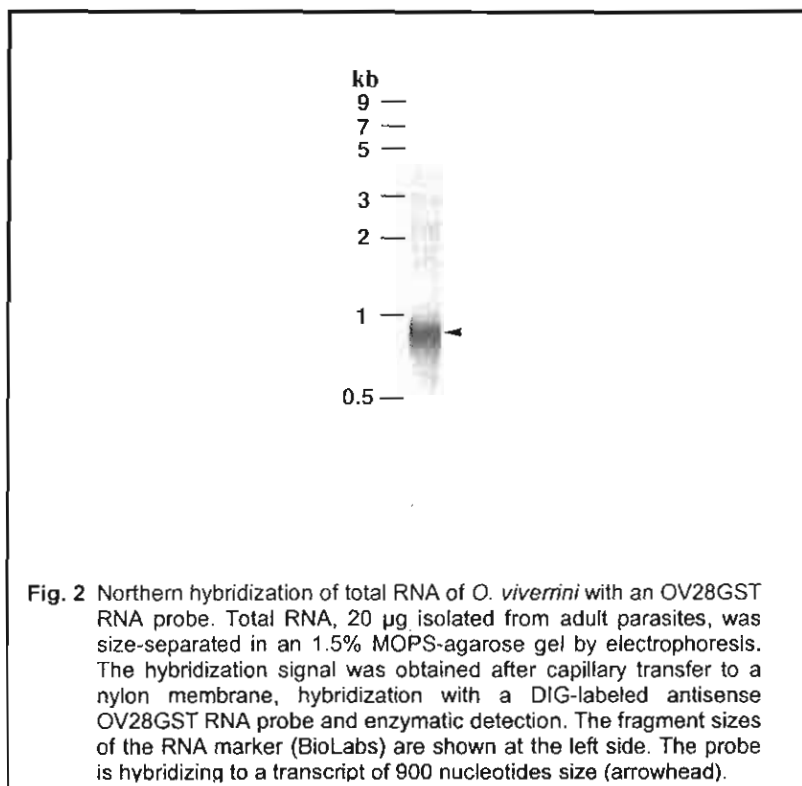
The distribution of OV28GST was studied in paraffin cross sections of adult *O. viverrini* using the anti-recOV28GST polyclonal antiserum as a probe. OV28GST protein was localized in the parasite's parenchymal cells (Fig. 5A) matching the results of RNA *in situ* hybridization and the localization of GST as reported for other trematodes.^{13,23-25} A negative control with preimmune serum did not show staining in the parenchymal cells (Fig. 5B).

Enzyme activity of recombinant OV28GST

The specific activity of recombinant OV28GST to the universal substrate CDNB was 5.73 $\mu\text{mol}/\text{minute}/\text{mg}$ protein.

DISCUSSION

In this report we describe the isolation and characterization of a cDNA from *O. viverrini* that encodes a 28 kDa glutathione S-transferase protein. It was isolated from an adult stage *O. viverrini* cDNA library. The OV28GST deduced amino acid sequence shows



overall identity with the highest score to the sigma class CS28GST of *C. sinensis* (57.1%). The deduced OV28GST protein is composed of 213 amino acids and therefore has nearly the same size as the GSTs of *C. sinensis*,¹³ *P. westermani*²³ and *Schistosoma*.²⁶ OV28GST was ex-

pressed as a soluble recombinant protein in *E. coli* and purified by glutathione affinity chromatography. The observed enzymatic activity of recombinant OV28GST confirmed the function suggested by sequence similarity to other trematode GSTs. The result of EITB

after SDS-PAGE shows that both recombinant OV28GST and native OV28GST run as 28 kDa proteins. Also the predicted secondary structure of OV28GST is conserved when compared to those of other helminthic GSTs. The conserved amino acids shared between squid GST, nematodes (*O. volvulus*,²⁷ *C. elegans*²⁸ and *A. suum*²⁹) and trematodes (lung, blood and liver flukes) are Tyr10, Phe11, Arg16, Glu18, Asp40 Trp41, Lys45, Pro54, Ser73 and Asp106. Northern hybridization using an antisense OV28GST RNA probe against total RNA of adult worms detected a transcript of approximately 900 nucleotides compatible with the 835 nucleotides size of the OV28GST cDNA. This cDNA obviously contains the full length mRNA of OV28GST. The mRNA distribution of OV28GST was observed by RNA *in situ* hybridization. The RNA was limited to the parenchymal cells in accordance with the protein location.

It is speculated that GSTs have an important role in parasite survival due to their abundance.³⁰ In mammalian liver cells, GSTs form 4% of the total soluble protein. Due to their activity, GSTs play a major role in detoxification of endogenous and exogenous toxins. With respect to *O. viverrini* these toxins may be generated by the parasite's own metabolism and/or through host responses to the infection.^{28,30,31} In Mammalia, eight classes of cytosolic GST have been characterized. In trematodes, 26 kDa and 28 kDa GSTs can be distinguished.²⁶ With respect to amino acid sequence, substrate specificity and inhibitor effects, it has been shown that 28 and 26 kDa types are similar to the sigma and mu classes of mammalian cytosolic GSTs. In *S. japonicum*,

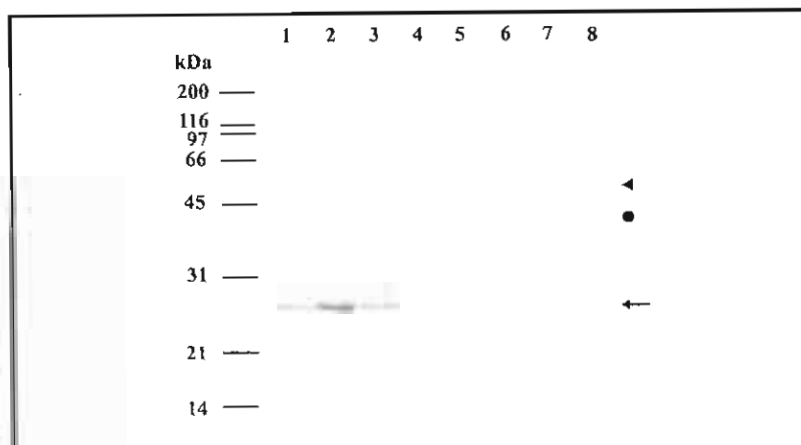


Fig. 4 Enzyme-linked immunoelectrotransfer blot (EITB) of crude worm extract, purified native and recombinant OV28GST. The preparations were separated by 12.5% SDS-PAGE, transferred onto a nitrocellulose membrane and incubated with anti-recOV28GST polyclonal antiserum. The signal was obtained after further incubation with an alkaline phosphatase rabbit anti-mouse conjugate. Lane 1: Purified native OVGST28, lane 2: recombinant OVGST28, lanes 3-8: crude worm extracts of *O. viverrini*, *S. japonicum*, *S. mansoni*, *S. mekongi*, *F. gigantica* and *Eurytrema* spp., respectively. Arrow, 28 kDa GST protein; arrow head 56 kDa putative GST dimer; circle, cross-reacting proteins.

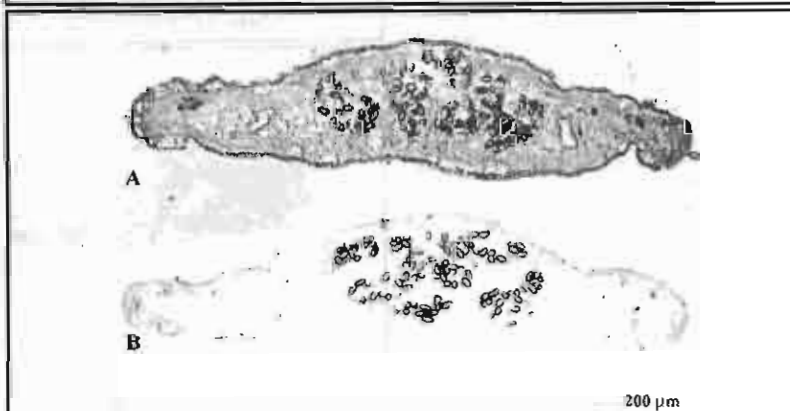


Fig. 5 Immunolocalization of OV28GST protein in cross sections of adult *O. viverrini*. The cross-sections were incubated with either preimmune serum or the anti-recOV28GST polyclonal antiserum. Detection was done by further incubation with horse radish peroxidase-conjugated ABC complex (DAKO) and diaminobenzidine substrate. A) anti-recOV28GST polyclonal antiserum, B) preimmune serum, size bar 200 μ m. In consistency with RNA *in situ* hybridization (Fig. 3), OV28GST protein is observed in parenchymal cells only.

no significant difference was observed between the tissue distributions of 26 and 28 kDa GST proteins by TEM.²⁴ Generally, parasitic trematodes seem to contain more 28 kDa

than 26 kDa GSTs (molar ratio of 28 to 26 kDa is 20:1 in *S. mansoni*, *S. haematobium*, *S. bovis*, *S. japonicum*, *P. westermani*^{25,26} and 14:1 in *C. sinensis*¹³). The functional speci-

ficiencies of these two enzymes are unknown but it can be assumed that their preference of substrate and responses to inhibitors are different. Identity of amino acid sequences between the 28 kDa and 26 kDa GSTs of the same species is low while the identity within each class is higher between different species. We suppose that more than one class of GST does exist in *O. viverrini*. After purification of soluble *O. viverrini* proteins by glutathione affinity chromatography and separation of the products by SDS-PAGE, two similarly sized 28-29 kDa proteins were observed. In an immunoblot, the 28 kDa protein showed strong reaction with anti-OV28GST polyclonal antibodies while the 29 kDa protein showed only a weak reaction. Crude worm proteins probed with anti-OV28GST polyclonal antibodies confirmed this result. A prominent band at 28 kDa was observed. This result implies that there is no or only weak cross reactivity of the anti OV28GST antibodies with other GSTs of *O. viverrini*. As mentioned earlier only important amino acids such as those found at the active site are conserved between the 26 and 28 kDa GSTs. Further studies are needed to identify additional GSTs and their function in *O. viverrini*. Also a putative 56 kDa GST dimer that reacted with the anti-OV28GST polyclonal antibody was observed as a weak signal in immunoblots (Fig. 4). This 56 kDa protein occurs in crude worm protein extracts, purified recombinant and native OV28GST with the same intensity. OV28GST protein could be detected by immunohistochemistry techniques in parenchymal cells exclusively. There was no signal in cells of vitelline tissue, tegument and the intestine epithelial lining.

This finding corresponds to results of TEM immunogold techniques applied to *S. mansoni* GST.²⁵ Using OV28GST for diagnostic application may be helpful for indicating opisthorchiasis. In several studies, the use of GST for diagnosis has been investigated.¹⁴ GST is also a candidate protein for the generation of vaccines against trematodes.^{32,33} Several studies have shown a significant decrease in infection rate after immunization with GST in experimental animals.^{33,35} Our analysis of OV28GST at the nucleic acid and protein level confirms the phylogenetic position of *O. viverrini* next to *C. sinensis*. It indicates the importance of OV28GST as a major detoxifying protein in *O. viverrini* and therefore a possible use of this protein in the diagnosis of opisthorchiasis viverrini.

ACKNOWLEDGEMENTS

We would like to express our gratitude to Dr. John Milne for critically reading this manuscript. This research was financial supported by the Royal Golden Jubilee Program of the Thailand Research Fund (RGJ-TRF), Deutscher Akademischer Austauschdienst (DAAD) and partially supported by a research grant from Thammasat University.

REFERENCES

1. Jongsuksuntigul P, Imsomboon T. Opisthorchiasis control in Thailand. *Acta Trop* 2003; 88: 229-32.
2. Jongsuksuntigul P, Imsomboon T. The impact of a decade long opisthorchiasis control program in northeastern Thailand. *Southeast Asian J Trop Med Public Health* 1997; 28: 551-7.
3. Mairiang E, Mairiang P. Clinical manifestation of opisthorchiasis and treatment. *Acta Tropica* 2003; 88: 221-7.
4. Harinasuta T, Riganti M, Bunnag D. *Opisthorchis viverrini* infection: pathogenesis and clinical features. *Arzneimittelforschung* 1984; 34: 1167-9.
5. Thamavit W, Bhamarapravati N, Saha-phong S, Vajrasthira S, Angsubhakorn S. Effects of dimethylnitrosamine on induction of cholangiocarcinoma in *Opisthorchis viverrini*-infected Syrian golden hamsters. *Cancer Res* 1978; 38: 4634-9.
6. Sripa B, Kaewkes S. Localisation of parasite antigens and inflammatory responses in experimental opisthorchiasis. *Int J Parasitol* 2000; 30: 735-40.
7. Sripa B, Kaewkes S. Gall bladder and extrahepatic bile duct changes in *Opisthorchis viverrini*-infected hamsters. *Acta Trop* 2002; 83: 29-36.
8. Bhamarapravati N, Thamavit W, Vajrasthira S. Liver changes in hamsters infected with a liver fluke of man, *Opisthorchis viverrini*. *Am J Trop Med Hyg* 1978; 27: 787-94.
9. Wongratanaheewin S, Sermswan RW, Sirisinha S. Immunology and molecular biology of *Opisthorchis viverrini* infection. *Acta Trop* 2003; 88: 195-207.
10. Poopyruchpong N, Viyanant V, Upatham ES, Srivatanakul P. Diagnosis of opisthorchiasis by enzyme-linked immunosorbent assay using partially purified antigens. *Asian Pac J Allergy Immunol* 1990; 8: 27-31.
11. Wongsaraj T, Sakolvaree Y, Chaicumpa W, Maleewong W, Kitikoon V, Tapchaisri P, Chongsa-nguan M, Cross JH. Affinity purified oval antigen for diagnosis of opisthorchiasis viverrini. *Asian Pac J Allergy Immunol* 2001; 19: 245-58.
12. Wongratanaheewin S, Pumidonming W, Sermswan RW, Maleewong W. Development of a PCR-based method for the detection of *Opisthorchis viverrini* in experimentally infected hamsters. *Parasitology* 2001; 122: 175-80.
13. Kang SY, Ahn IY, Park CY, Chung YB, Hong ST, Kong Y, Cho SY, Hong SJ. *Clonorchis sinensis*: molecular cloning and characterization of 28-kDa glutathione S-transferase. *Exp Parasitol* 2001; 97: 186-95.
14. Hong SJ, Yun Kim T, Gan XX, Shen LY, Sukontason K, Sukontason K, Kang SY. *Clonorchis sinensis*: glutathione S-transferase as a serodiagnostic antigen for detecting IgG and IgE antibodies. *Exp Parasitol* 2002; 101: 231-30.
15. Altschul SF, Madden TL, Schaffer AA, Zhang J, Zhang Z, Miller W, Lipman DJ. Gapped BLAST and PSI-BLAST: a new generation of protein database search programs. *Nucleic Acids Res* 1997; 25: 3389-402.

16. Thompson JD, Higgins DG, Gibson TJ. CLUSTAL W: improving the sensitivity of progressive multiple sequence alignment through sequence weighting, position-specific gap penalties and weight matrix choice. *Nucleic Acids Res* 1994; 22: 4673-80.
17. Rice P, Longden I, Bleasby A. EMBOSS: the European Molecular Biology Open Software Suite. *Trends Genet* 2000; 16: 276-7.
18. Rost B. PHD: predicting one-dimensional protein structure by profile-based neural networks. *Methods Enzymol* 1996; 266: 525-39.
19. Swoford D. PAUP: phylogenetic analysis using parsimony. version 4.0 beta10. Centre for Agriculture and Bioscience International, Camptaign, IL, 1999.
20. Braissant O, Wahli W. A simplified *in situ* hybridization protocol using non-radioactively labeled probes to detect abundant and rare mRNAs on tissue sections. *Biochemica* 1998; 1: 10-16.
21. Habig WH, Pabst MJ, Jakoby WB. Glutathione S-transferases. The first enzymatic step in mercapturic acid formation. *J Biol Chem* 1974; 249: 7130-9.
22. Viyanant V, Krailas D, Sobhon P, Upatham ES, Kusamran T, Chompoochan T, Thammasart S, Prasittirat P. Diagnosis of cattle fasciolosis by the detection of a circulating antigen using a monoclonal antibody. *Asian Pac J Allergy Immunol* 1997; 15: 153-9.
23. Hong SJ, Kang SY, Chung YB, Chung MH, Oh YJ, Kang I, Bahk YY, Kong Y, Cho SY. *Paragonimus westermani*: a cytosolic glutathione S-transferase of a sigma-class in adult stage. *Exp Parasitol* 2000; 94: 180-9.
24. Gobert GN, Stenzel DJ, McManus DP. Immunolocalisation of the glutathione S-transferases, GST-26 and GST-28, within adult *Schistosoma japonicum*. *Int J Parasitol* 1998; 28: 1437-43.
25. Liu JL, Fontaine J, Capron A, Grzyeh JM. Ultrastructural localization of Sm28 GST protective antigen in *Schistosoma mansoni* adult worms. *Parasitology* 1996; 113: 377-91.
26. Trottein F, Godin C, Pierce RJ, Sellin B, Taylor MG, Gorillot I, Silva MS, Lecocq JP, Capron A. Inter-species variation of schistosome 28-kDa glutathione S-transferases. *Mol Biochem Parasitol* 1992; 54: 63-72.
27. Liebau E, Walter RD, Henkle-Duhrsen K. Isolation, sequence and expression of an *Onchocerca volvulus* glutathione S-transferase cDNA. *Mol Biochem Parasitol* 1994; 63: 305-9.
28. Tawe WN, Eschbach ML, Walter RD, Henkle-Duhrsen K. Identification of stress-responsive genes in *Caenorhabditis elegans* using RT-PCR differential display. *Nucleic Acids Res* 1998; 26: 1621-7.
29. Liebau E, Schonberger OL, Walter RD, Henkle-Duhrsen KJ. Molecular cloning and expression of a cDNA encoding glutathione S-transferase from *Ascaris suum*. *Mol Biochem Parasitol* 1994; 63: 167-70.
30. Eaton DL, Bammler TK. Concise review of the glutathione S-transferases and their significance to toxicology. *Toxicol Sci* 1999; 49: 156-64.
31. Kampkötter A, Volkmann TE, de Castro SH, Leiers B, Klotz LO, Johnson TE, Link CD, Henkle-Duhrsen K. Functional analysis of the glutathione S-transferase 3 from *Onchocerca volvulus* (Ov-GST-3): a parasite GST confers increased resistance to oxidative stress in *Caenorhabditis elegans*. *J Mol Biol* 2003; 325: 25-37.
32. Sexton JL, Milner AR, Panaccio M, Waddington J, Wijffels G, Chandler D, Thompson C, Wilson L, Spithill TW, Mitchell GF, Campbell NJ. Glutathione S-transferase. Novel vaccine against *Fasciola hepatica* infection in sheep. *J Immunol* 1990; 145: 3905-10.
33. Liu SX, Song GC, Xu YX, Yang W, McManus DP. Anti-fecundity immunity induced in pigs vaccinated with recombinant *Schistosoma japonicum* 26 kDa glutathione-S-transferase. *Parasite Immunol* 1995; 17: 355-40.
34. Liu S, Song G, Xu Y, Yang W, McManus DP. Immunization of mice with recombinant Sj26GST induces a pronounced anti-fecundity effect after experimental infection with Chinese *Schistosoma japonicum*. *Vaccine* 1995; 13: 603-7.
35. Shuxian L, Yongkang H, Guangchen S, Xing-song L, Yuxin X, McManus DP. Anti-fecundity immunity to *Schistosoma japonicum* induced in Chinese water buffaloes (*Bos buffelus*) after vaccination with recombinant 26 kDa glutathione-S-transferase (reSj26GST). *Vet Parasitol* 1997; 69: 39-47.

Chromatin Organization and Basic Nuclear Proteins in the Male Germ Cells of *Rana tigerina*

SIRIKUL MANOCHANTR,¹ PRAPEE SRETARUGSA,² JITTIPAN CHAVADEJ,² AND PRASERT SOBHON^{2*}¹Department of Anatomy, Faculty of Medicine, Thammasart University, Rangsit Campus, Patumthani, Thailand²Department of Anatomy, Faculty of Science, Mahidol University, Bangkok, Thailand

ABSTRACT The process of chromatin condensation during spermiogenesis in *Rana tigerina* is similar to the heterochromatinization in somatic cells, where 30 nm fibers are coalesced together into a dense mass in spermatozoa without changing their initial size and nucleosomal organization. This conclusion was supported by the finding that the full set of core histones (H2A, H2B, H3, H4) are still present in sperm chromatin, but histone H1 is replaced by its variant, H1V. Rabbit anti-sera were raised against histone H3, H1, H1V, and H5 (H1 variant in chick erythrocyte). Anti-histone H1 antiserum cross-reacted with histone H1V, which implied the presence of a common epitope. Anti-histone H1V and H5 also showed cross-reaction with each other but not with histone H1, which implied the presence of a common epitope not shared by histone H1. Immunocytochemical studies, using the above antibodies as probes, showed that histones H3 is present in all steps of spermatogenic and spermiogenic cells, and somatic cells including red blood cells, Sertoli cells, and Leydig cells, while histone H1 is present in all of the cells mentioned except in spermatozoa where it is replaced by histone H1V. Histone H1V appears in the early spermatids starting from spermatid 1 (St1), and it persists throughout the course of spermatid differentiation into spermatozoa. Histone H1V is also found in chromosomes of metaphase spermatocyte and red blood cells. Thus histone H1V may cause the final and complete condensation of chromatin in *Rana* spermatozoa, a process which is similar to the heterochromatinization occurring in somatic cells such as metaphase chromosome and chick erythrocyte nucleus. *Mol. Reprod. Dev.* 70: 184–197, 2005. © 2005 Wiley-Liss, Inc.

Key Words: *R. tigerina*; spermatogenesis; spermiogenesis; chromatin; sperm basic nuclear proteins; immunolocalization

(Ward and Coffey, 1991), and the specific basic nuclear proteins complexed with DNA have long been regarded as an important contributing factor to variations in the chromatin condensation patterns in spermatozoa (Kierszenbaum and Tres, 1978; Balhorn, 1982; Oka et al., 1996; Balhorn et al., 1999). Ultrastructurally, at least two patterns of chromatin condensation could be discerned in mammalian spermatozoa (Ward et al., 1989; Balhorn et al., 1999). In human and primates, the fine granular chromatin substance of early spermatids gradually turned into coarser and denser bodies which eventually coalesce to form the compact homogenous mass in the mature spermatozoa (Holstein and Rosen-Runge, 1981; Allen et al., 1997; Balhorn et al., 1999). Alternatively, in most rodents the highly coiled 30 nm nucleosomal type chromatin fibers are transformed into larger and straightened (40–50 nm) fibers that are arranged in parallel during the early acrosomal stage (Balhorn et al., 1999; Wanichanon et al., 2001). These fibers appear to laterally fused into the larger fibers about 100 nm in width. Later the large fibers are completely fused to form compact chromatin (Ward and Coffey, 1991; Wanichanon et al., 2001). The changes in the compact state of spermatid chromatin are concomitant with the replacements of somatic-type histones and their testis-specific variants by transition proteins (TP), which are subsequently replaced by protamines (Balhorn, 1989; Hecht, 1989; Meistrich et al., 1994).

Protamines (MW 4,500–8,000) are smaller than histones (MW 10,000–20,000) but are considerably more basic in containing about 50 mol% arginines (Courtens et al., 1988). Protamines of eutherian mammals also contain about 10 mol% cysteines. Thus, protamines, by virtues of their greater basicity and strong disulfide cross-links, are believed to play a major role in forming the final complex with DNA and thus bring about its complete condensation in the mature spermatozoa in

INTRODUCTION

During spermatogenesis of vertebrates, the haploid phase of male germ cells undergo a series of morphological changes as they mature into spermatozoa. One of the most striking of which is the condensation of chromatin. Spermatozoal chromatin is thought to be much more compact than those in mitotic chromosomes

Grant sponsor: The Thailand Research Fund (Senior Research Scholar Fellowship to PS); Grant sponsor: National Science and Technology Development Agency (PhD Scholarship to SM).

*Correspondence to: Dr. Prasert Sobhon, PhD, Department of Anatomy, Faculty of Science, Mahidol University, Rama 6 Road, Bangkok 10400, Thailand. E-mail: aspsobhon@mahidol.ac.th

Received 30 April 2003; Accepted 20 July 2003

Published online in Wiley InterScience (www.interscience.wiley.com). DOI: 10.1002/mrd.20191

mammals (Bedford and Calvin, 1974; Balhorn et al., 1999). Immunolabeling studies have demonstrated that protamines appear in late spermatids in both human and rat (Le Lannic et al., 1993; Oko et al., 1996).

In addition to protamines, there is also a diversity in other basic proteins present in the spermatozoa of various animal phyla (Bloch, 1969). Electrophoretic, cytochemical, and amino acid analysis demonstrated that sperm basic nuclear proteins (SNBPs) vary considerably among anurans (Kasinsky et al., 1985). Amino acid sequence analysis of SNBPs in mature toad sperm (of *Bufo* genus) indicated that it is composed exclusively of two protamines with lower molecular weights than that of somatic histones, and they are rich in arginines (Takamune et al., 1991). On the other hand, the mature sperm of African clawed toad, *Xenopus laevis*, contain six different SNBPs in addition to four types of the core histones (Risley and Eckhardt, 1979; Mann et al., 1982). By contrast, only core histones and sperm specific H1 variant are present in sperm of bullfrog, *Rana catesbeiana*, while protamines are totally absent (Itoh et al., 1997). Therefore, questions arise whether 30 nm nucleosomal type chromatin fiber still exist in all sperm nuclei of all *Rana* species. And if this is the case, how are these somatic type chromatin fibers packed in the sperm nuclei? The present study was undertaken to investigate the pattern of chromatin organization, the profile of SNBPs, and the distribution of these proteins during spermatogenesis of *Rana tigerina*, a rice field frog commonly found in Thailand.

MATERIALS AND METHODS

Experimental Animals

R. tigerina, a species of rural rice field frogs commonly found in Thailand, were cultured in cement tanks. They were maintained in a natural environment having approximate 12-hr light/dark cycle. The ambient temperature was about 25–30°C, while the relative humidity ranged from 80 to 100%. Pelleted frog feeds were given once daily in the afternoon, and the water in the cement tanks was changed at alternate days. Only sexually mature frogs, generally more than 12 months old (Sretarugsa et al., 1997), were used in the experiment.

Specimen Preparation for Light and Transmission Electron Microscopy (TEM)

Mature male frogs were collected during the breeding season (April–October) (Sretarugsa et al., 1997), and anesthetized by being placed in an ice bath until they became immobile. The testes were removed and immediately fixed in the solution of 4% glutaraldehyde plus 2% paraformaldehyde in 0.1 M Millonig's buffer, pH 7.2, for 2 hr, followed by post-fixation in 1% osmium tetroxide in the same buffer for 1 hr. After fixation, specimens were dehydrated through an increasing concentrations of ethyl alcohol at 50, 70, 90, 95, and 100%, consecutively, cleared with propylene oxide and embedded in Araldite 502 resin.

In order to facilitate the recognition of various steps of the male germ cells, semithin sections of about 0.75–1 µm were cut with glass knives in a Porter-Blum MT-2 ultramicrotome, and stained with 1% methylene blue. The sections were examined and photographed in an Olympus Vanox microscope. Thin sections with an interference color of silver to silver-gold (about 60–90 nm thick) were also cut with glass knives and picked up on uncoated 300-mesh copper grids, stained by floating on saturated aqueous uranyl acetate and lead citrate for 30 min each. The sections were then examined in TEM H-300 at 75 kV.

Measurement of Chromatin Fibers

The male germ cells of *R. tigerina* were classified into various steps based on the patterns of chromatin organization, and ultrastructural characteristics. The sizes of chromatin fibers in at least ten cells from each step of the male germ cells were measured in electron microscopic negatives in a Nikon profile projector. Fibers were measured at random by recording the distance between their distinct edges. Catalase crystal with the lattice spacing of 87.5 Å (Agar Aids) were photographed at the same magnifications and used as the standard for measurement of chromatin fiber sizes. From the variation in sizes and the orientation of chromatin fibers, the pattern of chromatin organization and condensation were deduced.

Isolation of Nuclei From Frog Spermatozoa, Testicular Cells, and Chick Erythrocytes

Testes were cooled on ice immediately after removal and all of the following steps were performed at 4°C. The testes were minced into small pieces and homogenized gently in five volumes of homogenizing buffer (0.31 M sucrose, 3 mM MgCl₂, 5 mM potassium phosphate pH 6.0, 0.05% Triton X-100, 0.1 mM PMSF) using a motor-driven Teflon pestle. The homogenate was filtered through four layers of gauze and centrifuged at 600g for 10 min. To lyse the cells, the pellet was suspended in cold distilled water containing 0.1 mM PMSF. After being centrifuged, the pellet was resuspended in the MP solution (5 mM MgCl₂, 5 mM sodium phosphate, pH 6.5) using Pasteur pipette. An aliquote of 100 µl was taken for microscopic examination, and the remainder was centrifuged to recover the nuclei in the pellet fraction.

Spermatozoa aspirated from the cloaca after 1 hr of s-GaRH injection were isolated from semen by centrifugation and then resuspended in SMT solution (250 mM sucrose, 2 mM MgCl₂, and 10 mM Tris-HCl, pH 7.4). They were demembranated with 0.5% Triton X-100 in SMT solution for 10 min at room temperature and their nuclei were stored at -70°C in SMT buffer.

Erythrocytes were lysed in the hypotonic solution of 0.5% Triton X-100 in SMT solution and centrifuged. The pellets of nuclei were then resuspended in MP solution and centrifuged again. This step was repeated until the pellet of nuclei was clear from reddish tinge.

Isolated nuclei were suspended in SMT solution and stored at -70°C .

Extraction of Nuclear Proteins

The three types of nuclei obtained above were re-suspended in 1.0 ml cold distilled water using a Teflon homogenizer. After incubation, proteins were extracted with 0.25 N HCl and then precipitated with 20% trichloroacetic acid (TCA). The precipitate was recovered by centrifugation and washed with ice cold acidified acetone (200 ml of acetone plus 0.1 ml of 12 N HCl), followed with ice cold acetone, and then dried under vacuum (Platz et al., 1975).

Acid-Urea-Triton X-100-Polyacrylamide Gel Electrophoresis (AUT-PAGE)

Basic nuclear proteins were separated on slab gels (0.75 mm \times 8 cm \times 10 cm) containing 17% acrylamide, 2.5 M urea, 6 mM Triton X-100, and 5% acetic acid (Zweidler, 1978). Protein samples were dissolved in sample buffer (1–2 mg/ml), 9 M urea, 0.9 N acetic acid, 5% mercaptoethanol, and 0.2% pyronine-G. Electrophoresis was carried out at 120 V at constant voltage, with the cathode at the bottom of the gel, for 4 hr. The gel was fixed and stained with 0.125% Coomassie Brilliant Blue R-250 in 50% methanol and 10% acetic acid for 30 min, followed by destaining in 50% methanol and 10% acetic acid, 5% methanol and 7% acetic acid for 2 hr and overnight, respectively (Laemmli, 1970). The gels were stored in sealed plastic boxes containing 7% acetic acid, or they were dried onto cellophane paper for longer storage.

Antibodies Against Histones

In the present study, four polyclonal antibodies were raised in rabbits against testis-specific histones H3, H1, H1V, and against chick erythrocyte H5. These antibodies were used as probes in localizing the corresponding proteins in the male germ cells in the seminiferous epithelium of the testes. Histones and their variants were separated in 17% AUT-PAGE slab gel (1.5 mm \times 8 cm \times 10 cm) and identified by brief staining with 0.05% Coomassie Brilliant Blue R-250 in distilled water. Appropriate bands were excised from the gel and lyophilized for 24 h. For immunization, a portion of gel powder containing about 0.4 mg of protein was mixed with sterile water (equal) to one half of the original gel volume, and the solution emulsified with an equal volume of complete Freund's adjuvant (Sigma Co., St. Louis, MO). The antigen preparation was administered by intradermal injection into the back of the neck of male New Zealand white rabbits. The first booster injection containing the same ground gel emulsified with incomplete Freund's adjuvant was given at 6 weeks after the first immunization, followed by the second boost 6 weeks later. Fourteen days after the final boost, blood was drawn from the marginal ear vein to test for the presence of specific antibodies by immunoblotting.

Immunoblotting

The specificities of anti-histone antibodies were assessed by immunoblotting as followed. Total basic nuclear proteins from testicular nuclei and chick erythrocytes were separated in 17% AUT-PAGE as previously described. Proteins were transferred onto nitrocellulose membrane (with 0.45 μm pore size) positioned at the cathode side of the gel, using 0.9 N acetic acid pH 2.3, as the transfer buffer, at 400 mA for 2 hr. Following transfer, the proteins on nitrocellulose membranes were visualized by brief staining with 0.5% Ponceau S in distilled water, while the gels were stained in Coomassie blue to determine the efficiency of transfer. The membranes were incubated in the blocking buffer, 5% nonfat dry milk in 10 mM Tris-buffered saline, pH 7.4 (w/v), for 1.5 hr. The membranes were then incubated in the primary antibodies at the dilution of 1:10,000 for 1 hr, followed by washing with 10 mM Tris-buffered saline, pH 7.4 containing 0.1% Tween-20 (v/v). The secondary antibody, HRP-conjugated goat anti-rabbit IgG, was added at the dilution of 1:20,000 for 40 min, washed with 10 mM Tris-buffered saline, pH 7.4 containing 0.1% Tween-20 (v/v). Finally, the membranes were washed with 10 mM Tris-buffered saline, pH 7.4. The membranes were visualized in the solution of 0.03% 3,3',4,4'-tetraamine biphenyl DAB in 50 mM Tris, pH 7.4, containing 0.1% H_2O_2 (Ausubel et al., 1995). The reaction was terminated by rinsing the membranes in several changes of distilled water. The membranes were dried at room temperature and kept in plastic bags in the dark.

Tissue Preparation for Immunolocalization

The testes were obtained from sexually mature frogs. Pieces of testes were fixed in 1% glutaraldehyde plus 4% paraformaldehyde and 0.2% picric acid in Millonig's buffer for 2 hr at 4°C . Subsequently, the specimens were dehydrated sequentially in 70, 80, and 90% ethyl alcohol. Then infiltrated in the mixture of LR White resin (London Resin, Basingstoke, UK) and 90% alcohol at the ratio of 1:1 for 2 hr, and then in pure LR White resin for overnight before being embedded in a fresh batch of LR White resin. Anaerobic polymerization was performed at the temperature lower than 50°C for 24 hr.

Immunofluorescence

Semithin sections (0.75–1 μm thick) of LR white embedded specimen were cut with glass knives in a Porter-Blum MT-2 ultramicrotome and placed on gelatin-coated slide, then washed in 0.1 M PBS containing 0.1% Tween-20 (v/v). The sections were incubated in the blocking buffers, 0.15 M glycine in 0.1 M PBS, pH 7.4 and 4% bovine serum albumin (BSA) in 0.1 M PBS, pH 7.4, respectively. The sections were then incubated in primary antibodies (as prepared previously) diluted at 1:10 with 0.1 M PBS, pH 7.4, containing 1% BSA for 1 hr; the excess antibodies were washed off with

0.1 M PBS, pH 7.4, plus 0.1% Tween-20 (v/v), three times, 5 min each. Then, the sections were incubated in the secondary antibody, fluoresceine isothiocyanate (FITC)-conjugated goat anti-rabbit IgG, diluted at 1:200 with 0.1 M PBS, pH 7.4, containing 1% BSA for 30 min, and washed with 0.1 M PBS, pH 7.4, plus 0.1% Tween-20 (v/v), three times, 5 min each. The slides were mounted with glass cover slips by using antifade medium (Vecta shield) mounting media, sealed with nail polish, and observed under Nikon HB 10101 AF fluorescence microscope. For negative controls, the primary antibodies were omitted to assess the specificities of the immunostainings.

Immunoelectron Microscopy

LR white-embedded ultrathin sections (about 60–90 nm thick) of the testes were obtained and mounted on 300-mesh nickel grids. The applications of various solutions to the tissues sections were done by floating the grids, tissue-side down, on drops of the relevant solutions. The sections were first blocked for 15 min in 0.15 M glycine in 0.05 M PBS, pH 7.4, at room temperature, followed by 4% BSA in 0.05 M PBS, pH 7.4, for 2 hr at 4°C. Next, they were incubated for 2 hr with appropriate primary antibodies diluted at 1:10 in 0.05 M PBS, pH 7.4, plus 1% BSA (w/v) at 4°C. After extensive washing in 0.05 M PBS, pH 7.4, plus 0.05% Tween-20 (v/v), the sections were incubated for 30 min with protein A gold diluted at 1:200 in 0.05 M PBS, pH 7.4, plus 1% BSA (w/v). The grids were then extensively washed in 0.05 M PBS, pH 7.4, plus 0.05% Tween-20 (v/v), followed by distilled water before being dried. The sections were then counterstained with uranyl acetate and lead citrate, washed in distilled water, and dried. For negative controls, the sections were treated as above with the omission of the primary antibodies to assess the specificities of the immunostainings. Ultrathin sections were examined for immunogold labeling by TEM H-300 at 75 kV.

RESULTS

Chromatin Organization

The testis of *R. tigrina* contains convoluted seminiferous tubules, each of which is surrounded by a thick basement membrane (Fig. 1A). The seminiferous epithelium consists of two groups of cells, i.e., spermatogenic cells and follicular cells. The interstitial areas are filled with interstitial cells, blood vessels, and connective tissues (Fig. 1A). The differentiating male germ cells are always found in synchronously developing groups, each surrounded by processes of follicular cells, which is called a spermatocyst (Fig. 1B,C). TEM can reveal the detail of chromatin organization in various steps of male germ cells. Primary spermatogonium (Sg1) has a clear nucleus containing almost all euchromatin (Fig. 1D). Each cell divides mitotically and gives rise to secondary spermatogonia (Sg2) which are distinguished by the increasing amount of small heterochromatin blocks distributed throughout the nucleus (Fig. 1E). Sg2

gives rise to primary spermatocytes which then pass through six steps as in the first meiotic division of vertebrate male germ cells, i.e., leptotene (LSc), zygotene (ZSc), pachytene (PSc), diplotene (DSc), diakinesis (DiSc), and metaphase (MSc) primary spermatocytes. The nuclear volume of LSc (Fig. 1F) starts to increase again compared to Sg2, due to the need to accommodate the increased amount of duplicated chromosomal DNA, and chromatin is made of loosely packed 30 nm fibers linked by thin zig-zag 10 nm fibers (Fig. 1F, inset). The 30 nm chromatin fibers start to be folded into small, elongated heterochromatin blocks again in late LSc. These blocks are increasingly enlarged and coupled by the synaptonemal complexes, the tripartite structures, in ZSc and PSc (Fig. 1G,H); while individual 30 nm fibers in the blocks and around the synaptonemal complexes can still be perceived (Fig. 1G, inset). In DSc (Fig. 1I), DiSc and MSc (Fig. 2A) the heterochromatin blocks are more condensed into complete chromosomes. Despite this extreme condensation, 30 nm fibers still maintain their individuality (Figs. 1I and 2A, inset). Thus, it can be concluded that throughout the transformation of primary spermatocytes, 30 nm chromatin fibers become increasingly condensed into larger heterochromatin blocks, while still maintaining their individual identity, and 10 nm fibers are decreasing in quantity until they are entirely absent in MSc. After the chromosomes are separated and MSc gives rise to secondary spermatocytes (SSc) (Fig. 2B), the 30 nm fibers become loosened again, so that they could eventually be unfolded (Fig. 2B, inset) and become evenly distributed throughout the nucleus in spermatids 1 and 2 (St1 and 2, Fig. 2C,D), while 10 nm fibers reappear briefly (Fig. 2C). The 30 nm chromatin fibers are re-aggregated and packed tightly into an increasingly uniform dense mass in St3, St4 while the 10 nm disappear once again (Fig. 2E,F). Despite the increased chromatin condensation in St3, St4 the individualities of 30 nm fibers are still well preserved (Fig. 2E,F, insets). Only the completely opaque mass in spermatozoa that the individualities of 30 nm fibers disappear (Fig. 2G–I). This observation reveals that the 30 nm fibers do not increase in size nor change in conformation during spermatid differentiation, but they are brought close together, and finally become coalesced into the complete electron opaque mass in the nuclei of spermatozoa.

Basic Nuclear Proteins

Electrophoretic patterns of the acid-extracted basic nuclear proteins from testicular cells and spermatozoa of *R. tigrina* in 17% AUT-PAGE is compared to those of chick erythrocytes. Based on the electrophoretic mobilities, the order of migration of basic nuclear proteins in AUT-PAGE can be defined from the top (anode) to the bottom (cathode) of the gel as H2A, H3, H2B, H4, H1, H1V/H5 (Fig. 3A). The five main histone fractions, H2A, H3, H2B, H4, and H1 exist in all groups of cells except for the absence of H1 in *Rana* spermatozoa (Fig. 3A, lane c). All histone fractions from each cell type exhibit similar degree of mobilities. In addition to these highly

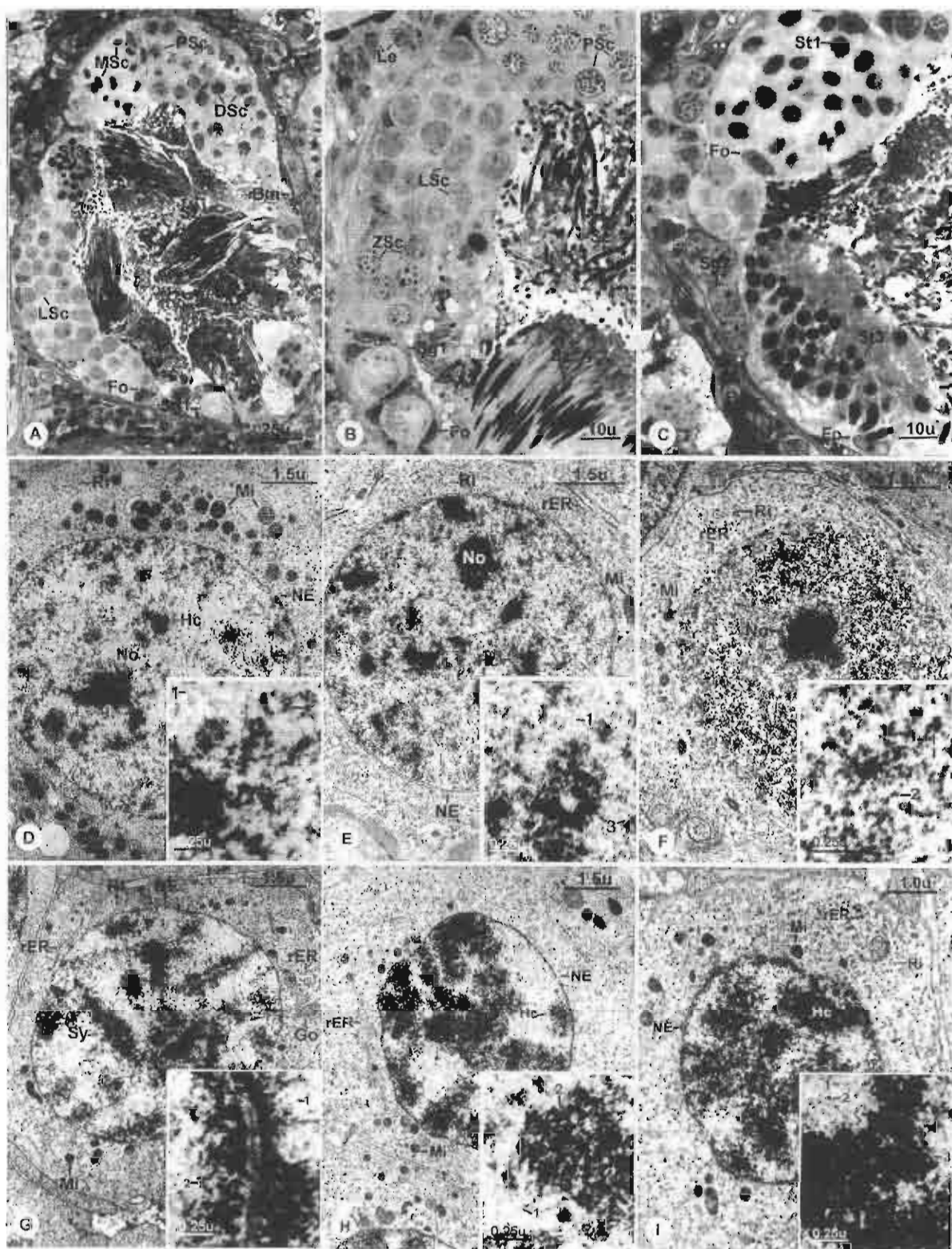


Fig. 1.

conserved bands, testicular cells and spermatozoa of *R. tigerina* possess two extra bands migrating slightly faster than those of H1 (arrowheads in Fig. 3A, lanes b, c). These proteins exhibit similar electrophoretic mobilities with histone H5 from chick erythrocytes (Fig. 3A, lane a), which imply their relatedness. These fast moving bands are probably equivalent to variants of histone H1 (H1V) as have been reported in *R. catesbaiana* spermatozoa (Itoh et al., 1997). Hence, it appears that these proteins are sperm-specific proteins unique to *Rana* species which may be involved in the condensation of chromatin like histone H5 in chick erythrocytes.

Characterization of Antibodies

The specificities of antibodies against H3, H1, H1V, and H5 are assayed by immunoblotting, which reveal that the tested antisera show specific reactivities exclusively to their corresponding antigens (Fig. 3B). All fractions of AUT-PAGE separated basic nuclear proteins extracted from chick erythrocytes and *Rana* testis are almost completely transferred onto nitrocellulose membranes as shown by Ponceau-S stained (Fig. 3B, lane 1). Rabbit anti-histone H3 antiserum recognizes the band corresponding to histone H3, and no cross-reaction with other histone bands are observed (Fig. 3B, lane 2). Anti-histone H1 antiserum recognizes only H1 and H1V (Fig. 3B, lane 3), which implies that these two histones share common epitope(s). Anti-histone H1V antiserum recognizes only H1V in *Rana* testicular cells and H5 in chick erythrocytes (Fig. 3B, lanes 4, 6), but not H1 (Fig. 3B, lane 4). Interestingly, anti-histone H5 antiserum reacts with histone H5 from chick erythrocytes as well as H1V from *R. tigerina* testis (Fig. 3B, lanes 5, 7). The cross immuno-reactivities of anti-histone H1V and anti-histone H5 antisera with histone H5 of chick erythrocytes and histone H1V of *R. tigerina* testicular cells implies that the two proteins are closely related (see Table 1 for summary).

Localization of Histones in the Male Germ Cells by Immunofluorescence

Anti-histone H3. Anti-H3, shows immuno-reactivity in the nuclei of all steps of the male germ cells. The fluorescence is intense in the chromatin, which exhibits the unique features according to specific steps of the cells (Fig. 4B). Primary spermatocytes show staining of their characteristic heterochromatin pattern (Fig. 4C). The uniformly intense immuno-staining is also seen in the nuclear of early spermatids (St1, St2) (Fig. 4C), late spermatids (St3, St4), and spermatozoa (Fig. 4B,C). Positive staining is also detected in the nuclei of follicular cells (Fig. 4C), interstitial cells and erythrocytes. In the tubules of negative control sections, there is neither immuno-staining in the nuclei of germ cells nor testicular somatic cells (Fig. 4A).

Anti-histone H1. The immuno-staining pattern of anti-H1 is similar to that of anti-H3 as intense fluorescence is observed in the nuclei of all steps of cells in spermatogenesis and spermiogenesis including spermatozoa (Fig. 4E,F). The nuclei of testicular somatic cells, i.e., follicular cell, Leydig cells, and erythrocytes in the blood vessels are all positively stained. Immuno-reactivity is not observed in the nuclei of cells in the control group (Fig. 4D).

Anti-histone H1V. Anti-H1V exhibits immuno-staining in the nuclei of St1 and the fluorescence is localized uniformly over each nucleus, while no fluorescence is observed in the cytoplasm (Fig. 4H). The nuclei of St1 2, 3, 4 are uniformly and intensely stained (Fig. 4I). Intense immuno-reactivity is also observed in the nuclei of spermatozoa (Fig. 4H,I). No immuno-staining is detected in the nuclei of spermatogonia and primary spermatocytes, except on the chromosomes of metaphase spermatocyte (Fig. 4H,I). No immuno-reactivity is observed in the nuclei of testicular somatic cells, Sertoli cells, and Leydig cells (Fig. 4I). Control sections do not show immuno-reactivity (Fig. 4G).

Fig. 1. A-C: Semithin sections of a frog's testis showing the histology of seminiferous tubules and the spermatocytes containing clones of synchronously developing male germ cells: primary spermatogonia (Sg1), secondary spermatogonia (Sg2), leptotene spermatocyte (LS), zygotene spermatocyte (ZS), pachytene spermatocyte (PS), diplotene spermatocyte (DS), anaphase spermatocyte (MS), secondary spermatocyte (SS), spermatid 1 (St1), spermatid 2 (St2), spermatid 3 (St3), spermatid 4 (St4), and spermatozoa (Sz). Each spermatocyte is surrounded by the processes of follicular cell (Fo). The interstitial areas are filled with interstitial Leydig cells (Le). **D:** Transmission electron micrographs of primary spermatogonia (Sg1): the nucleus (Nu) contains mostly euchromatin, which consists of two levels of fibers, 10 (1) and 30 (2) nm in width (inset). Tight aggregations of 30 nm fibers form heterochromatin blocks (He). The cytoplasm contains numerous ribosomes (Ri) and mitochondria (Mi). No, nucleolus; NE, nuclear envelope. **E:** Secondary spermatogonia (Sg2): small heterochromatin blocks (He) are increasing in number and scattered throughout the nucleus. Chromatin fibers (inset) are organized into two levels and in primary spermatogonia. The cytoplasm contains abundant ribosomes (Ri), mitochondria (Mi), and rough endoplasmic reticulum (rER). No, nucleolus; NE, nuclear envelope. **F:** Leptotene spermatocyte (LS): the nucleus has a round shape.

Its contains 10 nm (1) and 30 nm (2) chromatin fibers (inset). Small blocks of condensed chromatin (arrow) are evenly scattered throughout the nucleus. The cytoplasm contains abundant ribosomes (Ri), mitochondria (Mi), and rough endoplasmic reticulum (rER). No, nucleolus. **G:** Zygotene spermatocyte (ZS): in the nucleus (Nu), synaptonemal complex (Sy) is fully formed and becomes numerous. Chromatin fibers (inset) are still organized into two levels, i.e., 10 nm (1) and 30 nm (2). The cytoplasm contains ribosomes (Ri), mitochondria (Mi), Golgi complex (Go), and rough endoplasmic reticulum (rER). High magnification of synaptonemal complex is displayed in an inset. NE, nuclear envelope. **H:** Pachytene spermatocyte (PS): the nucleus exhibits long and thick intertwined heterochromatin blocks or cords (He). Chromatin fibers can be identified as two levels, and those within the heterochromatin blocks could still be visualized individually as 30 nm fibers (inset). The cytoplasm contains mitochondria (Mi), ribosomes (Ri), and rough endoplasmic reticulum (rER). NE, nuclear envelope. **I:** Diplotene spermatocyte (DS): the nucleus (Nu) shows long and thick heterochromatin blocks (He) aligned along the nuclear envelope (NE) in a cartwheel pattern. Most single chromatin fibers are 30 nm (2) in size while 10 nm (1) are much decreased in quantity (inset). The cytoplasm contains mitochondria (Mi), ribosomes (Ri), and rough endoplasmic reticulum (rER). NE, nuclear envelope.

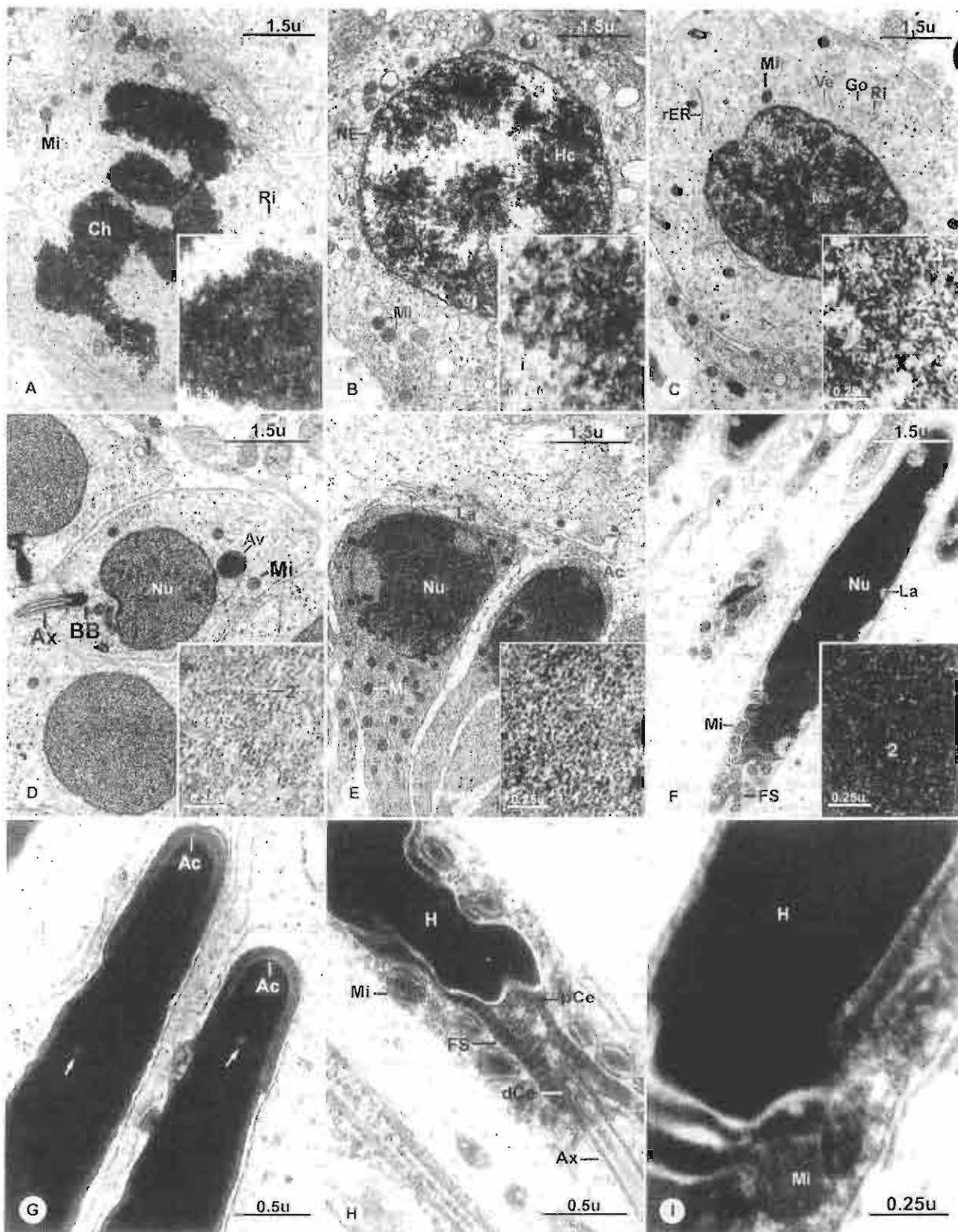


Fig. 2.

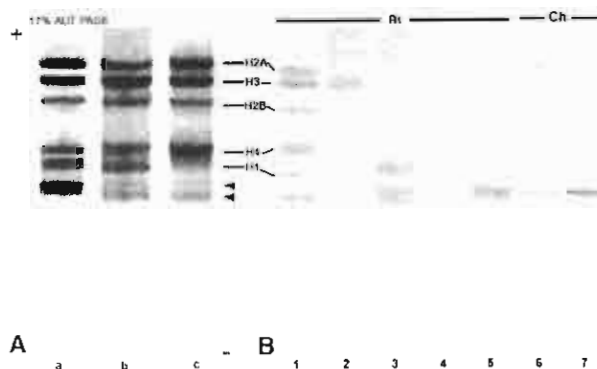


Fig. 3. A: AUT-PAGE (17%) analysis of the basic nuclear proteins from nuclei of testicular cells (lane b) and spermatozoa (lane c) from *R. tigrina*, in comparison to basic nuclear proteins from chick erythrocytes (lane a). Extracted proteins were applied to each well and electrophoresed from top (+) to bottom (-). Each lane shows the Coomassie blue-stained bands displaying all fractions of core histones (H2A, H2B, H3, H4) together with linker histone H1. Arrowheads indicated sperm-specific histones, H1V, of *R. tigrina*. B: Demonstration of the specificities of antibodies analyzed by Western blotting. The acid extracted proteins from *Rana* testis (two to five) and chick erythrocytes (six and seven) were electrophoresed through 17% AUT-PAGE, transferred onto nitrocellulose membranes and probed with rabbit anti-histone H3 antibody (lane 2), rabbit anti-histone H1 antibody (lane 3), rabbit anti-histone H1V antibody (lanes 4, 6), rabbit anti-histone H5 antibody (lanes 5, 7). Lane 1 is nitrocellulose membrane stained with Ponceau S, showing almost complete transfer of all histone fractions onto nitrocellulose strip. The results show the specificities of antibodies to corresponding antigens. The cross-reactivity between histone H1V and histone H5 are observed.

Anti-histone H5. Anti-H5 exhibits similar immunostaining pattern as anti-histone H1V antibody. A moderate fluorescence is observed over the nuclei of St1. In the St2, the nuclear fluorescence intensifies and is even more elevated in St3 and St4, as well as in spermatozoa (Fig. 4K,L). In contrast the immuno-staining is not observed in the nuclei of spermatogonia and spermatocytes except on the chromosomes of metaphase spermatocyte (Fig. 4K,L). The nuclei of follicular cells and interstitial cells do not show any immuno-reactivity

TABLE 1. Summary of the Specificities of Anti-Histone Antibodies

| Antibody | Antigen | | | |
|----------------------------|------------|------------|-------------|------------|
| | Histone H3 | Histone H1 | Histone H1V | Histone H5 |
| Rb α FH3 antiserum | * | | | |
| Rb α FH1 antiserum | | * | * | |
| Rb α FH1V antiserum | | | * | * |
| Rb α ChH5 antiserum | | | * | * |

Rb, rabbit; F, frog; Ch, chick.

Asterisks (*) indicate positive reaction.

(Fig. 4K). Control section does not show any immuno-reactivity (Fig. 4J).

Localization of Histones in the Male Germ Cells by Immunoelectron Microscopy

Anti-histone H3. Immunogold labels are present over the nuclei of all steps of spermatogenic and spermiogenic cells (Fig. 5A-F). The labeling is especially abundant in the areas of heterochromatin, with only occasional gold particles observed over the euchromatin (Fig. 5A). The concentration of label appears to be directly proportional to the condensation state of the heterochromatin (Fig. 5D-F). During the metaphase step, the chromosomes are intensely labeled while cytoplasm shows only minimal background label (Fig. 5C). Spermiogenic cells also exhibit numerous evenly distributed gold particles in the nuclei of St1 and 2 which contain uniformly condensed 30 nm chromatin fibers (Fig. 5D). The number of gold particles gradually increase in the nuclei of St3 and 4 (Fig. 5E). Immunolabeling is also conspicuous throughout the nuclei of spermatozoa (Fig. 5F). Gold particles are also distributed throughout the nuclei of testicular somatic cells,

Fig. 2. A: Diakinesis-metaphase spermatocytes (DiSc-MSc): the nucleus exhibits 30 nm chromatin fibers aggregated together to form long and large chromosomes (Ch) that begin to separate from each other in diakinesis step, and move to be aligned along the equatorial region in metaphase step. Only 30 nm fibers are present within the chromosomes, whose outlines could still be visualized (inset). The cytoplasm contains only a few organelles mainly mitochondria (Mi) and ribosomes (Ri). B: Secondary spermatocyte (SSc): the nucleus contains four to six blocks of heterochromatin (Hc) that are distributed on the inner facet of the nuclear envelope (NE). Chromatin fibers (inset) could be observed at two levels, i.e., 10 nm (1) and 30 nm (2). The heterochromatin is formed from loosely bound 30 nm fibers. The cytoplasm contains numerous mitochondria (Mi) and some vacuoles (Va). C: Spermatid 1 (St1): the nucleus (Nu) has a round to oval shape, and it contains chromatin appearing as fine granules (inset) which are the cross sections of 30 nm fibers (2), that become loosely packed throughout the nucleus. The cytoplasm contains mitochondria (Mi), relatively few ribosomes (Ri), rough endoplasmic reticulum (rER), and a few stacks of Golgi complex (Go) with smooth vesicles (Ve) associated with it. D: Spermatid 2 (St2): the nucleus (Nu) becomes oval shape, in which 30 nm fibers (2, inset) are loosely but evenly packed throughout the

nucleus. Acrosomal vesicles (Av) are present in the anterior end of the nucleus, while the developing tail appears as axoneme (Ax) outgrowing from basal body (BB) at the posterior end. E: Spermatid 3 (St3): the nucleus (Nu) becomes elongated and 30 nm fibers (2) are closely packed together (inset). Due to the increased condensation of chromatin, in most part some lightly stained areas (La) within the nucleus that contain fewer chromatin fibers appear. Fibers at 10 nm disappear completely. Flat acrosome (Ac) is present at the proximal end, while the numerous mitochondria (Mi) are present at the tail. F: Spermatid 4 (St4): the nuclear elongation is more pronounced while 30 nm fibers (2) become tightly packed, but the outlines of individual fibers are still visible (inset). Lightly stained areas (La) are also present. The cranial end of nucleus contains striated cylindrical fibrous sheath (FS) and numerous mitochondria (Mi). G-I: Spermatozoa (Sz): the head (H) contains completely condensed and electron opaque chromatin. Only few vacuoles (arrow) are present. Small U-shaped acrosome (Ac) can be observed over the anterior end of the nucleus in G. The proximal end of the tail consists of a pair of perpendicularly orientated centrioles (pCe, dCe) surrounded by the striated cylindrical fibrous sheath (FS) with rootlets. Axoneme (Ax) outgrows from the distal centriole. Mitochondria (Mi) surround the fibrous sheath.

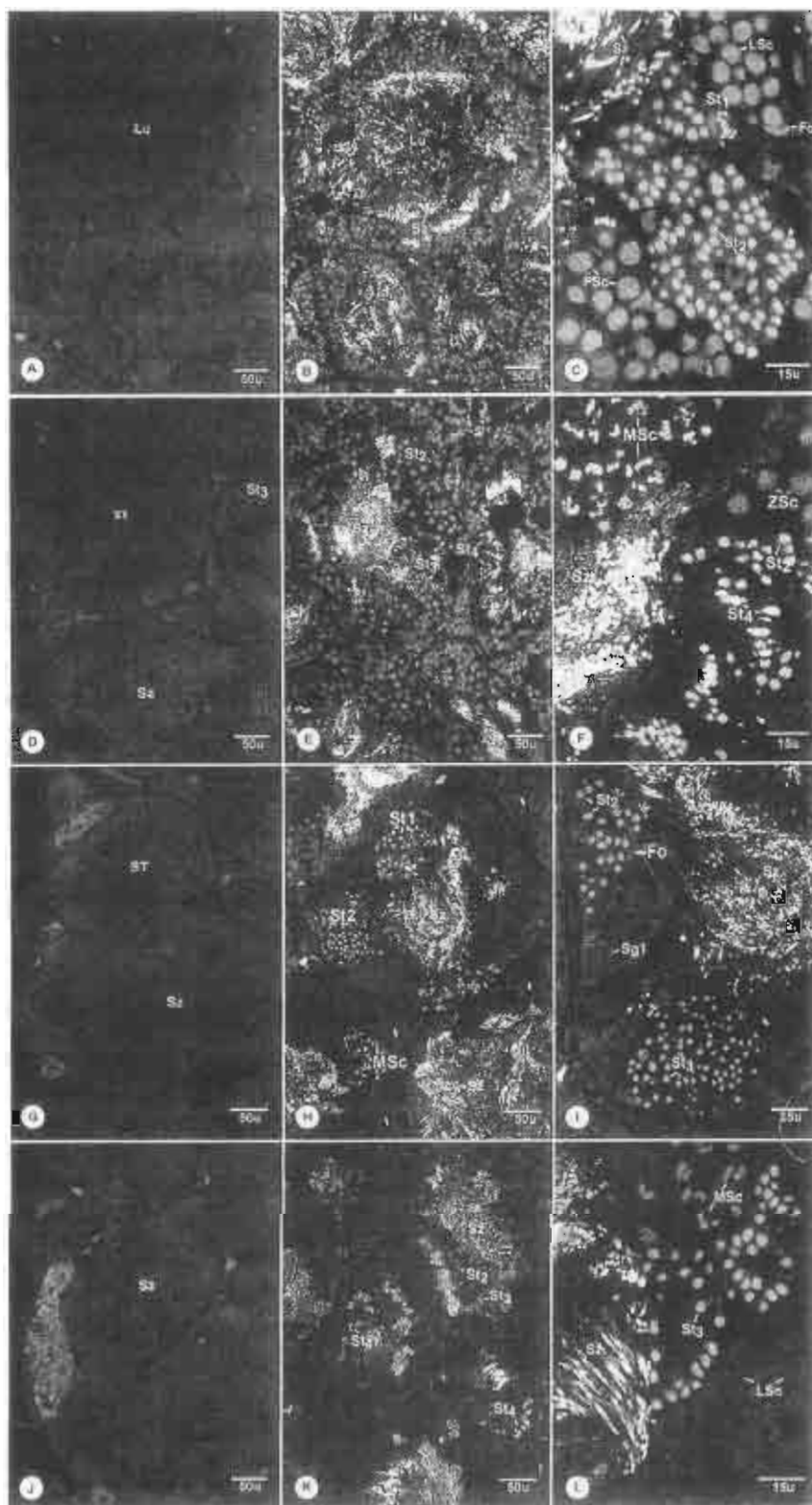


Fig. 4.

such as, erythrocytes, interstitial cells, and follicular cells (Fig. 5A). In control group, only a low nonspecific background labeling occurs over germ cells (data not shown).

Anti-histone H1. In general, anti-H1 exhibits similar pattern of immuno-labeling as anti-H3. The gold particles are distributed over the areas of the heterochromatin in the nuclei of spermatogonia and spermatocytes, and their abundance is directly proportional to the state of chromatin condensation (Fig. 5H–L). In contrast, only a few grains are found in the areas of euchromatin (Fig. 5I). High amount of immunogold labels also appear in the nuclei of cells during spermiogenesis, i.e., St1, 2, 3, and 4 (Fig. 5J,K), as well as in spermatozoa whose chromatin is totally condensed (Fig. 5L). Anti-H1 can also bind to the heterochromatin of testicular somatic cells, i.e., follicular and Sertoli cells, interstitial cells and erythrocytes (Fig. 5G). No labeling is observed in the cytoplasm of the cells at any steps of spermatogenetic and spermiogenesis (Fig. 5I). In the control group, which is incubated in the absence of primary antibody, no labeling is observed.

Anti-histone H1V. The nuclei of spermatogonia and spermatocytes do not show any labels (Fig. 5N), while the chromosomes of metaphase spermatocytes exhibit numerous gold labels (Fig. 5O). Gold labels are apparent over the granular chromatin of St1 and 2 (Fig. 5P). The chromatin becomes homogeneously condensed in St3 which coincides with a significant increase of the gold particles (Fig. 5Q). The gold labels continued to increase throughout the nuclei of St4 and become highly concentrated throughout the completely condensed chromatin in the nuclei of spermatozoa (Fig. 5R). No gold particle is observed over the chromatin in the nuclei of Sertoli cells and interstitial cells. In contrast, the labeling is very prominent over heterochromatin of erythrocyte nuclei (Fig. 5M). Only a very small amount of background labeling occurs in the control group.

Anti-histone H5. As with anti-H1V, the labeling with the anti-histone H5 antibody become quite evident only over the granular chromatin of St1 (Fig. 5U), while

the labels are absent in the earlier steps (Fig. 5S,T). In St2, the high concentration of the gold particles appears to be related to the increased chromatin condensation (Fig. 5V). Gold particles are still abundant over the more condensed chromatin of St3 and 4 (Fig. 5W), as well as in the nuclei of spermatozoa (Fig. 5X). Nuclei of spermatogenic cells are not labeled, and neither are those of follicular and interstitial cells. However, intense immunolabels can be observed over the chromosomes of metaphase spermatocytes and heterochromatin of erythrocyte nuclei. No labeling is observed in the nuclei of cells in control sections.

DISCUSSION

During the course of spermiogenesis in vertebrates, the paternal chromatin undergoes condensation, which starts in the early or mid stage spermatids and culminates in spermatozoa (Ward and Coffey, 1991; de Kretser et al., 1998; Balhorn et al., 1999). Although this condensation is the universal feature for almost all animal phyla, the specific patterns by which the chromatin is packed vary widely among different animal species (Ward and Coffey, 1991; Balhorn et al., 1999; Jameison, 1999; Sobhon et al., 2001; Wanichanon et al., 2001). These modes correlate with the presence of different testis specific basic nuclear proteins that replace somatic-type histones and interacting with DNA (Saperas et al., 1993; Soon et al., 1997; Balhorn et al., 1999). The most studied is the rodent model where TP proteins replace histones during middle stage spermatids (Meistrich et al., 1994; Oko et al., 1996), which, as the results, the chromatin loses its nucleosomal structure, and the transcription ceases (Kierszenbaum and Tres, 1975; Grimes and Smart, 1985). Protamines have high basicity and strong disulfide cross-links, so they finally complex with DNA and bring about its complete condensation in the mature spermatozoa in mammals (Bedford and Calvin, 1974; Balhorn et al., 1999). In contrast to mammalian spermiogenesis, the present ultrastructural study shows that during spermatogenesis and spermiogenesis in *R. tigrina* the chromatin

Fig. 4. Immunofluorescence micrographs of semithin sections of testes taken from mature frogs stained with polyclonal rabbit anti-frog histone antibody (RbαFH) and labeled with goat anti-rabbit IgG conjugated to FITC. RbαFH3 (A–C), RbαFH1 (D–F), RbαFH1V (G–I), RbαCH5 (J–L). A: Control section of immunocytochemically stained testis, there is no immunoreactive cells in the testis. Lu, lumen. B: Cross section of seminiferous tubules stained with RbαFH3, showing positive staining in the nuclei of all stages of the male germ cells as well as in the nuclei of erythrocyte, Sertoli cell, and Leydig cell (Le). Lu, lumen; Sz, spermatozoa; Fe, follicular cell. C: High magnification of (B) showing the positive staining exhibiting characteristic patterns of chromatin blocks in each cell stages: LSc, leptotene spermatocyte; PSc, pachytene spermatocyte; St1, spermatid 1; St2, spermatid 2; Sz, spermatozoa; Fe, follicular cell. D: Control section showing no positive staining in any part of the seminiferous tubule. ST, seminiferous tubule; St3, spermatid 3; Sz, spermatozoa. E: Low magnification micrograph showing intense immunoreactivity of RbαFH1 in the nuclei of all stages of the male germ cells. St2, spermatid 2; St3, spermatid 3; St4, spermatid 4; Sz, spermatozoa. F: High magnification micrograph of E displaying immunoreactivity of histone H1 in the characteristic chromatin patterns of various stages of the

male germ cells: ZSc, zygotene spermatocyte; MSc, metaphase spermatocyte; St2, spermatid 2; St4, spermatid 4; Sz, spermatozoa. G: There is no signal for immunoreactivity in any part of the testes of control group. ST, seminiferous tubule; Sz, spermatozoa. H: Low magnification micrograph showing positive immunoreactivity of histone H1V localized in the nuclei of spermatogenic cells: spermatid 1, spermatid 2, spermatid 3, spermatid 4, and spermatozoa (Sz). No label for histone H1V was observed in the nuclei of spermatogenic cells. I: Medium magnification micrograph of H, showing bright fluorescence in the nuclei of spermatid 2 (St2), spermatid 3 (St3), and spermatozoa (Sz). No label for histone H1V was observed in the nuclei of spermatogenic cells, such as primary spermatogonia, including somatic cells. J: Control section showing no immunoreactivity. ST, seminiferous tubule; Sz, spermatozoa. K: A low magnification showing intense immunoreactivity in the nuclei of spermatid 2 (St2), spermatid 3 (St3), spermatid 4 (St4), and spermatozoa (Sz). L: High magnification micrograph of K, showing intense immunoreactivity in the nuclei of spermatid 3 (St3) and spermatozoa (Sz). No immunoreactivity was observed in the nuclei of spermatogonia and spermatocytes such as leptotene spermatocyte (LSc), except for metaphase spermatocyte (MSc) which displays positive immunoreactivity for histone H5.

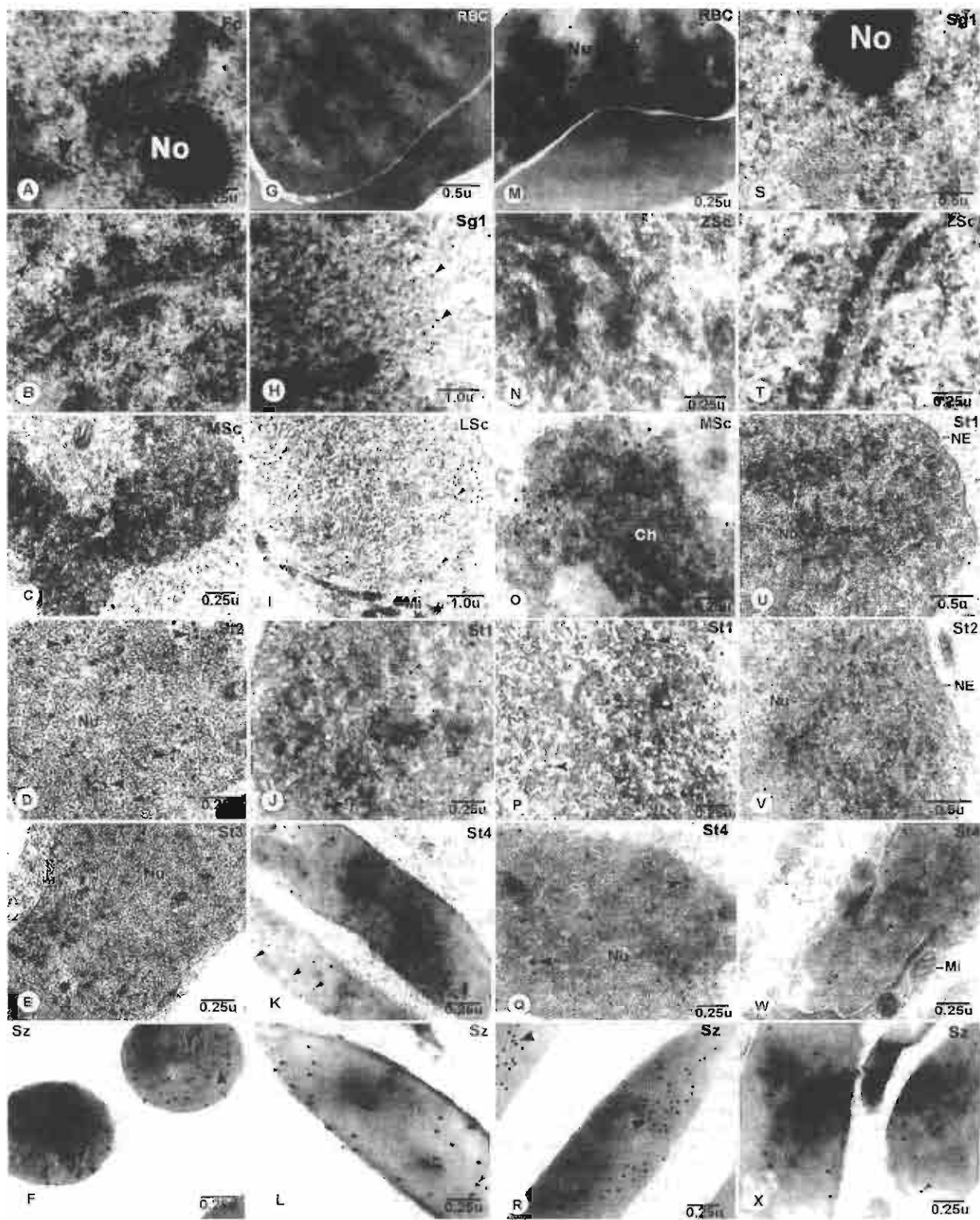


Fig. 5.

remains at two sizes, i.e., 10 and 30 nm fibers, a similar situation to the nucleosomal type of fibers existing in somatic cells. This observation is supported by the gel electrophoresis result which illustrates the presence of the full set of nucleosomal core histones (H2A, H2B, H3, H4) together with histone H1Vs in testicular as well as sperm cells, while there are no histone H1 and the higher electrophoretic mobility proteins, such as, protamines or protamine-like proteins in spermatozoa as found in other species (Alfonso and Kistler, 1993; Oki et al., 1996). This finding is similar to the study in *R. catesbeiana*, where there are no protamines in the spermatozoa of this species, while histone H1 variants (H1V) together with the full set of nucleosomal core histones are present (Itoh et al., 1997). From our data and that of Itoh et al. (1997), we believe that the fast moving bands of SNBPs of spermatozoa of *R. tigerina* is variants of histone H1 (H1V) and that these proteins are commonly found in all *Rana* species as suggested by Ausio (1999). It is possible that the final condensation of nucleosomal type fibers in sperm of *Rana* species is brought about by this. This is in contrast to the situation in *Bufo japonicus* spermatozoa where SNBPs comprise exclusively the fast moving, protamines, without any somatic histones (Takamune et al., 1991). The study of SNBPs in *Xenopus* revealed six difference species of proteins (SP 1–6), which are present in association with four types of core histones (Yokota et al., 1991). Thus, electrophoretic and amino acid composition data on the SNBPs of the genus *Bufo*, *Rana*, and *Xenopus* (Kasinsky et al., 1978, 1985; Yokota et al., 1991) suggested that there are a wide variety of these proteins, possessing properties similar to protamine or histones, or having intermediate properties. The situation in amphibians is similar to that in fishes which also show a remarkable diversity of SNBPs (Bloch, 1969). This diversity is in sharp contrast to the presence of protamines and the varying small amount of histones in sperm of aves and mammalian species (Takamune et al., 1991). The sequence of changes in sperm nuclear basic proteins has been studied by immunohistochemical techniques using polyclonal antibodies against various fractions of

histones, i.e., rabbit anti-frog histones (Rb α FH3, Rb α FH1, Rb α FH1V), and rabbit anti-chick histone H5 (Rb α ChH5) as probes. These antibodies react specifically with FH3, FH1, FH1V, and ChH5, respectively. Anti-histone H1 recognized both histones H1 and H1V in immunoblot; however, surprisingly anti-histone H1V antisera did not reacted with histone H1 in immunoblot. This may be because the two antibodies recognize different epitopes, i.e., the epitope recognized by Rb α FH1 is common to both histones, whereas the epitope recognized by Rb α FH1V is unique only to H1V. This finding gives additional support to the hypothesis that histone H1 and histone H1V is closely related (Ausio, 1999). Furthermore, Rb α FH1V also recognized histone H5 and vice versa, indicating that both proteins are similar and share common epitope. The high degree of structural similarity observed from the comparison of the partial amino acid sequences of the trypsin-resistant peptides of the histone H1 variants (Itoh et al., 1997), calf thymus histone H1 (Liao and Cole, 1981) chicken erythrocyte H5 (Briand et al., 1980) suggests the evolutionary link among all these proteins, and all could be regarded as belonging to the histone H1 family. Furthermore, there is no bands of proteins that move faster than H1V, such as TP or protamines as seen in SNBPs of mammals and other vertebrates (Oki et al., 1996; Balhorn et al., 1999). Thus one can conclude that there are no transitional proteins that replace histones in *Rana* spermatozoa. Eventhough *Rana* spermatozoa lack protamine, their chromatin can undergo complete condensation to the same degree as spermatozoa of mammals, at least as seen in TEM.

The immuno-localization study (summarized in Table 2) shows that rabbit anti-frog histone H3 (Rb α FH3) could stain nuclei of all steps of the cells: spermatogonia, spermatocyte, spermatid, spermatozoa, and even testicular somatic cells (follicular, Leydig, and red blood cells). Since histone H3 is one component of the nucleosomal core histones (van Holde, 1989), the expression of histone H3 in all spermatogenic cells is a strong evident pointing to the existence of nucleosomes in all stages of the male germ cells of *Rana*. In contrast, in the case of

Fig. 5. Transmission electron micrographs of thin sections of testes of *R. tigerina*, stained with polyclonal rabbit anti-frog histone antibody (Rb α FH) labeled with immunogold. **A–F:** Staining with Rb α FH3 demonstrating the immunogold labeling in the nuclei of spermatogenic cells: zygotene spermatocyte (ZSc), metaphase spermatocyte (MSc); spermatogenic cells: spermatid 2 (St2), spermatid 3 (St3), spermatozoa (Sz); somatic cells: follicular cells (Fol). No gold particle is observed in the cytoplasm of these cells. The gold particles are distributed mostly in the area of heterochromatin blocks (Hc), while they are occasionally found in the area of euchromatin. The round nucleolus (No) has no gold particle. Sy, synaptonemal complexes; Ch, chromosomes. **G–L:** Staining with Rb α FH1, intense immunogold labeling (arrowheads) over the area of heterochromatin in the nuclei of spermatogenic cells, i.e., primary spermatogonia (Sg1), leptotene spermatocyte (LS), spermatogenic cells, i.e., spermatid 1 (St1), spermatid 4 (St4), spermatozoa (Sz), and somatic cells, i.e., red blood cells (RBC). Only background labeling is present over the cytoplasm. Mi, mitochondria. **M–R:** Staining with Rb α FH1V, showing only background label in the nuclei and cytoplasm of spermatogenic cells, i.e., zygotene spermatocyte (ZSc) except

metaphase spermatocytes (MSc) which demonstrating the distribution of gold particles over the chromosomes. (Ch). No gold particle can be observed in the cytoplasm. Granular chromatin of spermatogenic cells, i.e., spermatid 1 (St1), spermatid 4 (St4), and spermatozoa (Sz) are strongly labeled. The density of gold particles appears directly proportional to the degree of condensation of the chromatin. The erythrocyte (RBC) also shows the immunogold labeling over the heterochromatin in its nucleus. Only background level of gold label can be observed in the cytoplasm. **S–X:** Staining with Rb α ChH5, showing only background level of gold label in the nuclei as well as in the cytoplasm of spermatogenic cells, which include primary spermatogonia (Sg1), zygotene spermatocyte (ZSc). The density of gold particle (arrowheads) appears evenly over the condensed chromatin of spermatogenic cells including spermatid 1 (St1), spermatid 2 (St2), spermatid 4 (St4), and spermatozoa (Sz). The density of gold particles appears directly proportional to state of condensation of chromatin. No gold particle is present in the cytoplasm. NL, nuclear envelope; Mi, mitochondria.

TABLE 2. Summary of the Immunolocalization Patterns of Antibodies to Various Histone Fractions in the Male Germ Cells of *Rana tigerina*

| | Antibodies | | | |
|-------------------------|-----------------|-----------------|------------------|------------------|
| | Rb α FH3 | Rb α FH1 | Rb α FH1V | Rb α ChH5 |
| Cell stages | | | | |
| Primary spermatogonia | * | * | | |
| Secondary spermatogonia | * | * | | |
| Leptotene spermatocyte | * | * | | |
| Zygotene spermatocyte | * | * | | |
| Pachytene spermatocyte | * | * | | |
| Diplotene spermatocyte | * | * | | |
| Metaphase spermatocyte | * | * | * | * |
| Secondary spermatocyte | * | * | | |
| St1 | * | * | * | * |
| St2 | * | * | * | * |
| St3 | * | * | * | * |
| St4 | * | * | * | * |
| Spermatozoa | * | * | * | * |
| Erythrocyte | * | * | * | * |
| Follicular cell | * | * | | |
| Sertoli cell | * | * | | |
| Leydig cell | * | * | | |

Spermatid 1, St1; Spermatid 2, St2; Spermatid 3, St3; Spermatid 4, St4.

Columns represent the antibodies. Rows represent the stages of male germ cells. Asterisk (*) means positive reaction.

mammals, during spermatogenesis even though a limited amount of nucleosomal organization is believed to be present up to spermatozoal stage, the majority of somatic-type histones including histone H3 are replaced by testis-specific histone variants (TH2A, TH2B, H1T) usually during the middle stages (acrosome phase) spermatids (Tanphaichitr et al., 1978; Meistrich et al., 1994; Oko et al., 1996). These testis specific histones are then replaced by transitional proteins (TP), and eventually by protamines in the late stage spermatids and immature spermatozoa (Alfonso and Kistler, 1993; Oko et al., 1996). Although, the labeling with Rb α FH1 shows similar result to the labeling with Rb α FH3 despite of absence of histone H1 in the spermatozoa of *R. tigerina* as shown by gel electrophoresis. Such positive reaction in spermatids and spermatozoa could be due to the binding on the common epitope presence in H1V even though H1 itself may be absent. However, the final confirmation of this result requires further experiment, such as in situ hybridization with specific probes for histone H1 and H1V mRNAs. Interestingly, antibody against histone H1V only stained nuclei of spermatids and spermatozoa but not the nuclei of spermatogenic cells and testicular somatic cells, except chromosomes of metaphase spermatocytes and the nuclei of red blood cells. Similar pattern was also found with Rb α ChH5, thus histone H1V and histone H5 are probably highly similar. Since the abundance of histone H1V appears concomitant with the commencement of nuclear condensation during the advance stage of spermiogenesis (i.e., St3 and St4), it is possible that H1V causes the final tight packing of nucleosomal type chromatin fibers in the nuclei of spermatids and mature spermatozoa of

R. tigerina. Furthermore, the tight packing of chromatin in *Rana* spermatozoa, chick erythrocytes, and metaphase chromosome may use a similar mechanism that is modulated by H1V or H5.

CONCLUSIONS

This study showed that chromatin organization in the *R. tigerina* spermatozoa occurs by the replacement of histone H1 with histone H1V during the course of differentiation of spermatids. Subsequently, H1V may play a role in the final and complete chromatin condensation without using protamine like in case of mammal spermatozoa. The absence of distinct ultrastructural changes in chromatin during frog spermiogenesis is correlated with the minimal changes in basic nuclear proteins. The presence of core histones suggests that nucleosomal organization is present throughout. Histone H1V, the lysine-rich variant of histone H1, may be the key factor that causes the tightly packed sperm chromatin. The similarity and higher amount of lysine/arginine content suggests histone H1V condenses chromatin of *R. tigerina* spermatozoa in the same manner as histone H5 which is known to cause in the heterochromatinization in the fully differentiated cells, such as chick erythrocytes.

REFERENCES

- Alfonso PJ, Kistler S. 1993. Immunohistochemical localization of spermatid nuclear transition protein 2 in the testes of rats and mice. Biol Reprod 48:522-529.
- Allen MJ, Bradbury EM, Balhorn R. 1997. AFM analysis of BNA-protamine complexes bound to mica. Nucleic Acids Res 25: 2221-2226.

- Ausio J. 1999. Histone H1 and evolution of sperm nuclear basic proteins. *J Biol Chem* 274:31115-31118.
- Ausubel FM, Brent R, Kingston RE, Moore DD, Seidman JG, Smith JA, Struhl K. 1995. Short protocols in molecular biology. New York: John Wiley & Sons. pp 10.1-11.31.
- Balhorn R. 1982. A model for the structure of chromatin in mammalian sperm. *J Cell Biol* 93:298-305.
- Balhorn R. 1989. Mammalian protamines: Structure and molecular interactions. In: Adolph KW, editor. Molecular biology of chromosome function. New York: Springer Verlag. pp 366-395.
- Balhorn R, Cosman M, Thornton K, Krishnan VV, Corzett M, Bench G, Kramer C, Lee IV J, Hud NV, Allen M, Prieto M, Meyer-Illse W, Brown JT, Kirz J, Zhang X, Bradbury EM, Maki G, Braun RE, Breed W. 1999. Protamine mediated condensation of DNA in mammalian sperm. In: Gagnon C, editor. The male gamete: From basic science to clinical applications. Vienna: Cache River Press. pp 55-70.
- Bedford JM, Calvin HJ. 1974. The occurrence and possible functional significance of -S-S- crosslinks in the sperm, with particular reference to eutherian mammals. *J Exp Zool* 188:137-158.
- Bloch DP. 1969. A catalog of sperm histones. *Genetics* 61:93-111.
- Briand G, Kmiecik D, Sautiere P, Wouters D, Borio-Loy O, Biserte G, Mazen A, Champagne M. 1980. Chicken erythrocyte histone H5. *FEBS Lett* 112:151-197.
- Courtens JL, Plöen L, Lair M. 1988. Immunocytochemical localization of protamine in the boar testis. *J Reprod Fertil* 82:635-643.
- de Krieger DM, Loveland KL, Meinhardt A, Simorangkir D, Wreford N. 1998. Spermatogenesis. *Hum Reprod* 13:1-5.
- Grimes SR, Smart PG. 1985. Changes in the structural organization of chromatin during spermatogenesis in the rat. *Biochim Biophys Acta* 824:128-139.
- Hecht NB. 1989. Mammalian protamines and their expression. In: Hrdlicka L, Stein G, Stein J, editor. Histones and other basic nuclear proteins. Boca Raton: CRC Press. pp 347-373.
- Holstein AF, Roosen-Runge EC. 1981. Atlas of human spermatogenesis. Berlin: Grosse Verlag. pp 1-224.
- Itoh T, Ausio J, Katagiri C. 1997. Histone H1 variants as sperm-specific nuclear proteins of *Rana catesbeiana*, and their role in maintaining a unique condensed state of sperm chromatin. *Mol Reprod Dev* 47:181-190.
- Jameison BGM. 1999. Spermatozoal phylogeny of vertebrates. In: Gagnon C, editor. The male gamete: From basic science to clinical applications. Vienna: Cache River Press. pp 304-328.
- Kasinsky HE, Huang SY, Kwauk S, Mann M, Sweeney MAJ, Yee B. 1978. On the diversity of sperm histones in the vertebrates: III. Electrophoretic variability of testis specific histone patterns in anura contrasts with relative constancy in squamata. *J Exp Zool* 203:109-126.
- Kasinsky HE, Huang SY, Mann M, Roca J, Subirana JA. 1985. On the diversity of sperm histones in the vertebrates: IV. Cytochemical and amino acid analysis in anura. *J Exp Zool* 234:33-46.
- Kierszenbaum AL, Tres LL. 1975. Structural and transcriptional features of the mouse spermatid genome. *J Cell Biol* 65:258-270.
- Kierszenbaum AL, Tres LL. 1978. The packaging unit: A basic structural feature for the condensation of late cricket spermatid nuclei. *J Cell Sci* 33:265-282.
- Laemmli UK. 1970. Cleavage of structural proteins during the assembly of the head of bacteriophage T4. *Nature* 227:680-685.
- Le Lannic G, Arkhis A, Vendrely E, Chevallier P, Dadoune JP. 1993. Protamine characterization and immunocytochemical applications of monoclonal antibodies to human sperm protamines. *Mol Reprod Dev* 36:106-112.
- Liao LW, Cole RD. 1981. The amino acid sequence of residues 1-104 of CTL-1: A bovine H1 histone. *J Biol Chem* 256:3024-3029.
- Mann M, Risley MS, Eckhardt RA, Kasinsky HE. 1982. Characterization of spermatid/sperm basic chromosomal proteins in the genus *Xenopus* (Anura, Pipidae). *J Exp Zool* 222:173-186.
- Meistrich ML, Trostle-Weige PK, Van Beek ME. 1994. Separation of specific stages of spermatids from vitamin A-synchronized rat testes for assessment of nucleoprotein changes during spermiogenesis. *Biol Reprod* 51:334-344.
- Oko RJ, Jando V, Wagner CL, Kistler WS, Herms LS. 1996. Chromatin reorganization in rat spermatids during the disappearance of testis-specific histone, H1t, and the appearance of transition proteins TP1 and TP2. *Biol Reprod* 54:1141-1157.
- Platz RD, Grimes SR, Meistrich ML, Hrdlicka LS. 1975. Changes in nuclear proteins of rat testis cells separated by velocity sedimentation. *J Biol Chem* 250:5791-5800.
- Risley MS, Eckhardt RA. 1979. Dissociation and separation of *Xenopus laevis* spermatogenic cells. *J Exp Zool* 207:93-106.
- Saperas N, Ribes E, Buesa C, Garcia-Hegardt F, Chiva M. 1993. Differences in chromatin condensation during spermiogenesis in two species of fish with distinct protamines. *J Exp Zool* 265:185-194.
- Sobhon P, Apisawetakan S, Linthong V, Pankao V, Wanichanon C, Weerachatanukul W, Meepool A, Krutachue M, Uptham ES, Punthong T. 2001. Ultrastructure of the differentiating male germ cells in *Halotis asinina* Linnaeus. *Inv Reprod Dev* 39:55-66.
- Soon LLL, Ausio J, Breed WG, Power JHT, Muller S. 1997. Isolation of histones and related chromatin structures from spermatozoa nuclei of a dasyurid marsupial, *Smutsomys crassicaudatus*. *J Exp Zool* 278:322-332.
- Sretarugsa P, Nakien V, Sobhon P, Chuvadej J, Krutachue M, Uptham ES. 1997. Structure of the testis of *Rana tigrina* and its changes during development and seasonal variation. *J Sci Soc Thailand* 23:75-86.
- Takamune K, Nishida H, Takai M, Katagiri C. 1991. Primary structure of toad sperm protamines and nucleotide sequence of their cDNAs. *Eur J Biochem* 196:401-406.
- Tanphaichitr N, Sobhon P, Taluppeth N, Chalermisarakul P. 1978. Basic nuclear proteins in testicular cells and ejaculated spermatozoa in man. *Exp Cell Res* 117:347-356.
- van Holde KE. 1989. Chromatin. New York: Springer-Verlag. pp 1-497.
- Wanichanon C, Weerachatanukul W, Suphamongkue W, Meepool A, Apisawetakan S, Linthong V, Sretarugsa P, Chuvadej J, Sobhon P. 2001. Chromatin condensation during spermiogenesis in rats. *Sci Asia* 27:211-220.
- Ward WS, Coffey DS. 1991. DNA packaging and organization in mammalian spermatozoa: Comparison with somatic cells. *Biol Reprod* 44:569-574.
- Ward WS, Partin AW, Coffey DS. 1989. DNA loop domains in mammalian spermatozoa. *Chromosoma* 98:153-159.
- Yokota T, Takamune K, Katagiri C. 1991. Nuclear basic proteins of *Xenopus laevis* sperm: Their characterization and synthesis during spermatogenesis. *Dev Growth Diff* 3:9-17.
- Zweidler A. 1978. Resolution of histones by polyacrylamide gel electrophoresis in presence of nonionic detergents. *Methods Cell Biol* 17:223-233.



Effects of praziquantel and artesunate on the tegument of adult *Schistosoma mekongi* harboured in mice

Wanee Jiraungkoorskul^{a,*}, Somphong Sahaphong^{a,b}, Prasert Sobhon^c,
Suda Riengrojpitak^a, Niwat Kangwanrangsana^a

^aDepartment of Pathobiology, Faculty of Science, Mahidol University, Rama VI road, Bangkok 10400, Thailand

^bMahidol University International College, Mahidol University Salaya Campus, Nakhonpathom 73170, Thailand

^cDepartment of Anatomy, Faculty of Science, Mahidol University, Rama VI road, Bangkok 10400, Thailand

Received 26 January 2005; accepted 19 April 2005

Available online 31 May 2005

Abstract

The effects of praziquantel and artesunate on the tegument of adult *Schistosoma mekongi* harboured in mice were compared using scanning electron microscopy (SEM). Forty-two mice infected with *S. mekongi* for 49 days were treated intragastrically with either 300 mg/kg praziquantel or 300 mg/kg artesunate. Mice were sacrificed 1 or 3 days post-treatment. Worms were collected by perfusion and examined by SEM. One to 3 days after administration of artesunate, the tegument of *S. mekongi* showed severe swelling, vacuolization, fusion of the tegumental ridges and loss or shortening of the spines on the trabeculae, collapse and peeling. Praziquantel induced similar tegumental alterations as those observed after administration of artesunate, but they were less severe. Three days post-treatment, there was evidence of recovery only in the case of praziquantel. The results of our study suggest that artesunate is more effective than praziquantel in causing tegumental damage in adult *S. mekongi*, and provides a basis for subsequent clinical trials.

© 2005 Elsevier Ireland Ltd. All rights reserved.

Keywords: Schistosomiasis; *Schistosoma mekongi*; Praziquantel; Artesunate; Scanning electron microscopy; Tegumental changes

1. Introduction

It is estimated that 200 million people in the world are currently affected by schistosomiasis, a disease caused by flatworms belonging to the genus *Schistosoma* [1–3]. There are five species that can parasitize humans, two of which are known as the Asian forms of schistosomiasis, i.e. *Schistosoma japonicum* and *Schistosoma mekongi*. Due to the characteristics of the intermediate host snail of *S. mekongi*, i.e. *Neotricula aperta*, transmission is restricted to the rocky banks of the Mekong River Basin. A seasonal cycle is consisting of a period of transmission in the dry season, from March to June both in Lao People's Democratic

Republic and Thailand [4,5]. Eggs are excreted by infected people. After reaching a freshwater body, eggs hatch to release miracidium that must penetrate the intermediate host snail for reproduction. Then cercariae are shed by the snail that can penetrate the intact skin of humans to complete the life cycle. Only few studies have been reported in the scientific literature on this schistosome species until 1992 when a focus of schistosomiasis mekongi was rediscovered in the province of Kracheh in northeast Cambodia [6,7].

In the second half of the 20th century a variety of different antischistosomal drugs were discovered with different modes of actions. The three drugs metrifonate, oxamniquine and praziquantel have been used for mass treatment in different parts of the world. However, metrifonate, which is only active against *Schistosoma haematobium*, was withdrawn from the market, on the

* Corresponding author. Tel.: +66 02 201 5563; fax: +66 02 354 7158.

E-mail address: wjra@mahidol.ac.th (W. Jiraungkoorskul).

basis of therapeutic and operational criteria [8]. Oxamniquine, singly active against *Schistosoma mansoni*, has been effectively and widely used in Brazil, but is currently being replaced by praziquantel [9]. Therefore, praziquantel has become the drug of choice as it is effective against all human schistosomes, is well tolerated and has become relatively inexpensive [3,10,11]. However, there is considerable concern about the development of praziquantel resistance [12]. Thus, there is a pressing need to look for new synthetic or natural antischistosomal drugs.

Qinghaosu (artemisinin) is an antimalarial drug which was isolated in 1972 from the Chinese traditional herb Qinghao (*Artemisia annua* L.) [13,14]. Qinghaosu and its derivatives, such as artesunate, artemether and arteether are safe, potent and well-tolerated compounds that are used as first-line antimalarial therapy in many tropical and sub-tropical countries. They have been widely used in Asia as they are efficacious against multidrug resistant strains of *Plasmodium falciparum* [15,16]. The derivative with the widest potential application is artesunate, a water-soluble drug that can be administered parenterally as well as by mouth and per rectum.

Studies in animal models indicated that artemether and artesunate are also effective against *S. japonicum* [17,18], *S. mansoni* [19,20] and *Schistosoma haematobium* [21]. Randomized controlled clinical trials confirmed that artemether results in no drug-related adverse effects, and significantly reduces the incidence and intensity of schistosome infections [22,23]. To the best of our knowledge no study has been done so far on the efficacy of the artemisinins against an *S. mekongi* infection. The purpose of the work presented here was to investigate the effects praziquantel and artesunate have on the tegument in adult *S. mekongi* harboured in mice using scanning electron microscopy (SEM).

2. Materials and methods

2.1. Snail

The freshwater snails *N. aperta* were collected at the Mekong River in Ubon Rajthani province, Thailand. They were maintained for the life cycle of *S. mekongi* in the Malacology Unit, Department of Biology, Faculty of Science, Mahidol University, Bangkok, Thailand.

2.2. Mice

ICR male mice were bred at the National Laboratory Animal Center, Nakhon Pathom, Thailand. Mice, 6 weeks old, mean weight 27.95 ± 1.39 g were used in this experiment. The animals were housed in the shoe box type cages ($18 \times 30 \times 13$ cm) containing sterile wood shaving bedding in a strictly hygienic conventional animal room at the

Faculty of Science, Mahidol University. Standard diet (Perfect companion Co. Ltd., Bangkok, Thailand) and tap water were available ad libitum. Room temperature was kept at $22-25^\circ\text{C}$ with relative humidity of 60–70% and a 12:12 hour light–dark cycle was maintained throughout. All experimental animals used in this study were approved following Guidelines for the Care and Use of Laboratory Animals, Mahidol University, authorized by the Animal Care and Use Committee, Faculty of Science, Mahidol University.

2.3. Drugs

Praziquantel and artesunate were the products of Atlantic Laboratories Corp. Ltd., Bangkok, Thailand (lot no. 000491 and 030601, respectively). For administration, all drugs were suspended in 7% Tween 80 and 3% ethanol at a final concentration of 30 mg/ml. The volume of the dose given to each mouse was 0.1 ml/mg.

2.4. Experimental design

Mice ($n=42$) were infected individually with 30 *S. mekongi* cercariae shed from experimentally infected *N. aperta*, after exposure to artificial light for at least 4 h, by the looping method [24]. Forty-nine days postinfection (PI), mice were randomly assigned to three equally-sized groups: group 1 was the control group receiving 7% Tween 80 + 3% ethanol; group 2 was the praziquantel treatment group receiving intragastrically a single dose of 300 mg/kg praziquantel; and group 3 was the artesunate treatment group receiving intragastrically a single dose of 300 mg/kg artesunate.

On days 1 and 3 post-treatment and at the same time points for the non-treated control group, 7 mice from each group were sacrificed by overinhalation of ether. Adult worms were collected from mice by the perfusion method using 0.1 M citrate in 0.15 M NaCl solution [24]. The worms were washed several times with normal saline solution and fixed in fixative solution for scanning electron microscopic examination.

2.5. Scanning electron microscopic examination

Worms were fixed in 2.5% glutaraldehyde-phosphate buffer (0.1 mol/L, pH 7.4) at 4°C for 24 h and post-fixed in 1% osmium tetroxide for 1 h. They were dehydrated through a graded series of ethanol, dried in a Hitachi HCP-2 critical point dryer machine using liquid carbon dioxide as a transitional medium. After drying, they were mounted on aluminium stubs and coated with platinum and palladium in an ion-sputtering apparatus, Hitachi E-102, at 10–15 mA for 6 min. They were examined and photographed in a Hitachi scanning electron microscope S-2500 (Hitachi High Technologies Co., Hitachi-Naka City, Japan), operating at 15 kV [25].

3. Results

3.1. Control group

The surface topography of *S. mekongi*, as studied by SEM, was reported in great detail in previous studies [26–28]. In brief, the adult male worm is thicker and shorter than the female worm and has a longitudinal cleft, the gynaecophoral canal, in which the female is held during copulation (Fig. 1A). The tegument of the adult male worm can be divided into three parts: (1) the anterior part which is the area from the oral sucker to the beginning of the gynaecophoral canal; (2) the middle part which is the largest portion of the body containing most of the gynaecophoral canal normally occupied by a female; and (3) the posterior part which comprises the area behind the region where the body of the female usually emerges from the gynaecophoral canal (Fig. 1A, B). There are numerous large trabeculae with numerous spines on the tegument covering the middle part of the male body (Fig. 1D). The surface of the adult

female worm is also divided into three parts, similar to those described in male (Fig. 1A, B). Male and female worms have an oral and a ventral sucker situated near the anterior end (Fig. 1C).

3.2. Effects of praziquantel

One day after administration of 300 mg/kg of praziquantel to mice infected with 49-day old *S. mekongi*, a few blebs were observed on the oral sucker of one male specimen (Fig. 2A). All worms showed slight to moderate focal damage of the dorsal surface of the tegument. The male worms showed changes in the trabeculae, namely swelling and shortening or even loss of the spines on the surface. There were numerous blebs around the trabeculae (Fig. 2B). In female worms, slight to moderate peeling of the dorsal surface was seen (Fig. 2C). Three days post-treatment, some worms showed apparent recovery of the tegument induced by praziquantel. Most of the trabeculae showed normal and intact appearance (Fig. 2D).

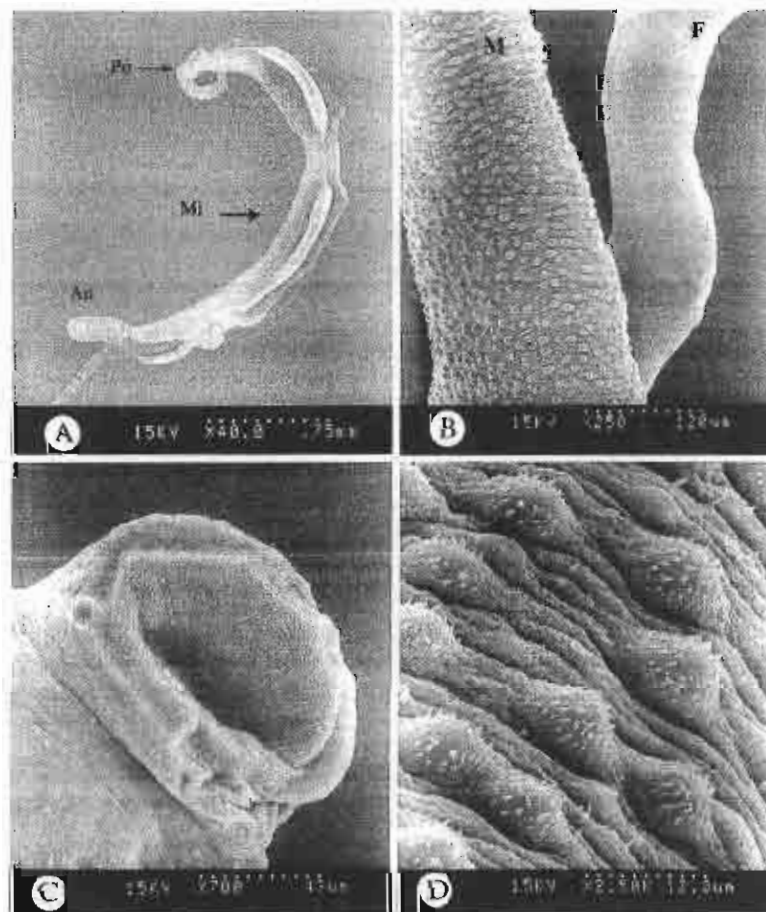


Fig. 1. Micrographs of adult male and female *S. mekongi* from untreated control group. (A) Male and female, lower magnification of the body surface showing anterior (An), middle (Mi) and posterior (Po) parts ($\times 40$). (B) Male (M) and female (F), higher magnification of the tegument of the middle part ($\times 250$). (C) Male, normal appearance of the oral sucker ($\times 200$). (D) Male, the tegument showing numerous large trabeculae with numerous spines ($\times 2500$).

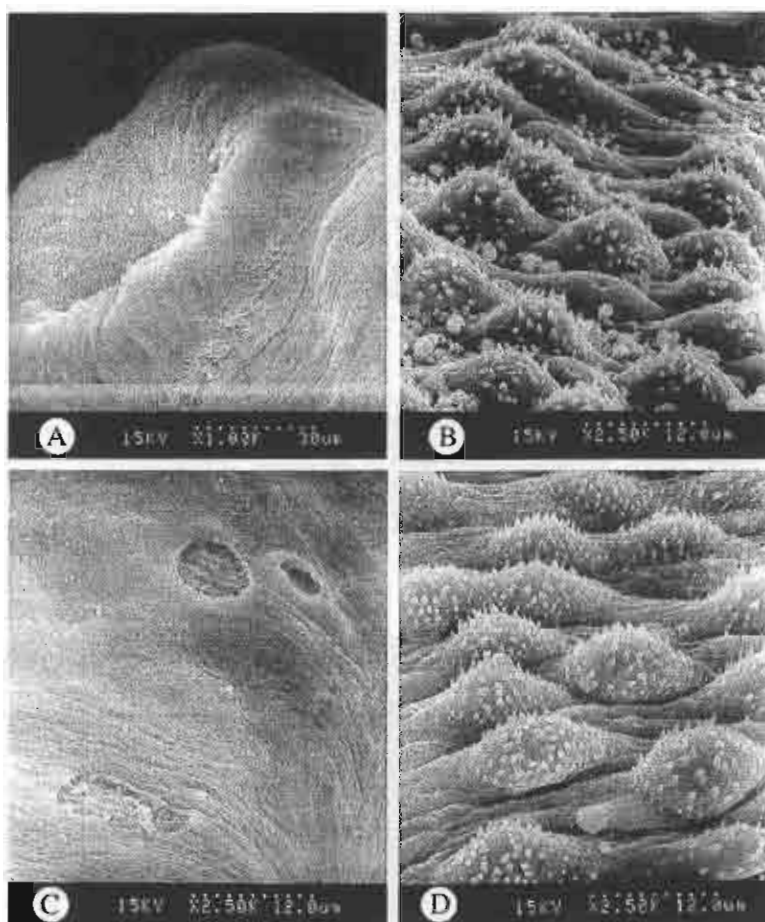


Fig. 2. Micrographs showing tegumental alterations in adult *S. mekongi* recovered from mice 1 day (A–C) and 3 days (D) after intragastric administration of a single dose of 300 mg/kg praziquantel. (A) Male, the oral sucker showing a few blebs ($\times 1000$). (B) Male, the tegument showing moderate swelling and shortening of the spines on the surface of trabeculae with numerous vesicles around trabeculae ($\times 2500$). (C) Female, moderate peeling of tegumental dorsal surfaces ($\times 2500$). (D) Male, the tegument showing recovery and normal appearance of the trabeculae ($\times 2500$).

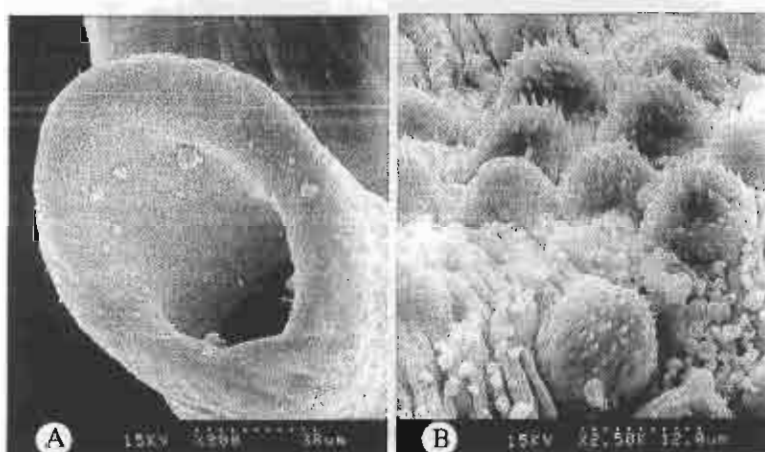


Fig. 3. Micrographs showing tegumental alterations in adult *S. mekongi* recovered from mice 1 day after intragastric administration of a single dose of 300 mg/kg artesunate. (A) Male, the oral sucker showing a few blebs (800). (B) Male, the tegument showing moderate to severe swelling, shortening and loss of the spines on the surface of trabeculae with numerous blebs around trabeculae ($\times 2500$).

3.3. Effects of artesunate

One day after a single dose of 300 mg/kg artesunate was given to mice infected with 49-day old *S. mekongi*, a few blebs were observed on the oral sucker of male worms (Fig. 3A). All worms showed moderate to severe focal damage of the tegument. In male worms, the lesions were similar to those observed after praziquantel treatment, but showed a somewhat higher severity. For example, some of the trabeculae were swollen and shortened, and some showed complete loss of the spines on the surface. In addition, there were numerous blebs around the trabeculae (Fig. 3B). Three days post-treatment, severe swelling was usually accompanied by vacuolization and disruption (Fig. 4A). Some areas of the swollen tegument coalesced and formed a mass with some cracks or superficial peeling. Numerous small blebs, protruding from the surface of the trabeculae, were also seen (Fig. 4B). Extensive peeling of the middle dorsal surface was observed (Fig. 4C). The alterations on the ventral surface were similar to those on the dorsal surface. In female worms, the most prominent

alteration was severe swelling and extensive peeling and erosion of the tegument (Fig. 4D).

4. Discussion

Praziquantel is active against all human schistosome species, can be easily administered, results in high cure and egg-reduction rates, with no or only mild and transient side-effects [3,10,11]. However, field studies in a *S. mansoni* focus in Senegal showed low cure rates after praziquantel treatment [29,30]. In mice, the possibility of selecting schistosomes insensitive to praziquantel has been shown after treatments with subcurative multiple doses of praziquantel [31]. These observations raised concern about praziquantel tolerance or resistance. Chinese scientists have discovered that derivatives of artemisinin, which are already widely and effectively used in the treatment of malaria [13,14], also display antischistosomal properties. Praziquantel and the artemisinins (i.e. artemether and artesunate) act against different developmental stages of the parasite.

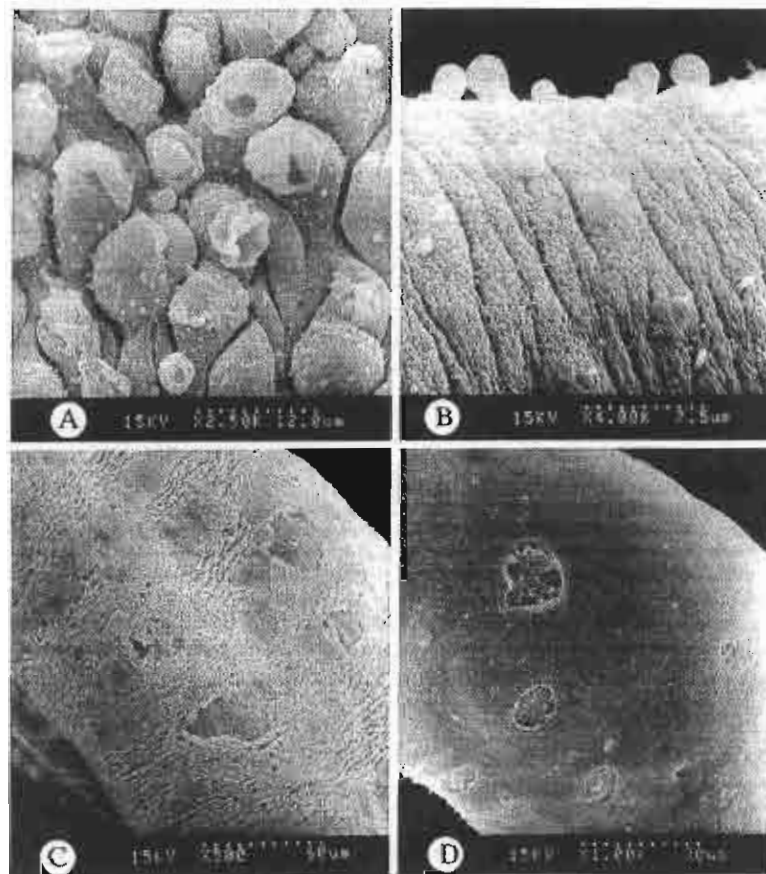


Fig. 4. Micrographs showing tegumental alterations in adult *S. mekongi* recovered from mice 3 days after intragastric administration of a single dose of 300 mg/kg artesunate. (A) Male, the trabeculae showing severe swelling, vacuolization and disruption ($\times 2500$). (B) Male, numerous small blebs protruding from the surface of the tegument ($\times 4000$). (C) Male, extensive peeling of the middle dorsal surface of tegument ($\times 500$). (D) Female, severe swelling and extensive peeling or erosion of the tegument ($\times 1000$).

Artemether has been shown to be active against the juvenile stages of schistosomes in experimentally infected animals, while it was less effective on adult worms [17,18,21,32], and the onset of the action of artemether on schistosomula of *S. japonicum* and *S. mansoni* was prompter than that of praziquantel [33]. However, in a recent study carried out in an area highly endemic for *S. mansoni* in Senegal, cure and egg count reduction rates obtained 5 weeks after the administration of artesunate were significantly lower than those obtained with praziquantel, but at 10 weeks there were no significant differences [34].

The tegument of schistosomes is an important target for antischistosomal drugs. The present study is the first to document tegumental alterations in *S. mekongi* induced by a derivative of artemisinin. The experimental focus was on adult *S. mekongi* harboured in mice, and tegumental alterations following the administration of a single dose of either praziquantel or artesunate were assessed by means of SEM. Both drugs induced damage to the oral sucker of male worms. Both sexes showed extensive tegumental alterations, with swelling, vacuolization or blebbing, fusion and peeling of the surfaces. Tegumental damage became apparent 1 day after administration of artesunate and usually increased in intensity 3 days post-treatment. These alterations in the tegument following treatment at the same dose and route of administration were similar to those previously obtained with adult *S. mansoni* treated with praziquantel [35] and with juvenile *S. haematobium* treated with artemether [36]. The observed morphological alterations could be a mechanism for the killing of the worms by these drugs. Such damage to the suckers must result in a loss of ability to adhere to blood vessels rendering ingestion of nutrients from the blood more difficult [37]. The damage to the tegument along the worm's body would have impaired the functioning of the tegument and also destroyed the defense system of the worm, so that it could easily be attacked by the host's immune system [37]. Some worms showed only slight damage or even normal tegument 3 days after praziquantel had been administered, suggesting that they could have recovered from the initial tegumental damage. We found no adherence of host leukocytes to the damaged tegumental surface in this study. This is in agreement with an earlier SEM study with juvenile *S. haematobium* [36], but in contrast to *S. mansoni* schistosomula, where adherence of host leukocytes on the damaged tegument was usually observed [37]. Xiao and co-workers suggested that the procedures of collecting parasites by repeated rinsing with Hank's balance salt solution before fixation for subsequent SEM examination might result in a loss of adhered leukocytes [36].

Although the mechanism of action of the artemisinins has not been clarified yet, recent in vitro studies with adult worms of *S. mansoni*, *S. japonicum* and *S. haematobium* indicated that artemether interacts with haemin to exert a toxic effect on the worms [38]. In view of these findings, it has been speculated that artemether might be activated

within schistosomes by heme or another iron compound, as it is in malaria parasites, to produce a toxic compound [39].

We conclude that artesunate is more active than praziquantel in causing damage to the tegument of adult *S. mekongi*. However, several questions remain to be answered, such as whether *S. mekongi* also shows the typical stage specific susceptibilities to artesunate or artemether as has been observed previously with *S. japonicum* and *S. mansoni*. A series of clinical trials in humans have been carried out defining the use of artemisinins for the prevention of schistosomiasis in different epidemiological settings. In view of artemisinins widely used in malaria endemic settings of Southeast Asia, including areas where *S. mekongi* remains endemic, some clinical trials in these areas might be feasible.

Acknowledgements

This study was funded by the Thailand Research Fund (TRF) and the Commission on Higher Education: the New Researchers Grant 2003.

References

- [1] Ross AGP, Bartley PB, Sleight AC, Olds GR, Li YS, Whitten GM, et al. N Engl J Med 2002;346:1212–20.
- [2] Chitsulo L, Engels D, Montresor A, Savioli L. The global status of schistosomiasis and its control. Acta Trop 2000;77:41–51.
- [3] World Health Organization. Prevention and control of schistosomiasis and soil-transmitted helminthiasis: report of a WHO expert committee. Geneva: World Health Organization; 2002. WHO Technical Report Series No. 912.
- [4] Urbani C, Sinoun M, Socheat D, Pholsena K, Strandgaard H, Odermatt P, et al. Epidemiology and control of mekongi schistosomiasis. Acta Trop 2002;82:157–68.
- [5] Ohmae H, Sinoun M, Kirinoki M, Matsumoto J, Chigusa Y, Socheat D, et al. Schistosomiasis mekongi: from discovery to control. Parasitol Int 2004;53:135–42.
- [6] Biays S, Stich AH, Odermatt P, Long C, Yersin C, Men C, et al. Foyer de bilharziose à *Schistosoma mekongi* redécouvert au Nord du Cambodge: I. Perception culturelle de la maladie; description et suivi de 20 cas cliniques graves. Trop Med Int Health 1999;4:662–73.
- [7] Stich AH, Biays S, Odermatt P, Men C, Saem C, Sokha K, et al. Foci of Schistosomiasis mekongi, Northern Cambodia: II. Distribution of infection and morbidity. Trop Med Int Health 1999;4:674–85.
- [8] Feldmeier H, Chitsulo L. Therapeutic and operational profiles of metrifonate and praziquantel in *Schistosoma haematobium* infection. Arzneimittelforschung 1999;49:557–65.
- [9] Machado PA. The Brazilian program for schistosomiasis control, 1975–1979. Am J Trop Med Hyg 1982;31:76–86.
- [10] Fenwick A, Savioli L, Engels D, Bergquist NR, Todd MH. Drugs for the control of parasitic diseases: current status and development in schistosomiasis. Trends Parasitol 2003;19:509–15.
- [11] Utzinger J, Keiser J. Schistosomiasis and soil-transmitted helminthiasis: common drugs for treatment and control. Expert Opin Pharmacother 2004;5:263–85.
- [12] Sangster NC. Managing parasiticide resistance. Vet Parasitol 2001;98:89–109.
- [13] Qinghaosu Antimalarial Coordinating Research Group (QACRG). Antimalarial studies on Qinghaosu. Chin Med J 1979;92:811–6.

- [14] Li Y, Wu YL. An over four millennium story behind qinghaosu (artemisinin) — a fantastic antimalarial drug from a traditional Chinese herb. *Curr Med Chem* 2003;10:2197–230.
- [15] Guerin PJ, Olliaro P, Nosten F, Druilhe P, Laxminarayan R, Binka F, et al. Malaria: current status of control, diagnosis, treatment, and a proposed agenda for research and development. *Lancet Infect Dis* 2002;2:564–73.
- [16] Myint HY, Tipmanee P, Nosten F, Day NP, Pukrittayakamee S, Loarcesuwan S, et al. A systematic overview of published antimalarial drug trials. *Trans R Soc Trop Med Hyg* 2004;98:73–81.
- [17] Xiao SH, You JQ, Yang YQ, Wang CZ. Experimental studies on early treatment of schistosomal infection with artemether. *Southeast Asian J Trop Med Public Health* 1995;26:306–18.
- [18] Li S, Wu L, Liu Z. Studies on prophylactic effect of artesunate on schistosomiasis japonica. *Chin Med J* 1996;109:848–53.
- [19] Xiao SH, Catto BA. In vitro and in vivo studies of the effect of artemether on *Schistosoma mansoni*. *Antimicrob Agents Chemother* 1989;33:1557–62.
- [20] Xiao SH, Chollet J, Weiss NA, Bergquist RN, Tanner M. Preventive effect of artemether in experimental animals infected with *Schistosoma mansoni*. *Parasitol Int* 2000;49:19–24.
- [21] Xiao SH, Utzinger J, Chollet J, Enslin Y, N'Goran EK, Tanner M. Effect of artemether against *Schistosoma haematobium* in experimentally infected hamsters. *Int J Parasitol* 2000;30:1001–6.
- [22] Utzinger J, Xiao SH, N'Goran EK, Bergquist R, Tanner M. The potential of artemether for the control of schistosomiasis. *Int J Parasitol* 2001;31:1549–62.
- [23] Xiao SH, Tanner M, N'Goran EK, Utzinger J, Chollet J, Bergquist R, et al. Recent investigations of artemether, a novel agent for the prevention of schistosomiasis japonica, mansoni and haematobia. *Acta Trop* 2002;82:175–81.
- [24] Sommani S, Kitikoon V, Schneider CR, Harinasuta C, Pathammawong O. Mekong schistosomiasis: I. Life cycle of *Schistosoma japonicum*, Mekong strain in the laboratory. *Southeast Asian J Trop Med Public Health* 1973;4:218–25.
- [25] Gretchen LH. Animal tissue techniques. 3rd ed. San Francisco: W.H. Freeman and Company; 1972.
- [26] Sobhon P, Upatham ES. Snail hosts, life-cycle, and tegumental structure of oriental schistosomes. Geneva, Switzerland: UNDP/World Bank/WHO Special Programme for Research and Training in Tropical Diseases (TDR); 1990.
- [27] Sobhon P, Upatham ES, McLaren D. Topography and ultra-structure of the tegument of adult *Schistosoma mekongi*. *Parasitology* 1984;89: 511–21.
- [28] Vongpayabal P, Sobhon P, Upatham ES, Wanichanon C, Mitrakond V, Tanphaichitr N, et al. Scanning electron microscopic study of the tegumental surface of adult *Schistosoma mekongi*. *Parasitology* 1982;85:325–32.
- [29] Stelma FF, Talla I, Sow S, Kongs A, Niang M, Polman K, et al. Efficacy and side effects of praziquantel in an epidemic focus of *Schistosoma mansoni*. *Am J Trop Med Hyg* 1995;53:167–70.
- [30] Guisse F, Polman K, Stelma FF, Mbaye A, Talla I, Niang M, et al. Therapeutic evaluation of two different dose regimens of praziquantel in a recent *Schistosoma mansoni* focus in northern Senegal. *Am J Trop Med Hyg* 1997;56:511–4.
- [31] Fallon PG, Doenhoff MJ. Drug-resistant schistosomiasis: resistance to praziquantel and oxamniquine induced in *Schistosoma mansoni* in mice is drug specific. *Am J Trop Med Hyg* 1994;51:83–8.
- [32] Sabah AA, Fletcher C, Webbe G, Doenhoff MJ. *Schistosoma mansoni*: chemotherapy of infections of different ages. *Exp Parasitol* 1986;61:294–303.
- [33] Utzinger J, Chollet J, You JQ, Mei JY, Tanner M, Xiao SH. Effect of combined treatment with praziquantel and artemether on *Schistosoma japonicum* and *Schistosoma mansoni* in experimentally infected animals. *Acta Trop* 2001;80:9–18.
- [34] De Clercq D, Vermeysse J, Verle P, Niasse F, Kongs A, Diop M. Efficacy of artesunate against *Schistosoma mansoni* infections in Richard Toll, Senegal. *Trans R Soc Trop Med Hyg* 2000;94:90–1.
- [35] Xiao SH, Shen BG, Chollet J, Tanner M. Tegumental changes in adult *Schistosoma mansoni* harboured in mice treated with praziquantel enantiomers. *Acta Trop* 2000;76:107–17.
- [36] Xiao SH, Shen BG, Chollet J, Utzinger J, Tanner M. Tegumental alterations in juvenile *Schistosoma haematobium* harboured in hamsters following artemether treatment. *Parasitol Int* 2001;50: 175–83.
- [37] Xiao SH, Shen BG, Chollet J, Tanner M. Tegumental changes in 21-day-old *Schistosoma mansoni* harboured in mice treated with artemether. *Acta Trop* 2000;75:341–8.
- [38] Xiao SH, Chollet J, Utzinger J, Matile H, Mei JY, Tanner M. Artemether administered together with haemin damages schistosomes in vitro. *Trans R Soc Trop Med Hyg* 2001;95:67–71.
- [39] Meshnick SR, Taylor TB, Kamchonwongpaisan S. Artemisinin and the antimalarial endoperoxides: from herbal remedy to targeted chemotherapy. *Microbiol Rev* 1996;60:301–15.

Title: Development and roles of vitelline cells in the eggshell formation
in *Fasciola gigantica*

Authors: Ardool Meepool^{1,2}, Chaitip Wanichanon², Vitoon Viyanant³
and Prasert Sobhon²

Affiliations: Department of Medical Science¹, Faculty of Science,
Burapha University, Chonburi, Thailand
Departments of Anatomy², Faculty of Science, Mahidol
University, Bangkok, Thailand
Faculty of Allied Health Sciences³, Thammasat University,
Khong Luang, Prathum Thani, Thailand

Corresponding author:

Name: Prof. Dr. Prasert Sobhon,

Affiliations: Departments of Anatomy, Faculty of Science,
Mahidol University, Bangkok, Thailand, 10600

Telephone No.: 02-201-5406

Fax No.: 02-354-7168

Email address: pcpso@mahidol.ac.th

Development and roles of vitelline cells in the eggshell formation in *Fasciola gigantica*

SUMMARY

In *Fasciola gigantica*, vitelline cells are the major contributors to the formation of the egg's shell. These cells develop in vitelline follicles that are located in the posterior one-third of the adult parasite's body, and the areas lateral to the uterus and the testis. Mature vitelline cells are released and transported to the Mehlis' gland-ootype complex via a series of vitelline ducts. Based on ultrastructural features the developing vitelline cells are classified into stem cell, developing and mature vitelline cells. The developing vitelline cells are divided into 4 steps: non synthetic, protein synthetic, glycogen synthetic and glycan vesicle synthetic steps. The mature vitelline cells are detached from the nurse cells, and pass successively into interfollicular lumen, longitudinal and transverse vitelline ducts, to be stored in the vitelline reservoir before being transported to the ootype via the median vitelline duct. The ova are transported from the ovary through the oviduct into the ootype, and finally into the proximal part of the uterus where fertilization occurs and the eggshell is being formed. Each fertilized ovum is surrounded by a number of vitelline cells that secrete eggshell globules, that upon being activated by Mehlis' gland secretions, start to coalesce into the definitive eggshell. The glycan vesicles remain with other broken down product of vitelline cells as the nascent substance, possibly as the nutritive substance, around the ovum.

Key words: *Fasciola gigantica*, vitelline cell, eggshell formation, reproductive system, ultrastructure

INTRODUCTION

In parasitic trematodes the egg formation takes place in the Mehlis' gland-ootype complex, where the oviduct and vitelline duct join together to form the ootype. An egg is composed of a zygote cell surrounding by a numbers of vitelline cells covered by the eggshell. The vitelline cells play three important roles in reproduction: first they produce and secrete proteins to form the eggshell surrounding the zygote and vitelline cells themselves, thus forming the mature egg (Rao, 1958; Irwin and Threadgold, 1972; Awad and Probert, 1990). Second, they supply nutrients to the zygote during its development to miracidium (Irwin and Threadglod, 1970). And third released products from vitelline cells generate hydrostatic pressure to rupture the eggshell at the time of miracidium hatching (Schmidt, 1998). Up to now, the histology, ultrastructure and development of vitelline cells, and the mechanism of eggshell formation have been studied only in *F. hepatica* and some schistosome species (Irwin and Threadglod, 1970; Erasmias, 1973; Threadgold, 1982; Awad and Probert, 1990), while that of *F. gigantica* has not yet been investigated. In the present study we reported on the detailed ultrastructure of the differentiating vitelline cells and the corresponding process of eggshell formation in *F. gigantica*. The basic knowledge obtained from this study will provide the detailed structure in which the eggshell molecules could be identified and localized, thus aiding the identification of fasciola's egg. At present, the currently used method for identifying fasciolosis is by examining the structure and counting the number of eggs by sedimentation-techniques (Conceicao et al, 2002, Gonzalez-Lanza et al., 1989, Happich and Boray, 1969). Judging the unique characteristics of the fasciola's egg through a microscope require experience, whereas if monoclonal antibody could be developed against one of these

eggshell molecules it could be used to specifically immuno-stain the eggs, and thus facilitate identification process even by the less experienced examiner.

MATERIALS AND METHODS

Live adult parasites were recovered from bile ducts and gall bladders of cattle and water buffaloes killed at the abattoirs. Subsequently, they were washed in normal saline several times. The parasites were then separated into two groups: the first was fixed with 10% formaldehyde and stained with nitrate-nitrite technique for DOPA residue according to the technique described by Waite and Benedict (1984). Briefly, the fixed parasites were incubated in 0.5 M HCl for 30 min and transferred to nitrite reagent (1.45 M sodium nitrite and 0.41 M sodium molybdate) for 10 min, and finally the color was developed by incubating in 1M NaOH for 10min. Then the stained parasites were dehydrated, clear, mounted onto microscopic slides and photographed. The second group was fixed in Kanovsky's fixative (2% glutaraldehyde, 4% paraformaldehyde in 0.1M cacodylate buffer, pH7.4), at 4°C, overnight. Fixed specimens were washed and stored in 0.1 cacodylate buffer until processed further. The remaining specimens were cut into small pieces, post-fixed in 1% osmium tetroxide in 0.1M cacodylate buffer and 0.5% aqueous uranyl acetate containing 45 mg/ml sucrose, for 1 h each. After washing, they were dehydrated in graded series of ethanol, infiltrated with propylene oxide twice and transferred into the mixtures of propylene oxide and Aradite 502 resin at the ratios of 2:1 and 1:2, for 1 h and overnight, respectively. After that, the specimens were embedded in Aradite 502 resin and polymerized at room temperature for 1 day and at 45 °C and 60 °C for 2 days each. The embedded specimens were sectioned into 500-700 nm semithin and 60-90 nm thin sections. The formers were stained with methylene blue and PAS as followed: semithin sections were incubated in 1% periodic acid for 10 min at 37 °C,

followed by Schiff reagent for 10 min at 37 °C, and then counterstained with methylene blue for 1 min at 37 °C. The stained sections were observed and photographed under a light microscope, (Nikon E 600 equipped with DXM1200 digital camera). The ultrathin sections were double-stained with uranyl acetate and lead citrate, and observed under a Hitachi 300 transmission electron microscope, at 75kV.

RESULT

Vitelline Gland

Vitelline gland is the largest organ of adult *F. gigantica*. The extent and content of the gland are readily demonstrated by DOPA staining which is the major constituent of the eggshell proteins (Fig 1A). The gland is composed of numerous vitelline follicles, distributed lateral to the uterus and at the location posterior to the testis. Mature vitelline cells develop in the vitelline follicles and are transported along interfollicular, longitudinal and transverse vitelline ducts to be stored in the vitelline reservoir beneath the Mehlis' gland-ootype complex, the site of the egg formation (Fig 1A). Each of the two longitudinal vitelline ducts is composed of two parts: the anterior and the posterior longitudinal vitelline ducts. The former collects vitelline cells from vitelline follicles located lateral to the uterus, while the latter collects cells from the areas lateral and posterior to the testis. The left and right transverse vitelline ducts, located between the testis and the uterus, are the confluence of the anterior and posterior longitudinal vitelline ducts of each side, and they run towards the central part of the parasite's body to enter the vitelline reservoir at the midline (Fig 1A). After that, the median vitelline duct extends from the anterior border of the vitelline reservoir into the central part of the Mehlis' gland to join up with the oviduct which becomes the ootype. Before joining with the median vitelline duct, the oviduct merges

with the Laurer's canal, which is a small duct running from the dorsal surface of the parasite's body towards the Mehlis' gland-ootype complex.

Development and differentiation of the vitelline cells

Each vitelline follicle is filled with stem cells, 4 stages of developing and mature vitelline cells, and nurse cells (Fig 1B-D). The wall of each vitelline follicle is lined by nurse cells that send their processes to surround the developing vitelline cells. The basal surface of these cells is attached to the basement membrane where cytoplasmic processes of parenchymal cells come into contact with the follicle to supply nutrients and transport away waste products (Fig 2A; 4A, B).

Stem cell

The stem cells are located close to the wall of the follicle, and they are small cells, about 4-6 μm in diameter, with small amount of cytoplasm containing polysomes and few mitochondria (Fig. 2A). They tend to show mitotic division since they are actively dividing and will transform into the next stage.

Developing vitelline cells

Step 1 (ER-Golgi proliferation)

This cell stage is about 6-8 μm in diameter and distinguished by the increasing amount of cytoplasmic organelles. Their cytoplasm contains more organelles than the stem cells particularly mitochondria and rough endoplasmic reticulum (Fig. 2B), however, there is still no secretory granules. This cell loses contact with the basement membrane and start to move towards the center of the follicle (Fig 1B).

Step 2 (eggshell granules formation)

This stage is distinguished by the presence of the electron dense eggshell granules in their cytoplasm, and the increasing amount of rough endoplasmic

reticulum and Golgi complexes. The eggshell granules initially appear as single round dense granules in the early stage, then they coalesce together to become the eggshell globules in the later stage (Fig. 1B-D; 2C, D). Each eggshell globule is firstly formed as a small globule in which several nearby eggshell granules are packed together by fusion of their membrane, while the granules content remain separated from each other. As the result the tightly aggregated granules become surrounded within the same membrane compartment (Fig 2D). Then other granules synthesized later are added to this small eggshell globule resulting in its growth to the larger size and eventually becoming the mature globules. In the late stage, almost all of the eggshell granules are fused to form numerous eggshell globules, which occupy the entire cytoplasm.

Step 3 (glycogen synthesis and storage)

This step is characterized by the presence of glycogen particles in the central part of the cytoplasm. Initially the storage sites of glycogen are the lightly PAS-stained areas distributed randomly within the central part of the cytoplasm (Fig. 1D). When observed under the transmission electron microscope, these areas are filled with numerous small glycogen particles (Fig. 3A, B). Later, these glycogen storage areas increase in size and merge together to become the larger and more intense PAS-stained areas, which finally become a continuous zone completely surrounding the nucleus, and represent the major proportion of the cytoplasm. Concurrently, the increased glycogen deposit pushes all the eggshell globules towards the cells' periphery, and finally most come to be located underneath the cell membrane (Fig 3A, B). In late stage, there is only a thin rim of cytoplasm containing RER appearing around the nucleus, while the eggshell globules are located close to the cell membrane (Fig 2B-D; 3A, C).

Step 4 (glycan vesicle synthesis)

This step is defined when the glycan vesicles start to be formed from the cytoplasm surrounding the nucleus. The glycan vesicles appear as numerous small membrane-bound vesicles (Fig. 3C). As they become mature, these vesicles increase in size and are translocated into the glycogen storage area, and finally are disconnected from the cytoplasm surrounding the nucleus to become mature vesicles that are free floating in the glycogen storage area (Fig 3D). Under the light microscope, these vesicles are PAS positive, and their staining intensity increases as they mature like the glycogen storage area, but the mature vesicles appear to have greater intensity (Fig. 1D). Under the TEM, these vesicles are filled with numerous small dense particles similar to the glycogen particles stored in the cytoplasm, but these particles are more closely packed together (Fig 3C inset, 3D inset).

The mature vitelline cells

This cell is characterized by the intensely PAS-stained cytoplasm when observed under LM (Fig 1D), and under TEM, contains lightly electron-stained cytoplasm filled with glycogen, glycan vesicles, and eggshell globules. They are completely detached from the processes of the nurse cells and are released into the center of the follicle (Fig 1D). The mature cells are transported consecutively via the interfollicular, longitudinal, and transverse vitelline ducts to be stored in the vitelline reservoir located close to the posterior part of the Mehlis' gland.

The nurse cells

The nurse cells are the epithelial cells lining the wall of the vitelline follicles. Their basal membrane attaches to the basal lamina which makes contact with the cytoplasmic processes of parenchyma cells to exchange the nutrients and waste

products (Fig 2A; 4A, B). These cells have numerous long cytoplasmic processes projecting out to embrace the developing vitelline cells (Fig 2A-D)

Vitelline Duct

The vitelline ducts are lined with a thin layer of epithelial cells attached to the well defined basal lamina. The apical surface has long stereocilia or cytoplasmic lamellae projecting into the lumen which is filled with mature vitelline cells (Fig 4C, D). The epithelium is surrounded by a thin layer of muscle cells and parenchymal cells (Fig 4C, D)

The eggshell Formation

Mature vitelline cells and ova are transported via the median vitelline duct and oviduct which are converged to form the ootype that continues into the proximal part of the uterus, where the eggs are formed. The egg formation starts when the vitelline cells are transported pass the ootype where the cytoplasmic processes of the Mehlis' gland cells open and release their granules into the ootype lumen (Fig 5A, B). By as yet unknown mechanism, vitelline cells release their eggshell globules after they pass into the proximal part of the uterus. Then, these released eggshell globules fuse together to form the immature eggshell around an ovum surrounded by about 30 mature vitelline cells (Fig 5C, D; 6A). The immature egg with thin and incompletely fused eggshell is transported into the middle part of the uterus where numerous spermatozoa are stored (Fig 5E). These spermatozoa pass into the egg interior through the holes in the immature eggshell to fertilize with the ovum. Subsequently, the remaining eggshell globules are released from vitelline cells inside the immature eggshell. These granules move outwards to the periphery where they fuse with the internal surface of the eggshell, resulting in the filling of the holes, the thickening, and finally the complete formation of the eggshell around the fertilized ovum (Fig 5F; 6B-D). The glycan vesicles and glycogen particles are broken down and their released

materials nourish the developing embryo, which turn into miracidium when the egg is released from the mature parasites.

DISCUSSION

In *Fasciola gigantica*, vitelline cells differentiate in a continuous process within the vitelline follicles. They are classified into two major phases: growth and synthesis phases. The growth phase consists of the stem cell and step 1 cell when the cells rapidly increase in size and the number of the cytoplasmic organelles, notably rough endoplasmic reticulum and Golgi complexes. The synthesis phase is subdivided into protein synthesis (step 2) and glycogen synthesis phase (step 3 and 4). Protein synthesis phase is signified by the presence of the eggshell granules (containing eggshell proteins) which later coalesce to form globules. The glycogenesis is defined when glycogen particles (step 3) and glycan vesicles (step 4) are formed. In *F. hepatica*, the growing stage also include stem cells and immature stage while the synthesis phase is divided into the intermediate type I and II and mature cell (Irwin and Threadgold, 1970; Threadgold, 1982). Besides protein and glycogen synthesis, lipid synthesis is also found in the synthesis phase of the vitelline cells of *S. japonicum* and *S. mattheei* (Erasmus et al., 1982) but not in *Fasciola* spp.

In *F. hepatica*, the eggshell globules are synthesized in the RER and packed as small granules via the Golgi complexes before they become fused together. The fusion of these granules occurs only between the covering membranes, since individual granules are still separated from each other. This could be because the granules' content is composed mainly of the positively charged egg shell precursor proteins in the acidic environment (Colhoun et al., 1998). In addition to the eggshell proteins, phenol oxidase, the key enzyme in the tanning process of the eggshell, is

synthesized as the proenzyme in the vitelline cells and stored together with the eggshell precursor protein in the eggshell globules (Threadgold, 1982). Moreover, the same globule may contain a proteolytic enzyme that activates the prophenol oxidase and triggers the tanning process (Wells and Cordingley, 1991). It is believed that, the acidic pH within the globule clusters inhibits most of the reactions in the compartment, so the cross-linking reactions do not occur. When these globules are released into the ootype lumen where the pH is higher than in the globules, the prophenol oxidase enzyme is converted to the active form that starts the cross linking or tanning process (Wells and Cordingley, 1991).

The eggshell precursor proteins have been studied in some parasites but the most extensively studied is that of *F. hepatica*. These proteins could be studied by using acid urea extraction and separation by acid urea gel electrophoresis stained with nitrite molybdate, which is the specific staining for DOPA containing protein (Waite and Rice-Ficht, 1987). Such studies show three distinct bands designated as vitelline protein A, B and C (Waite and Rice-Ficht, 1987). Vitelline protein B is the most abundant and best investigated protein which represents about 6-7% of total protein of the adult fluke. Two mRNA sequences of these proteins have been identified and localized within the developing and maturing vitelline cells and the genes have been designated as vitelline B1 and B2 (Rice-Ficht, et al 1992). Both mRNA sequences encode for 272 amino acids (MW 31 kD) and containing high content of glycine, tyrosine, aspartate, histidine and lysine. The tyrosine residues are converted to 3, 4-dihydroxyphenyl-L-alanine (DOPA) residues during co- or post-translational processing by the enzyme tyrosyl 3-hydroxylase. The native protein contains 10 DOPA residues for 100 amino acids (Waite and Rice-Ficht, 1987). On the other hand vitelline C has a molecular weight ranging from 16,000 to 18,500 kD with the most

abundant at 17,500 kD. Compared to protein B, this group of protein is different in having very high histidine, low aspartate and tyrosine, and no lysine. The amount of glycine, histidine and DOPA is over 80% of the total amino acids, whereas in protein B these residues account for only 32% (Waite and Rice-ficht, 1989). The vitelline protein A has MW 70 kD while other details have not yet been obtained. In contrast, no study along this line has been done in *F. gigantica*.

At present our group is trying to develop a monoclonal antibody (MoAb) against one of these eggshell proteins and the most likely to be obtained is MoAb against vitelline B because of its abundance. It is hoped that such MoAb could be used to specifically immuno-stain the eggs in the feces of infected animals and thus help to facilitate the identification of fasciolosis by *F. gigantica*. Furthermore, the detailed knowledge on the fine structure of eggshell and its formation, as well as distribution of vitelline proteins, will serve as the normal base line for studying the effects of any future candidate vaccines that are designed to disrupt the eggshell protein synthesis and the eggshell's formation. In fact one such vaccine, employing the combination of cathepsin L and hemoprotein, has been shown to suppress the production of eggs as well as lower their viability (Dalton et al, 1996). Even though such a vaccine may not be able to completely cure the infected animals, it certainly could lessen the infection incidences by reducing the dissemination of fasciola eggs from the infected animals in the field and water reservoirs.

In *F. gigantica*, glycogenesis occurs in the late synthetic phase, ie, the glycogen and glycan vesicle synthesis steps. These two types of glycogen storage are similar to that observed in the cestode, *Caryophyllidea* (Swiderski and Xylander, 2000) and in *F. hepatica* (Irwin and Threadgold, 1970). The first or alpha type glycogen particles are distributed throughout the electronlucent area of cytoplasm,

while the beta type are stored in the membrane-bound vesicles wrongly called “yolk” globules, which is believed to be the key storage sites of nutrient supply for the larval development (Irwin and Threadgold, 1970). Recently, it was suggested that these yolk globules do not play role in supplying glucose to the developing miracidium so they were renamed glycan vesicles (Schmidt, 1998). These glycan vesicles persist with their membrane intact until the miracidium hatches from the eggshell. It is believed that the break down of glycan vesicle membrane release the content that increases the osmotic pressure that draws water from the outside into the inside of the egg, resulting in the increasing of hydrostatic pressure that helps to push the operculum open (Schmidt, 1998).

By as yet unknown mechanism, when the vitelline cells passes into the ootype lumen, the Mehlis’ gland cells are triggered to release their secretions into the ootype lumen which percolate to vitelline cells inside the ovum complex. It is believed that the Mehlis’ gland secretions activate the vitelline cells to exocytose the eggshell globules via the calcium dependent process (Skuce and Fairweather, 1988; Wells and Cordingley, 1991; Colhoun et al., 1998). In the ootype lumen, the phenol oxidase enzyme, which is co-packaged in the eggshell globules, changes the tyrosine residue in the eggshell proteins to DOPA and o-quinone, which are then cross-linked with the lysine residues which are present on the other chains of the eggshell precursor proteins. This finally results in the formation of the hard eggshell (Seed et al., 1978). It is notable that in *F. gigantica*, the new material from the vitelline globules is added onto the inner surface of the maturing eggshell.

ACKNOWLEDGEMENT

This investigation was supported by the Thailand Research Fund (Senior Research Scholar Fellowship to P. Sobhon)

REFERENCES

- Awad AHH, Probert AJ. Scanning and transmission electron microscopy of the female reproductive system of *Schistosoma margrebowiei*. J Helminth 1990; 64: 181-192.
- Colhoun LM, Fairweather I, Brennan GP. Observations on the mechanism of eggshell formation in the liver fluke, *Fasciola hepatica*. Parasitology 1998; 116: 555-567.
- Conceicao MA, Durao RM, Costa IH, da Costa JM. Evaluation of a simple sedimentation method (modified McMaster) for diagnosis of bovine fascioliosis. Vet Parasitol. 2002;105: 337-43.
- Dalton JP, McGonigle S, Rolph, TP. Andrews SJ. Induction of protective immunity in cattle against infection with *Fasciola hepatica* by vaccination with cathepsin L proteinases and with hemoglobin. Infect Immun. 1996, 64: 5066-74.
- Erasmus DA. A comparative study of the reproductive system of mature, immature and "unisexual" female *Schistosoma mansoni*. Parasitology 1973; 67: 165-83.
- Erasmus DA, Popiel I, Shaw JR. A comparative study of the vitelline cell in *Schistosoma mansoni*, *S. heamatobium*, *S. japonicum* and *S. matteei*. Parasitology 1982; 84: 286-287.
- Gonzalez-Lanza C, Manga-Gonzalez Y, Del-Pozo-Carnero P, Hidalgo-Arguello R.. Dynamics of elimination of the eggs of *Fasciola hepatica* (trematoda, digenea) in the faeces of cattle in the Porma Basin, Spain. Vet. Parasitol. 1989, 34: 35-43.
- Happich FA, Boray JC. Quantitative diagnosis of chronic fasciolosis. I. Comparative studies on quantitative faecal examinations for chronic *Fasciola hepatica* in sheep. Aust. Vet. J. 1969. 45: 326-328.

- Irwin SWB, Threadgold LT. Electron microscope studies on *Fasciola hepatica* VIII: The development of the vitelline cells. *Exp Parasitol* 1970; 28: 399-411.
- Irwin SWB, Threadgold LT. Electron microscope studies on *Fasciola hepatica* X: Egg formation. *Exp Parasitol* 1972; 31: 321-331.
- Rao KH. Observation of the Mehlis' gland complex in the liver fluke *Fasciola hepatica*. *J Parasitol* 1958; 45: 347-351.
- Rice-Ficht AC, Dusek KA, Kochevar GJ, Waite JH. Eggshell precursor proteins of *Fasciola hepatica*, I. Structure and expression of vitelline protein B. *Mol Biochem Parasitol* 1992; 54: 129-141.
- Schmidt J. Glycan vesicle formation in vitellocytes and hatching vacuoles in eggs of *Echinostoma caproni* and *Fasciola hepatica* (Digenea). *Tissue Cell* 1998; 30: 416-426.
- Seed JL, Michael B, Bennett JL. Phenol oxidase activity: Induction in female *Shistosomes* by *in vitro* incubation. *J Parasitol* 1978; 64:283-289.
- Skuce PJ, Fairweather I. *Fasciola hepatica*: perturbation of secretory activity in the vitelline cells by the sodium ionophore monensin. *Exp Parasitol* 1988; 65: 20-30.
- Swiderski Z, Xylander WE. Vitellocytes and vitellogenesis in cestodes in relation to embryonic development, egg production and life cycle. *Int J Parasitol* 2000; 30: 805-817.
- Threadgold LT. *Fasciola hepatica*: Stereological analysis of vitelline cell development. *Exp Parasitol* 1982; 54: 352-365.
- Waite JH, Benedict CV. Assay of dihydroxyphenylalanine (DOPA) in invertebrate structural proteins. *Methods in Enzymology* 1984; 107: 397-413

Wait HJ, Rice-Ficht AC. Presclerotized eggshell protein from the liver fluke *Fasciola hepatica*. Biochem 1987; 26: 7819-7825.

Wait HJ, Rice-Ficht AC. A histidine-rich protein from the vitellaria of the liver fluke *Fasciola hepatica*. Biochem 1989; 28: 6104-6110.

Wells KE, Cordingley JS. *Schistosoma mansoni*: eggshell formation is regulated by pH and calcium. Exp Parasitol 1991; 73: 295-310.

Figure 1

- A) A micrograph of the DOPA stained of the cephalic part of a whole-mounted adult parasite showing relationship of the vitelline gland (Vg), anterior (aLd) and posterior (pLd) longitudinal and transverse vitelline duct (Td), vitelline reservoir (Vr), ootype (Ot), uterus (Ut), Testis (Te) and ventral (Vs), oral (Os) suckers
- B-D) Light micrographs of semithin sections of vitelline follicles stained with methylene blue (B, C) and PAS and methylene blue (D), showing the stem cell (St), step 1, 2, 3 and 4 of developing vitelline cells, and mature vitelline cell (M); Eg - eggshell granules, Gv - glycan vesicles, Va – vacuole like structures, Pc – parenchymal cells, Bl – bladder, Mu - muscle

Figure 2

- A) A TEM micrograph of stem cell showing small heterochromatin blocks (Hc) distributed throughout the nucleus, and cytoplasm containing mitochondria (Mi) and abundant ribosomes. The nurse cell (Nc) lines the wall of the follicle, where it contact with the parenchyma cells (Pc), and sends its cytoplasmic process (Np) to surround the outer surface of the developing vitelline cells. 1, 3 - developing vitelline cells step 1 and 3.
- B) A TEM micrograph of developing vitelline cell step 1 which is a larger cell whose nucleus (Nu) contains small amount of heterochromatin (Hc), while the cytoplasm contains more mitochondria (Mi) and rough endoplasmic reticulum (RER).
- C, D) Low (C) and high (D) magnification TEM micrographs of developing vitelline cell step 2 showing eggshell granules (Gr) and eggshell globules (Eg) in the central part of cytoplasm. RER – rough endoplasmic reticulum, Nu –nucleus, Np - nurse cell process

Figure 3

- A, B) Low (A) and high (B) magnification TEM micrographs of developing vitelline cell step 3, showing numerous glycogen particles (Gy) in the lightly stained area of the cytoplasm in the central part of cytoplasm. RER and eggshell globules (Eg) are dislocated to the cell periphery. Nu – nucleus, Np – nurse cell process.
- C) A TEM micrograph of developing vitelline cell at the beginning of step 4 showing small glycan vesicles (Gv) at the perinuclear region. Inset shows high magnification of the newly formed (arrow) and small glycan vesicles containing electron dense particles similar to glycogen particles. Eg - eggshell globule, Nu - nucleus
- D) The TEM micrograph of developing vitelline cell at the late step 4 showing large glycan vesicles (Gv) detached from the nuclear islet, and some vesicles floating freely in the lightly stained area of the cytoplasm. Inset shows high magnification of the glycan vesicle containing electron dense particles similar to the glycogen particles. Eg - eggshell globule, Nu - nucleus, Bl = bladder

Figure 4

A, B) Low (A) and high (B) magnification TEM micrographs of the wall of the vitelline follicle showing the nurse cell and its cytoplasmic process (Np) surrounding the developing vitelline cell step 3 (3). Nu – nucleus, Eg – eggshell globule, Pc – parenchymal cells

C, D) TEM micrographs of the vitelline duct showing simple epithelial cell (Ep) with long stereocilia (Sc). This epithelium is surrounded by an incomplete layer of thin muscle (Mu) and parenchymal cells (Pc). Vc - mature vitelline cell, Bm = basement membrane, Mu – muscle, Bl - bladder

Figure 5

Light micrographs of semithin sections of the ootype (A, B) and the proximal part of the uterus (C-F) stained with methylene blue

- A) The ootype epithelium (Ep) is penetrated by cytoplasmic processes of Mehlis' gland cell (arrows), and the ootype lumen contains vitelline cells (Vc) with intact eggshell granules (Eg). Mu = muscle
- B) The ootype epithelium (Ep) penetrated by cytoplasmic processes of Mehlis' gland cell (arrows), and the ootype lumen contains vitelline cells (Vc) with intact (Eg) and the released eggshell granules (Eg'). Mu = muscle
- C) Vitelline cells (Vc) and eggshell granule (Eg') are shown in the uterine lumen. Ep – uterine epithelium, Mu – muscle, Gv – glycan vesicle, Nu – nucleus of vitelline cell
- D) The immature eggshell (Sh) is formed by the coalescence of the eggshell granules (Eg') supposedly released from several eggshell granule-free vitelline cells (Vc) surrounding the ovum (Om). Ep – uterine epithelium, Mu – muscle, Gv – glycan vesicle, Nu – nucleus of vitelline cell
- E) A micrograph of the uterus outside the Mehlis' gland area, showing an immature egg containing vitelline cells (Vc) and some released eggshell granules (Eg'). The immature eggshell (Sh) still has several holes (arrow) that are the site where the sperm (Sz), stored in the uterine lumen, can gain access into the egg for fertilization. Op – operculum
- F) The mature egg showing thick and completely continuous eggshell (Sh) surrounding the degenerating vitelline cells (Dv) around the zygote (Zy). Op – operculum

Figure 6

TEM micrographs of the proximal part of the uterus

- A) Few loosely aggregated eggshell granules (Eg) are seen in the periphery of the vitelline cell (Vc). These eggshell granules are probably released by the nearby vitelline cell (Vc) and become distributed in uterine lumen outside the vitelline cell. Ep = uterine epithelium, Mu = muscle
- B) An immature eggshell (Sh) surround the vitelline cells (Vc) that are releasing a large number of the eggshell granules (Eg), some of which are coalesced with the inner facet of the eggshell (Sh). Ep = uterine epithelium, Mu = muscle
- C, D) Numerous eggshell granules (Eg) are incorporated into the internal surface of the immature eggshell (Sh - arrows) while the vitelline cell (Vc) is breaking down. Gv = glycogen vesicle, RER = rough endoplasmic reticulum

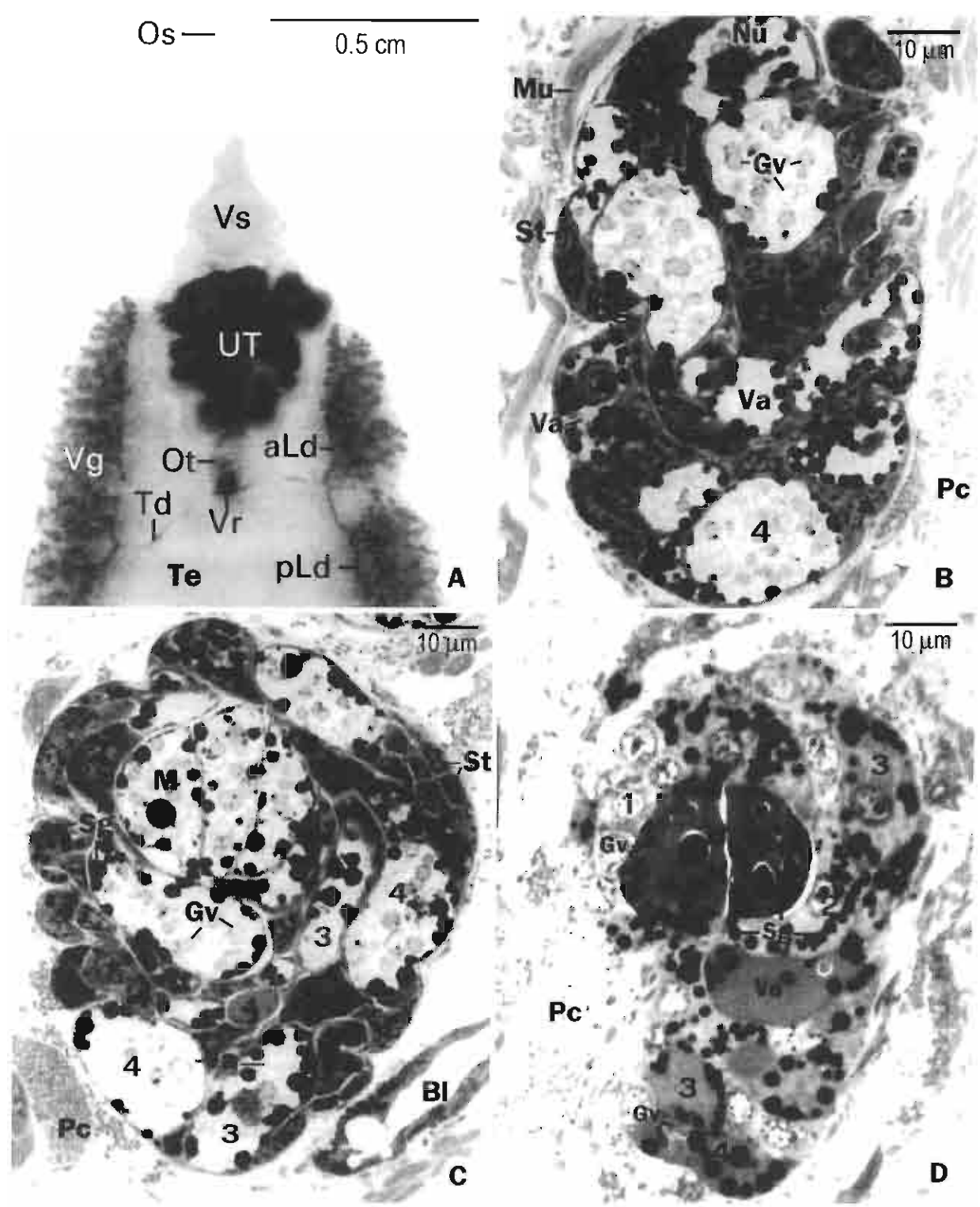


Figure 1

Title: Development and roles of vitelline cells in the eggshell formation in *Fasciola gigantica*

Authors: Ardool Meepool, Chaitip Wanichanon, Vitoon Viyanant and Prasert Sobhon



Os ————— 0.5 cm

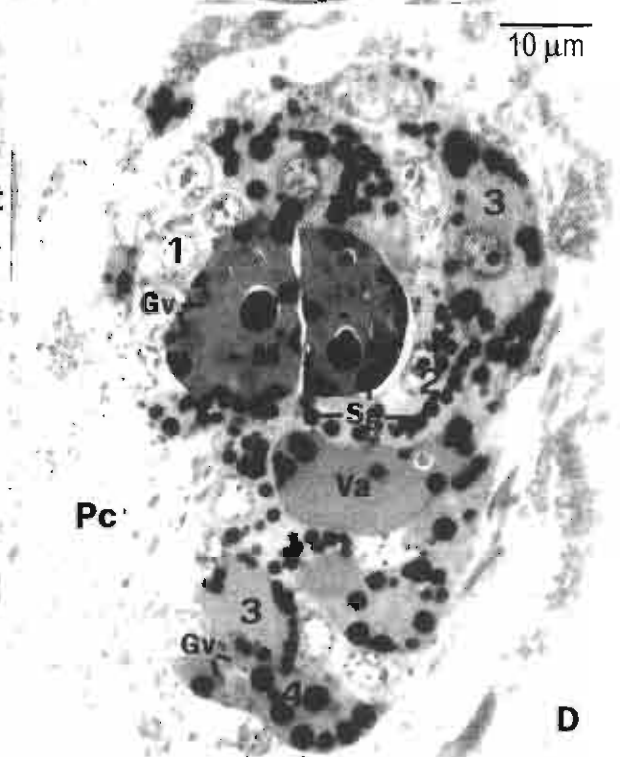
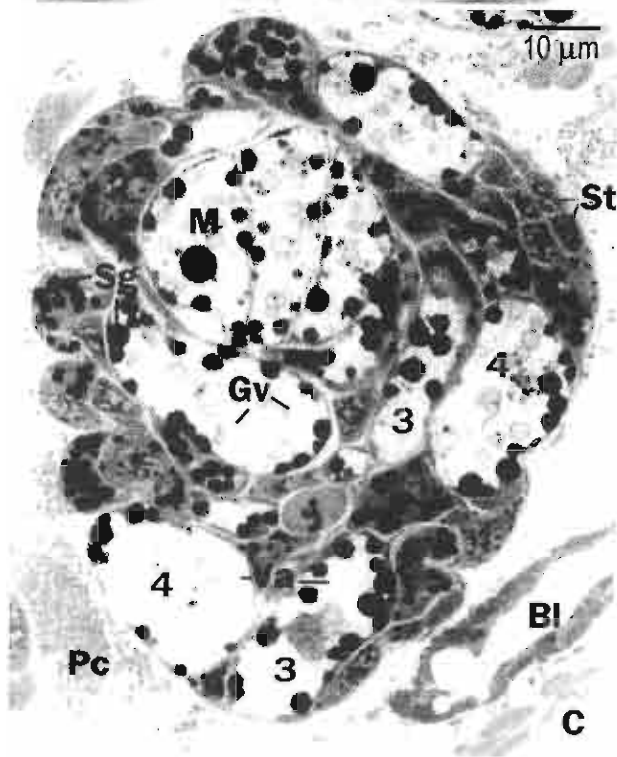
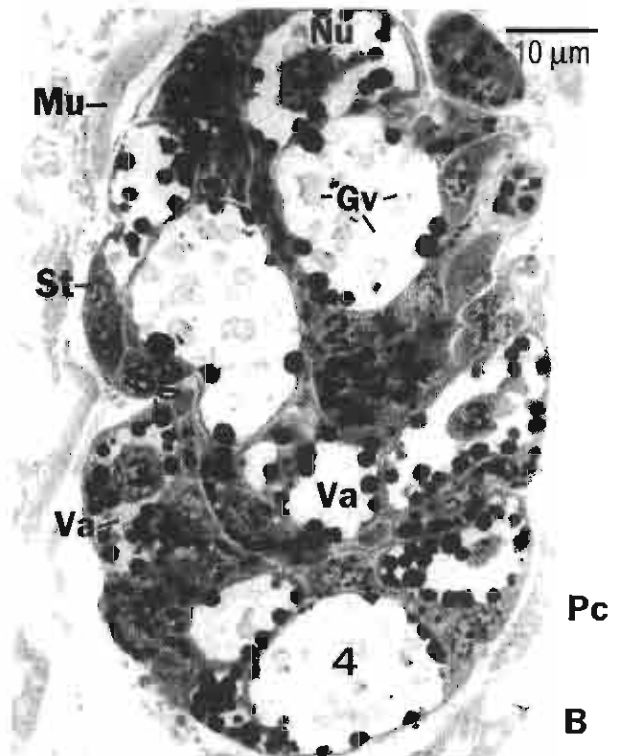
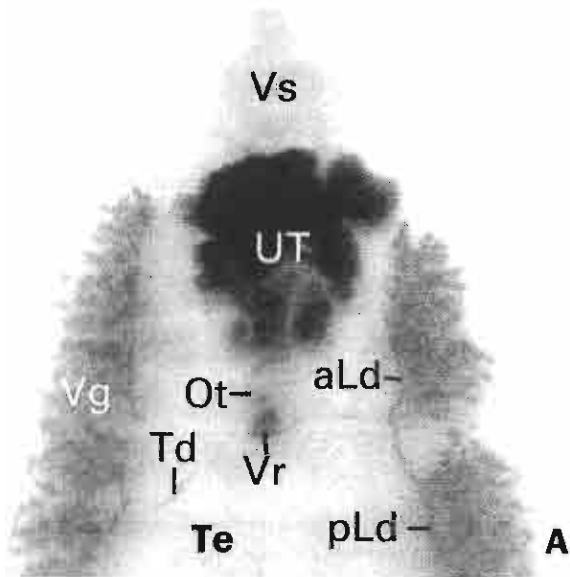


Figure 1

Title: Development and roles of vitelline cells in the eggshell formation in *Fasciola gigantica*

Authors: Ardool Meepool, Chaitip Wanichanon, Vitoon Viyanant and Prasert Sobhon



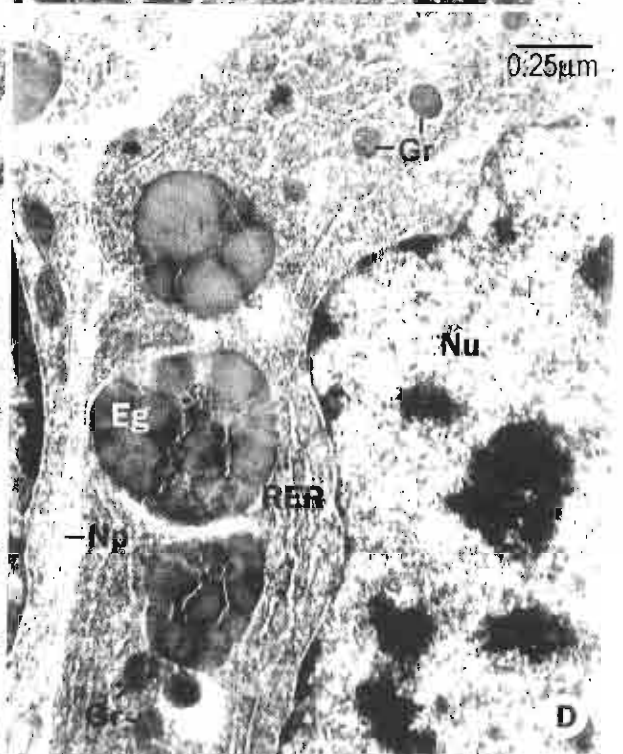
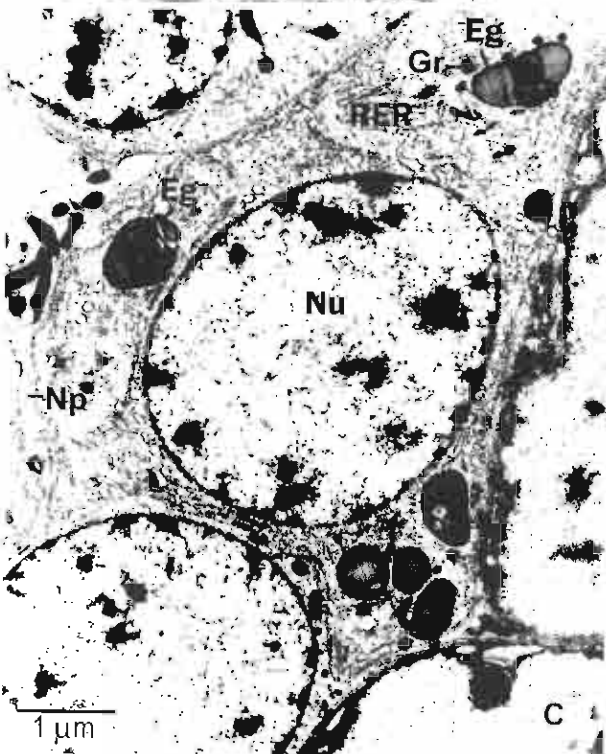
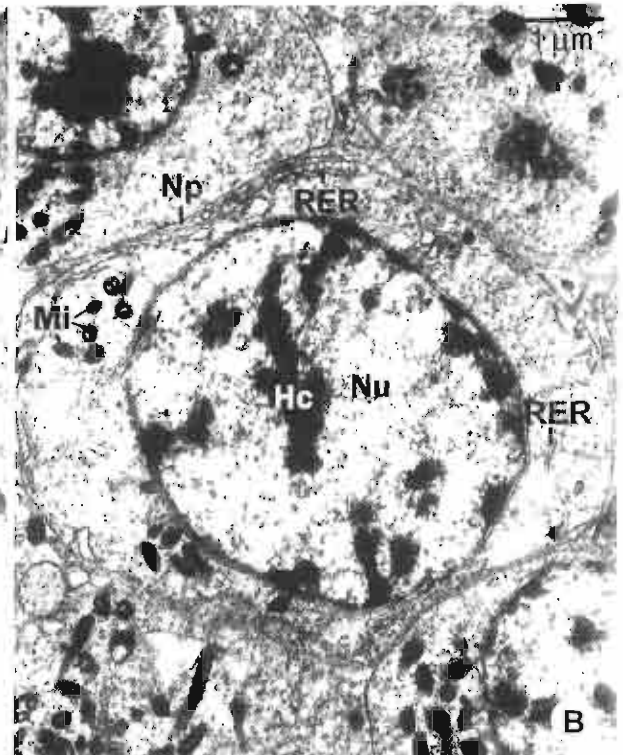
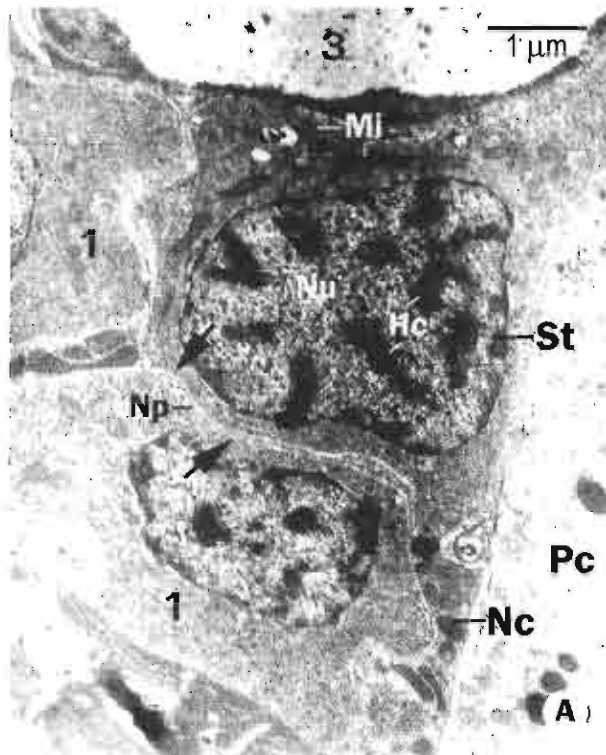


Figure 2

Title: Development and roles of vitelline cells in the eggshell formation in *Fasciola gigantica*

Authors: Ardool Meepool, Chaitip Wanichanon, Vitoon Viyanant and Prasert Sobhon



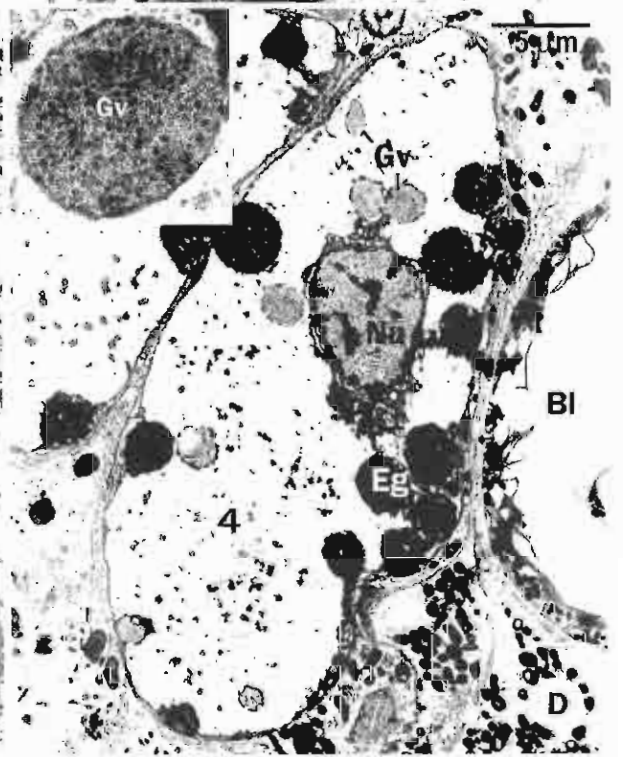
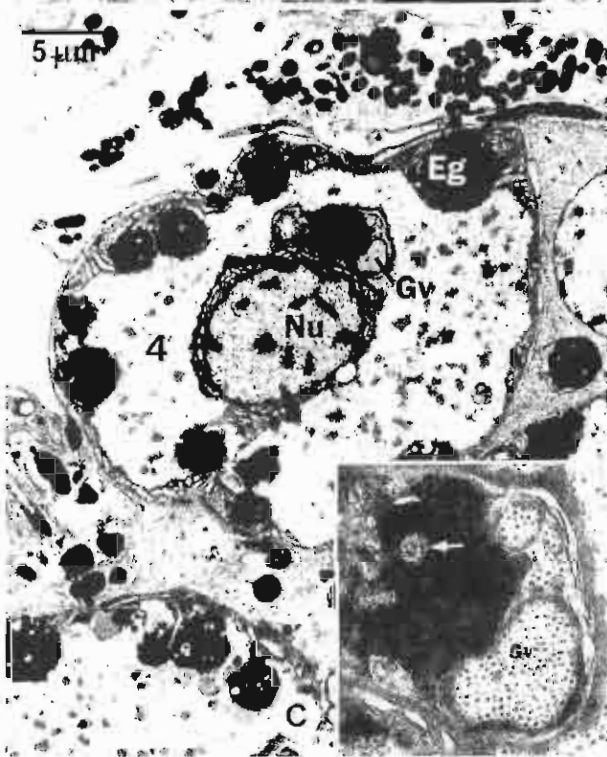
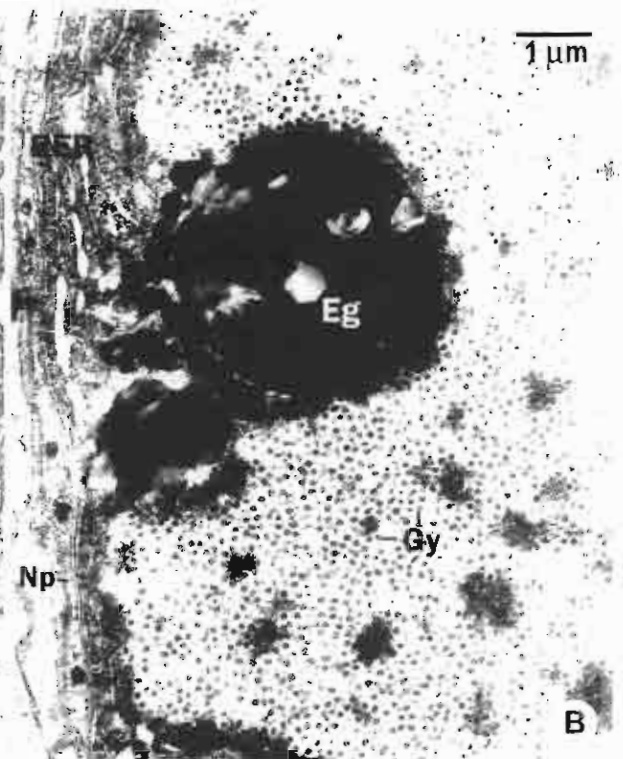
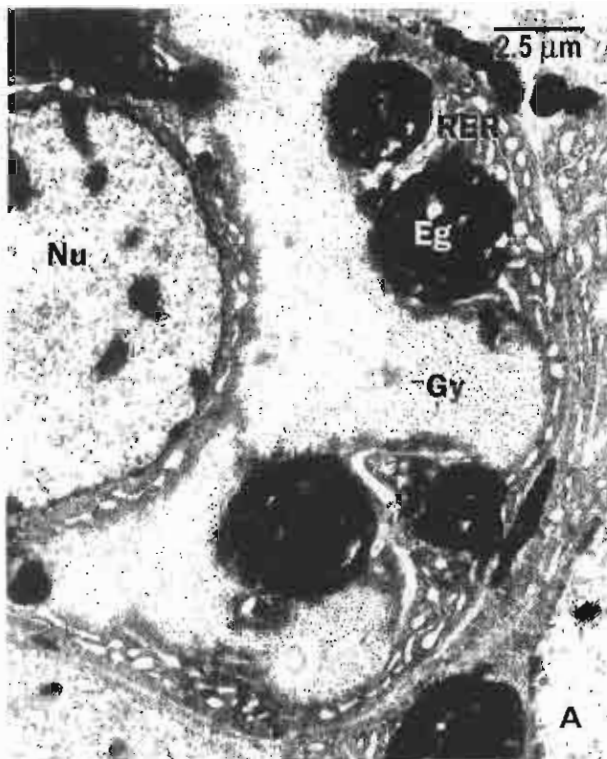


Figure 3

Title: Development and roles of vitelline cells in the eggshell formation in *Fasciola gigantica*

Authors: Ardool Meepool, Chaitip Wanichanon, Vitoon Viyanant and Prasert Sobhon



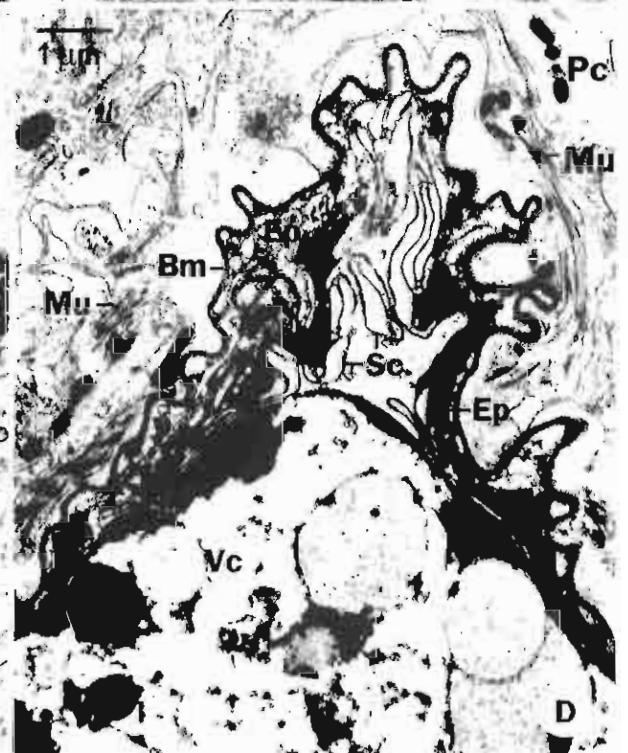
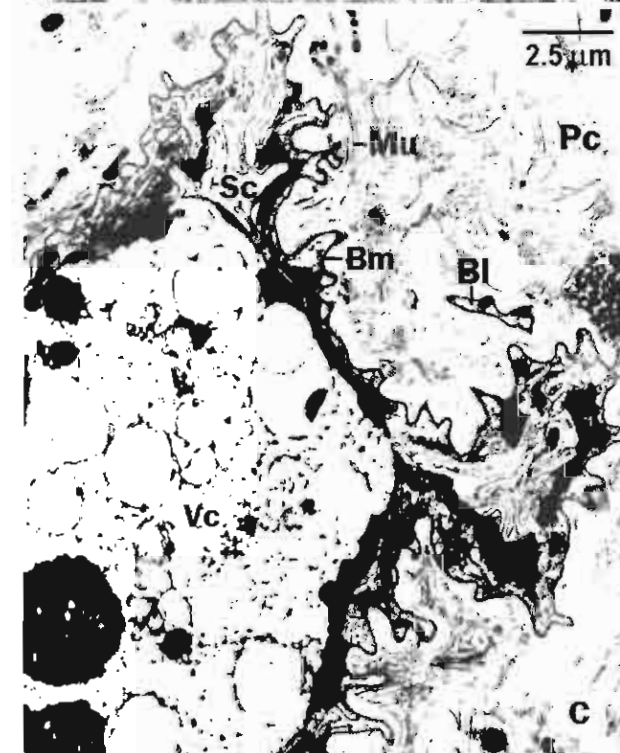
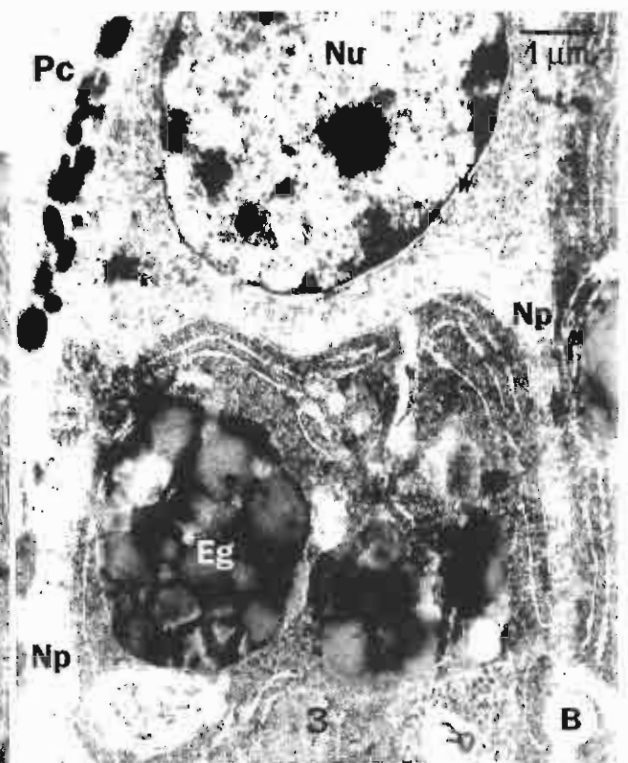
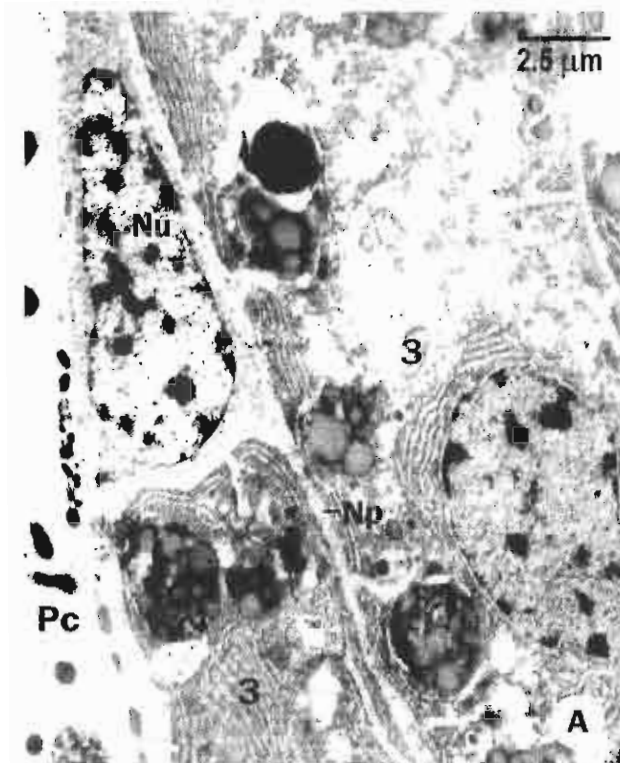


Figure 4

Title: Development and roles of vitelline cells in the eggshell formation in *Fasciola gigantica*

Authors: Ardool Meepool, Chaitip Wanichanon, Vitoon Viyanant and Prasert Sobhon



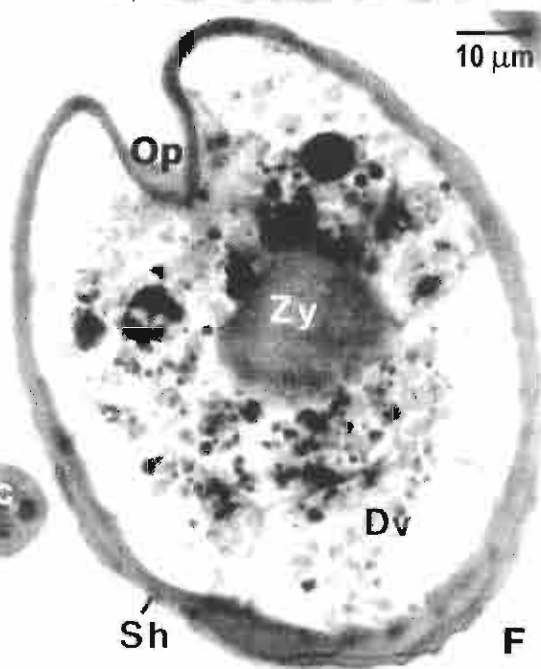
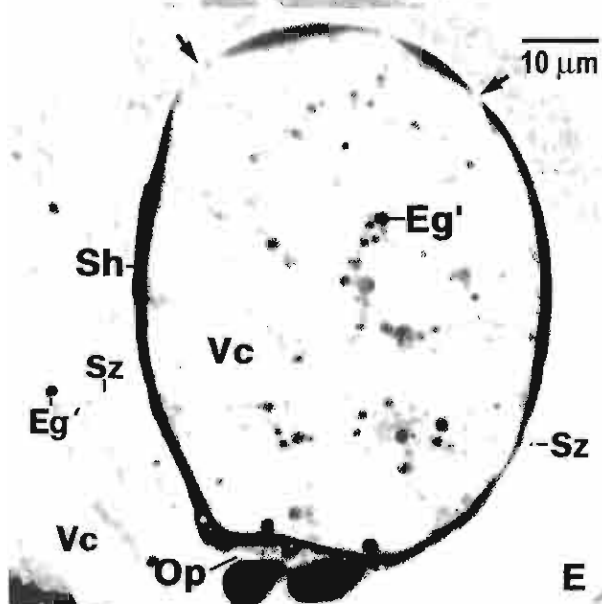
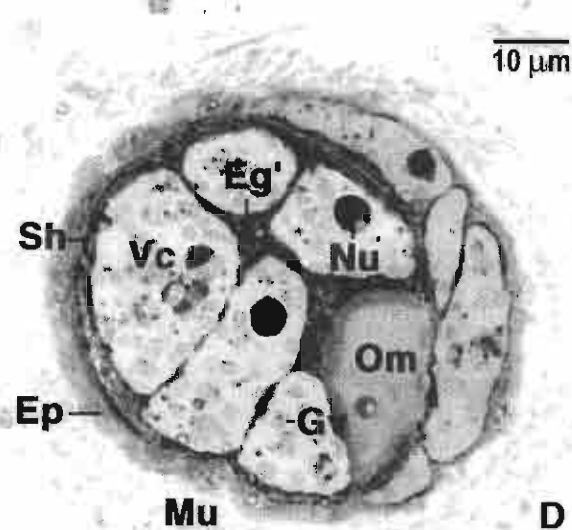
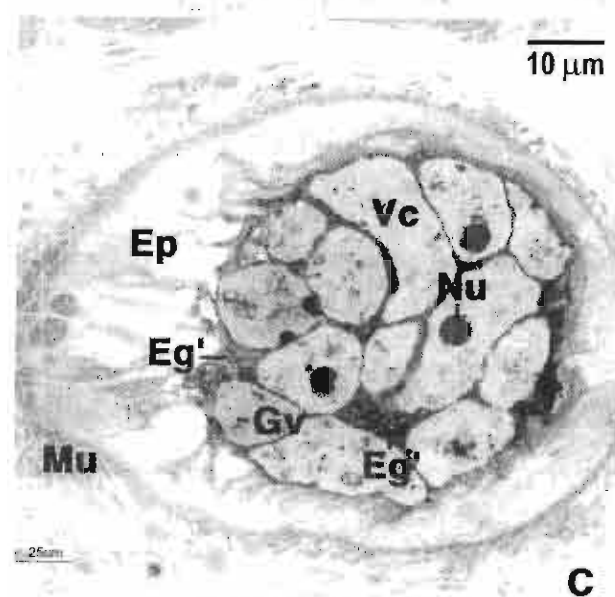
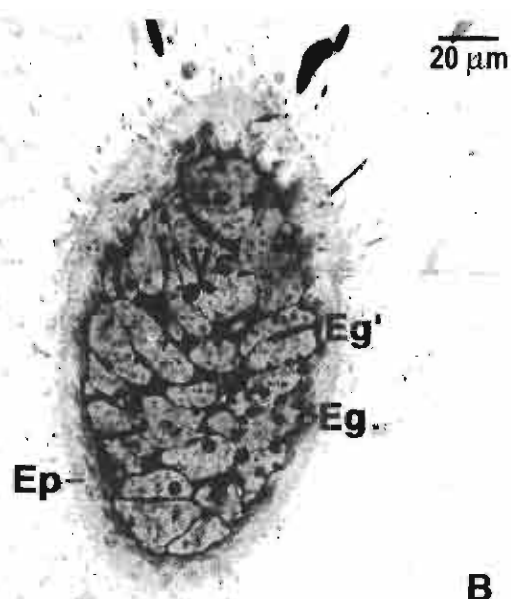
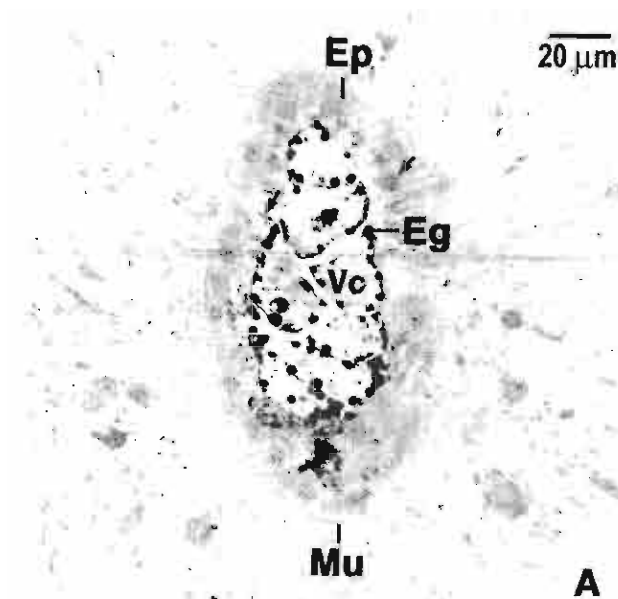


Figure 5

Title: Development and roles of vitelline cells in the eggshell formation in *Fasciola gigantica*

Authors: Ardool Meepool, Chaitip Wanichanon, Vitoon Viyanant and Prasert Sobhon



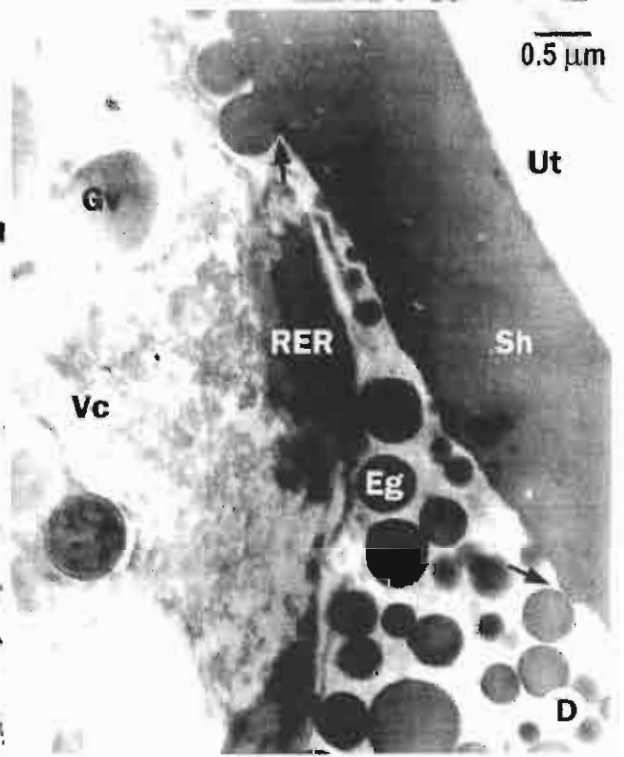
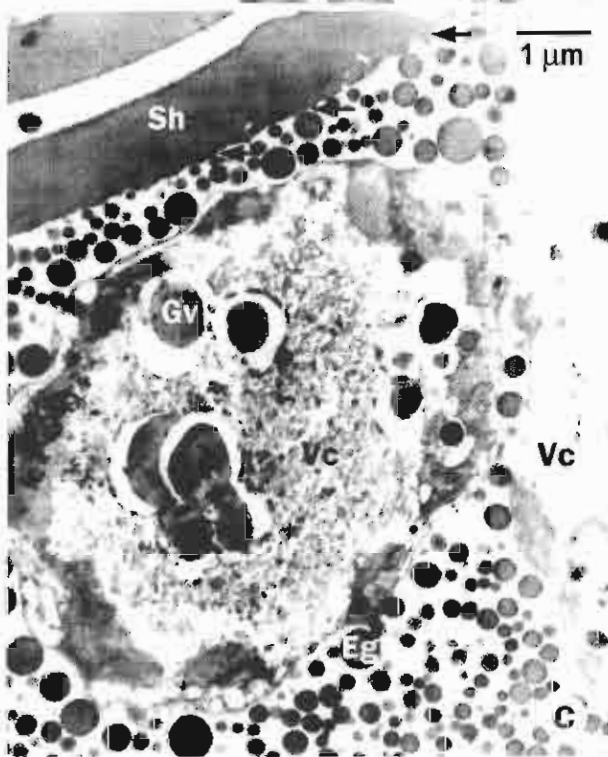
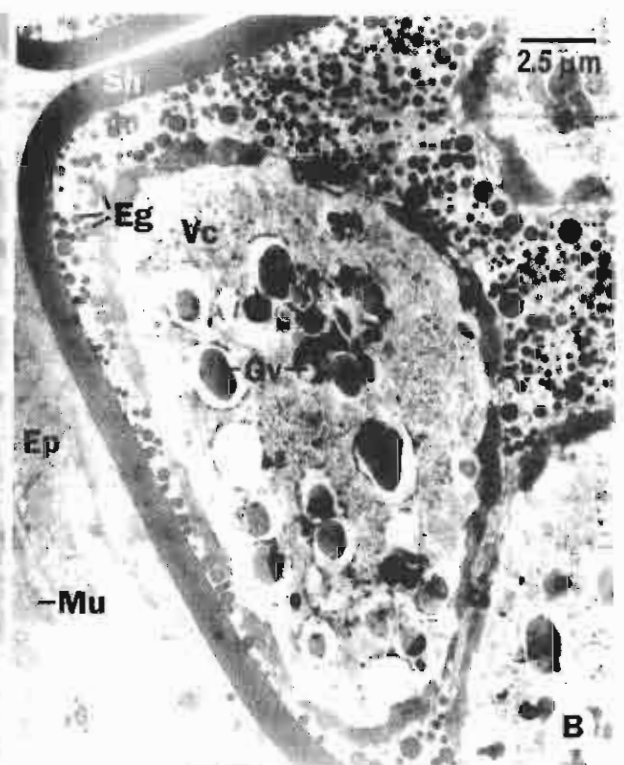
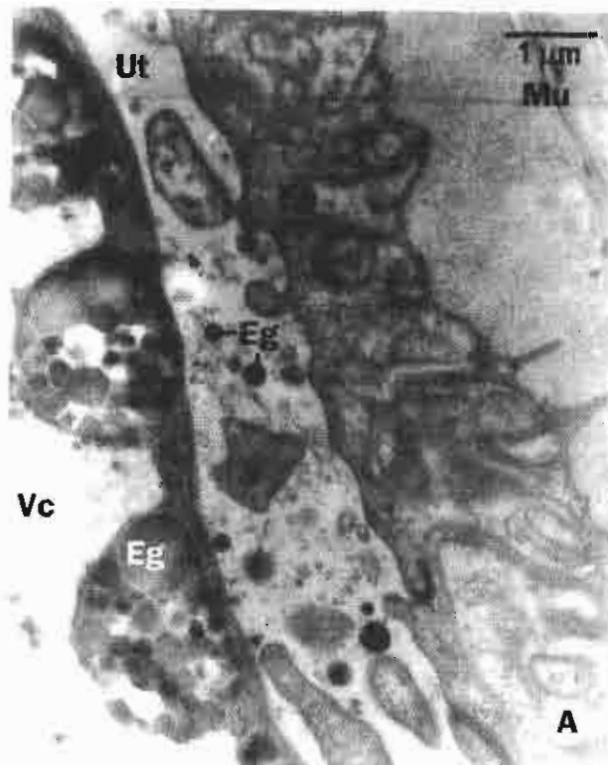


Figure 6

Title: Development and roles of vitelline cells in the eggshell formation in *Fasciola gigantica*

Authors: Ardool Meepool, Chaitip Wanichanon, Vitoon Viyanant and Prasert Sobhon



scpso

From: "VETPAR" <vetpar@elsevier.com>
To: <scps**o**@mucc.mahidol.ac.th>
Sent: Wednesday, March 30, 2005 2:33 PM
Subject: Elsevier Editorial System Registration

Dear Dr Sobhon,

Thank you for registering for the Elsevier Editorial Systems online submission and peer review tracking system for Veterinary Parasitology.

Here is your username and confidential password, which you need to access the system at <http://ees.elsevier.com/vetpar/>

Username: scps**o**
Password: sobhon22

Please save this information in a safe place.

You can change your password and other personal information at <http://ees.elsevier.com/vetpar/>. (log in as Author and choose 'change details' from the top menu).

Kind regards,

Editorial Office Staff
Veterinary Parasitology

3/30/2005

Department of Anatomy, Faculty of Science
Mahidol University, Rama VI Road
Bangkok, 10400 (Thailand)
Tel: 662-245-5198
Fax: 662-247-9880

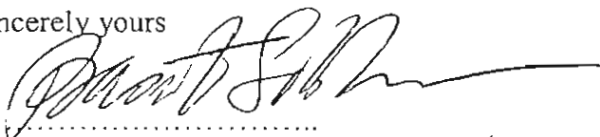
March 25, 2005

The Editor,
The Editorial Office of *Veterinary Parasitology*
P.O. Box 993
1000 AZ Amsterdam
The Netherlands

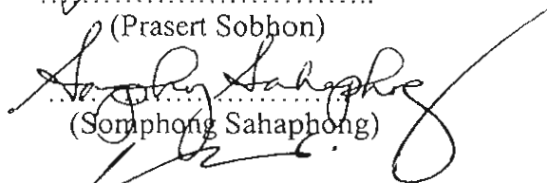
Dear Editor,

On behalf of all the coauthors I would like to submit the manuscript entitled "Immunolocalization of cytoskeletal components in the tegument of the 3-week-old juvenile and adult *Fasciola gigantica*" to be considered for publication in *Veterinary Parasitology*. The work as reported has not been, and is not intended to be, published anywhere except in *Veterinary Parasitology*. We thank you very much for your kind attention and consideration.

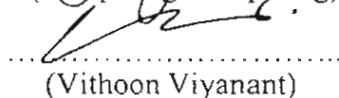
Sincerely yours



.....
(Prasert Sobhon)



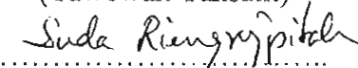
.....
(Somphong Sahaphong)



.....
(Vithoon Viyanant)

.....
Tawewan Tansatit

.....
(Tawewan Tansatit)



.....
(Suda Riengrojpitak)

*Corresponding Author : Prasert Sobhon

Title: Immunolocalization of cytoskeletal components in the tegument of the
3-week-old juvenile and adult *Fasciola gigantica*

Authors: T. TANSATIT¹, S. SAHAPHONG^{1,3}, S. RIENGROJPITAK¹, V.
VIYANANT⁴ AND P. SOBHON²

Affiliations: *Departments of ¹Pathobiology and ²Anatomy, Faculty of Science,
Mahidol University, RamaVI Rd., Bangkok, 10400, Thailand.*

*³International College, Mahidol University, Salaya Campus, Nakhonpathom
73170, Thailand.*

*⁴Faculty of Allied Health Sciences, Thammasat University, Phahonyothin Rd.,
Klongluang, Pathumthani, 12120, Thailand.*

Correspondences and reprint request to: Dr. Prasert Sobhon Ph.D.

Department of Anatomy,

Faculty of Science, Mahidol University

RamaVI Rd., Bangkok 10400, Thailand

Tel. : 66-2-201-5406.

Fax: 66-2-247-9880.

E-mail: scpsob@mahidol.ac.th

Abstract

Components of three cytoskeletal elements, namely, microtubule, intermediate and actin filaments have been localised in the tegument of the 3-week-old juvenile and adult *Fasciola gigantica* by means of immunofluorescence and immunoperoxidase techniques, using mouse monoclonal anti-alpha-tubulin, anti-cytokeratin antibodies and biotinylated-phalloidin, respectively. The presence of tubulin, indicative of microtubules, was demonstrated in the tegumental cell bodies, their cytoplasmic processes, and the basal layer of the tegumental syncytium. Cytokeratin, representing one type of intermediate filaments, was detected in the tegumental cell bodies, their cytoplasmic processes, tegumental syncytium and spines. Phalloidin, which could bind to actin, a subunit of microfilament, was detected in the tegumental cell bodies and their processes, and the microtrabecular network which form the scaffold of the tegumental syncytium. In tegument, cell bodies and their processes, tubulin and actin appeared as long bundles and network, which could mediate the movement of secretory granules from the cell bodies towards the basal as well as the apical layer of the tegument. Cytokeratin-based intermediate filament may serve to reinforce the integrity of the tegumental syncytium.

Keywords

Fasciola gigantica, Tegument, Cytoskeleton, Tubulin, Actin, Cytokeratin

Introduction

In trematodes, the tegument is the interface layer between the parasites and their environment. It represents a site where considerable biochemical, physiological and host immune reactions interplay. In *fasciola* spp., the tegument plays crucial roles in maintaining homeostasis, including absorption of the nutrient, exchange of the waste molecules, regulation of ionic equilibrium, and protection from host immune responses (Fairweather et al, 1999). In addition, tegument is the major site from which antigens are released to stimulate the host

immune responses (Hanna and Trudgett, 1983; Sobhon et al, 1996). In trematodes, the cytoskeleton is thought to play important roles in maintaining the tegumental architecture, transportation of tegumental granules from tegumental cells to the syncytium, thus are directly involved in the synthesis and turnover of the surface membrane and its outer coat (Wilson and Barnes, 1974; Sobhon and Apinhasmit, 1995; Fairweather et al, 1999). The cytoskeleton, especially microtubules and actin filaments represent a potential target for anthelmintic drugs (Lacey, 1988; Sobhon and Upatham, 1990a). Several anthelmintic drugs act by damaging the tegument cytoskeleton (Sobhon and Upatham, 1990b; Stitt and Fairweather, 1994; Apinhasmit and Sobhon, 1996; Meaney et al, 2002; Meaney et al, 2003; Meaney et al, 2004). However only few studies have been carried out on the distribution and arrangement of the cytoskeletal components and their role in organizing the unique structure of the tegument. In *Schistosoma mansoni*, actin filaments have been found in the tegument and surface spines by immunocytochemical analysis (Cohen et al, 1982; Abbas and Cain, 1987; Matsumoto et al, 1988; MacGregor and Shore, 1990) while intermediate filaments existed at the base of spines (Abbas and Cain, 1987). Cytokeratin was exhibited in the tegument and the spines of *S. mansoni* (Diogo et al, 1994). In *F. hepatica*, actin filaments have been immunocytochemically demonstrated in the tegumental cell bodies and tegumental spines (Stitt et al, 1992a) and tubulin in the tegumental cell bodies, their cytoplasmic processes and the syncytium (Stitt et al, 1992b). In the present report, we have localised the distribution of tubulin, cytokeratin and actin in the tegument and its associated structures in 3-week-old juvenile and adult *F. gigantica* by using immunofluorescence and immunoperoxidase techniques.

Materials and Methods

Specimens preparation

Juvenile flukes were recovered from the liver parenchyma of male Golden Syrian hamsters at 3 weeks after being infected orally by feeding metacercariae of *F. gigantica*. Adult parasites were collected from the bile ducts and gall bladder of infected cattle and buffaloes at the local abattoir. They were washed several times with 0.85% NaCl solution before being processed for further study. The localization of cytoskeletal components in the tegument of adult and 3-week-old juvenile *F. gigantica* was performed by standard indirect immunofluorescence and the avidin-biotin immunoperoxidase methods.

For the immunofluorescence technique, the flukes were fixed in 4% (w/v) paraformaldehyde in 0.1 M phosphate buffered saline (PBS) pH 7.4 at 4 °C for 4 hours. After washing, the specimens were immersed in 5% (w/v) sucrose in 0.1 M PBS at 4 °C for 24 hours and transferred to 30% (w/v) sucrose in 0.1 M PBS at 4 °C, then embedded in the Tissue Tek O.C.T. medium and frozen at -30 °C. The sections were cut at the thickness of 3-5 µm in a Leica CM 1800 cryostat, and mounted on 3-aminopropyl-triethoxy-silane (APES) (Sigma-Aldrich Co., Saint Louis, MO, USA) coated slides.

For immunoperoxidase staining, the parasites were fixed in 10% buffered formalin, dehydrated through graded series of alcohol, embedded in paraplast, cut at the thickness of 5 µm and placed on APES-coated slides.

Indirect immunofluorescence detection

For localization of microtubules and intermediate filaments, the sections were incubated in 0.1% glycine in 10 mM PBS, and subsequently in 4% bovine serum albumin (BSA) to block non-specific bindings for 15 and 30 min, respectively. Then the sections were covered with mouse monoclonal anti-alpha-tubulin or monoclonal anti-cytokeratin antibody (Zymed Co., San Francisco, CA, USA) for 1 hour at room temperature at the dilution 1:500

and 1:100, respectively. After washing with 10 mM PBS, pH 7.4, 3 times for 10 min each, the sections were treated with fluorescein isothiocyanate (FITC)-conjugated goat anti-mouse IgG solution (Sigma-Aldrich Co.), at 1:100 dilution, for 30 min.

For localizing actin, the sections were treated with 1% Triton-X 100 in PBS for 10 min. After washing with 10 mM PBS, pH 7.4 for 5 min, the sections were incubated in biotinylated-phalloidin solution (Molecular Probes Inc., OR, USA) at 1:20 dilution for 1 hour at room temperature. The sections were rinsed three times with PBS for 10 min each, then covered with streptavidin-FITC (Zymed Co.), at 1:100 dilution for 30 min. Finally, the treated sections were rinsed thoroughly with PBS and mounted in Vectashield (Vector Laboratories Inc., Burlingame, CA, USA), observed and photographed under a Nikon HB 10101 AF fluorescence microscope.

Immunoperoxidase detection

The immunoperoxidase staining was done by using a Vectastain Universal Quick kit (Vector Laboratories, Inc). The deparaffinised sections were hydrated and treated with 3% H₂O₂ in tap water for 30 min to destroy endogenous peroxidase. Prior to the primary antibody incubation, the sections were submitted to treatment in microwave oven, using three 5 minute cycles at 700 w in 10 mM citric acid, pH 6.0 (Shi et al, 1991). For microtubule and intermediate filament localizations, the sections were blocked for non-specific staining with 2.5% normal blocking serum for 10 min, then incubated for 1 hour at room temperature with mouse monoclonal anti-alpha-tubulin or anti-cytokeratin antibodies. After washing three times in 10 mM PBS, pH 7.5 for 10 min each, the sections were subsequently incubated in the biotinylated secondary antibody and streptavidin-peroxidase solution (Vector Laboratories, Inc) for 15 min and 10 min, respectively. For actin filament localization, the deparaffinised sections were hydrated and permeabilised with 1% Triton-X 100 in PBS for 10 min before being covered with biotinylated-phalloidin solution overnight, at 4 °C, and subsequently

incubated with streptavidin-HRP solution (Sigma). Then, color products in the treated sections were developed in 0.03% diaminobenzidine tetrahydrochloride (DAB) in 0.1% H_2O_2 solution (Vector Laboratories, Inc). After counterstaining with Mayer hematoxylin, the stained sections were dehydrated, mounted, and viewed under an Olympus microscope.

For the negative controls in both immunofluorescence and immunoperoxidase experiments, the sections were incubated in the normal mouse serum without primary antibodies.

Results

The distribution pattern of the cytoskeletal proteins in the tegument of 3-week-old juvenile and adult stages was similar, and thus was described simultaneously.

Tubulin

By indirect immunofluorescence, tubulins were detected in the tegumental cell bodies, their processes running between the muscle, and the basal part of the tegumental syncytium (Fig. 1C,D). In the tegumental cell, intense staining was observed in the cytoplasm around the nucleus, and in the cytoplasmic processes running between the muscle fibers to join the tegumental syncytium (Fig. 1D). While in the tegument itself, intense staining was seen only at the basal layer (Fig. 1D). The cells of parenchyma and caecal epithelium also exhibited strong fluorescence (Fig. 1C). Immunoperoxidase staining showed similar distribution of tubulin which is indicative of the presence of microtubules as in the immunofluorescence experiment (Fig. 2C,D), though the major structures (eg. tegument, muscle) could be more clearly observed.

Cytokeratin

Strong immunofluorescence of cytokeratin was observed in the cytoplasm of the tegumental cell around the nucleus (Fig. 1E,F). Moderate fluorescence was observed in the cytoplasmic processes situated between muscle cells, whereas the whole width of the

tegumental syncytium was also moderately and homogeneously fluoresce (Fig. 1E,F). Tegumental spines showed intense fluoresce of cytokeratin in all parts (Fig. 1E inset,F). The parenchymal and caecal epithelial cells exhibited moderate fluorescence (Fig. 1E). The immunoperoxidase detected similar distribution pattern of cytokeratin except in the syncytium and tegumental spines where the intense immunostain appeared in patches, particular in the apical layer of the tegument and the tip of the spines (Fig. 2E,F), while only very light staining was visible in the rest of the tegumental syncytium and the cytoplasmic processes of tegumental cells (Fig. 2E,F).

Actin

Both indirect immunofluorescence and immunoperoxidase could detect strong staining of biotinylated-phalloidin in the tegumental cell bodies, their cytoplasmic processes, almost the whole thickness of the tegumental syncytium and subtegumental muscle layers (Fig. 1G,H, Fig. 2G,H). In the tegumental cell bodies and their processes, strong fluorescence was visible in area around the nuclei, while in some cells the fluorescence was so strong that the nuclei were masked (Fig. 1G,H). Moderate staining appeared in the subtegumental muscle layers, the parenchymal and caecal epithelial cells. In the tegumental syncytium, intense and uniform staining occupied the basal two-third of the width of the syncytium in all area of the fluke body, but not the spines (Fig. 1G,H, Fig. 2G,H).

Discussion

The tegument of both adult and juvenile stages *F. gigantica* is made up of a syncytium that is connected to the processes of tegumental cells situated underneath the muscular layers. The detailed arrangement of the cytoskeleton in tegument of adult *F. gigantica* was first observed by Sobhon et al (2000) using conventional transmission electron microscopy (TEM). The tegument was divided into four layers based on the presence of various organelles and the density of the cytoskeleton elements. The main body of the tegument is

composed of the network of fine filaments appearing as microtrabecular network. Microtubules were shown concentrated in the processes of tegumental cells and the fourth, or basal layer of the tegument. While bundles of fibrils similar to intermediate filaments appeared in patches underneath the surface membrane. The presence of high concentration of tubulin in the tegumental cell bodies and their processes agrees with the ultrastructural observation. The presence of tubulin only in the basal layer of the tegumental syncytium of *F. gigantica* differs from that of *F. hepatica* reported by Stitt et al (1992b), which showed the presence of microtubules oriented vertically and horizontally in the syncytium and along the apical and basal boundaries of the syncytium.

Using phalloidin, a compound known to bind to filamentous actin (F-actin) (Cooper, 1987), actin filaments were detected in almost the whole thickness of tegumental syncytium. This corresponds to the presence of microtrabecular network in the third and fourth layers of adult's tegument and juveniles' as viewed by TEM (Sobhon et al, 2000; Khawsuk, 2003) and were similar to the pattern reported earlier in the tegument of the oriental schistosomes, ie, *S. japonicum* and *S. mekongi* (Sobhon and Upatham, 1990a). These result suggested that actin may form the major part of the microtrabecular network. However, direct labelling studies by immunoelectron microscopy needed to be done. Surprisingly, actin was not detected in the spines of *F. gigantica* in both adult or juvenile stages which is in contrast to other reports which showed actin as the major components of spines in *F. hepatica* (Stitt et al, 1992a) and *S. mansoni* (Abbas and Cain, 1987; Cohen et al, 1982; MacGregor and Shore, 1990; Matsumoto et al, 1988).

In diverse eukaryotic cells, microtubules and actin filaments networks cooperate functionally during a wide variety of cellular functions, especially in vesicle and organelle transport (Goode et al, 2000; Rogers and Gelfand, 2000). In general, microtubules are utilized for the long-range transport while actin filaments are used for the short-range transport

(Goode et al, 2000). Vesicles are transported using microtubules in the initial fast motion towards the cell periphery, followed by the dispersion of vesicles throughout the cytoplasm by the action of actin fibers (Goode et al, 2000). In fasciola as well as schistosoma spp, microtubules and actin filaments are believed to be involved in the movement of tegumental granules from the tegumental cell bodies to the syncytium (Wilson and Barnes, 1974), and their distribution at definite sites within the tegumental syncytium may be determined by actin filaments in the microtrabecular network.

The present study has demonstrated for the first time the presence of cytokeratin, which is one form of intermediate filament, in the tegument of fasciola parasite. Intense staining was observed at the apical surface of the tegumental syncytium, perhaps corresponding to the patches of bundles of thin fibrils found underneath the surface membrane (Sobhon et al, 2000). Light staining occurred throughout the width of the syncytium, which suggested the distribution of intermediate filament across the whole tegument. These observations are similar to that by Diogo et al (1994) who revealed the cytokeratin network in the tegument, and also the presence of this protein in the spines of both male and female *S. mansoni*.

The distribution pattern of cytokeratins in the tegumental cell bodies and the cytoplasmic processes is somewhat overlapping with that of microtubules and actin filaments. It is possible that in the cell bodies, cytokeratins form a scaffold linking microtubules and actin filaments (Houseweart and Cleveland, 1998; Herrmann and Aebi, 2000) in maintaining the position of the nucleus, determining the cell shape, as well as protecting cells from mechanical stresses (Goldman et al, 1996; Galou et al, 1997; Coulombe et al, 2002). Similarly, in the tegumental syncytium, the cytokeratin-associated intermediate filaments may play important roles in maintaining the integrity, and specific shape as well as surface contour of the syncytium, which is so unique for this species (Daengprasert et al, 2000).

Our finding also indicated that *F.gigantica* spines were, at least in part, composed of cytokeratin, since this protein could be detected by both immunofluorescence and immunoperoxidase stainings. The flukes use their spines in maintaining position in the host's bile ducts, eroding the epithelium and also puncturing the blood vessels (Fairweather et al, 1999). In this regards it would be expedient if the spines are composed in part of cytokeratin which contribute to their rigidity.

Acknowledgements

This work was supported by the Thailand Research Fund (Senior Research Scholar Fellowship to Prasert Sobhon) and by The Ministry of University Affairs and Faculty of Graduate Studies, Mahidol University (to Tawewan Tansatit).

References

- Abbas, M.K., Cain, D., 1987. Actin and intermediate-sized filaments of the spines and cytoskeleton of *Schistosoma mansoni*. Parasitol Res. 73, 66-74.
- Apinhasmit, W., Sobhon, P., 1996. *Opisthorchis viverrini*: effect of praziquantel on the adult tegument. Southeast Asian J Trop Med Public Health. 27, 304-311.
- Cohen, C., Reinhardt B., Castellani, L., Norton, P., Stirewalt, M., 1982. Schistosome surface spines are "crystals" of actin. J Cell Biol. 95, 987-988.
- Cooper, J.A., 1987. Effects of cytochalasin and phalloidin on actin. J Cell Biol. 104, 1473-1487.
- Coulombe, P.A., Omary, M.B., 2002. "Hard" and "soft" principles defining the structure, function and regulation of keratin intermediate filaments. Curr Opin Cell Biol. 14, 110-122.
- Diogo, C.M., Mendonca, M.C.R., Savino, W., Katz, N., Tendler, M., 1994. Immunoreactivity of a cytokeratin-related polypeptide from adult *Schistosoma mansoni*. Int J Parasitol. 24, 727-732.

- Fairweather, I., Lawence, T., Threadgold, L.T., Hanna, R.E.B., 1999. Development of *Fasciola hepatica* in the mammalian hosts. In: Dalton, J.P.(Ed.), Fasciolosis, CABI Publishing, Wallingford, UK, pp.47-111.
- Galou, M., Gao, J., Humbert, J., Mathias, M., Li, Z., Paulin, D., Patrick, V., 1997. The importance of intermediate filaments in the adaptation of tissue to mechanical stress: evidence from gene knockout studies. *Biol Cell*. 98, 85-97.
- Goldman, R.D., Khuon, S., Chou, Y., Opal, P., Steinert, P., 1996. The function of intermediate filaments in cell shape and cytoskeletal integrity. *J Cell Biol*. 134, 971-983.
- Goode, B.L., Drubrin, D.G., Barnes, G., 2000. Functional cooperation between the microtubule and actin cytoskeletons. *Curr Opin Cell Biol*. 12, 63-71.
- Hanna, R.E.B., Trudgett, A.G., 1983. *Fasciola hepatica*: development of monoclonal antibodies and their use to characterize a glycocalyx antigen in migrating flukes. *Parasite Immunol*. 5, 409-425.
- Herrmann, H., Aebi, U., 2000. Intermediate filaments and their associates: multi-talented structural elements specifying cytoarchitecture and cytodynamics. *Curr Opin Cell Biol*. 12, 79-90.
- Houseweart, M.K., Cleveland, D.W., 1998. Intermediate filaments and their associated proteins: multiple dynamic personalities. *Curr Opin Cell Biol*. 10, 93-101.
- Khawsuk, W., 2003. Development of *Fasciola gigantica* tegument, Identification and Localization of associated antigens [Ph.D. Thesis in Anatomy], Faculty of Graduate Studies, Mahidol University.
- Lacey, E., 1988. The role of the cytoskeletal protein, tubulin, in the mode of action and mechanism of drug resistance to benzimidazoles. *Int J Parasitol*. 18, 885-936.
- MacGregor, A.N., Shore, S.J., 1990. Immunostaining of cytoskeletal proteins in adult *Schistosoma mansoni*. *Int J Parasitol*. 20, 279-284.

Matsumoto, Y., Perry, G., Levine, R.J.C., Blanton, R., Mahmoud, A.A.F., Aikawa, M., 1988.

Paramyosin and actin in schistosomal teguments. *Nature*. 333, 76-78.

Meaney, M., Fairweather, I., Brennan, G.P., Ramasamy, P., Subramanian, P.B., 2002.

Fasciola gigantica: tegumental surface alterations following treatment in vitro with the sulphoxide metabolite of triclabendazole. *Parasitol Res.* 88, 315-325.

Meaney, M., Fairweather, I., Brennan, G.P., McDowell, L.S.L., Forbes, A.B., 2003. *Fasciola*

hepatica: effects of the fasciolicide clorsulon *in vitro* and *in vivo* on the tegument surface, and a comparison of the effects on young-and old-mature flukes. *Parasitol Res.* 91, 238-250.

Meaney, M., Fairweather, I., Brennan, G.P., Forbes, A.B., 2004. Transmission electron

microscopy study of the ultrastructural changes induced in the tegument and gut of

Fasciola hepatica following *in vivo* drug treatment with clorsulon. *Parasitol Res.* 92, 232-241.

Rogers, S.L., Gelfand, V.I., 2000. Membrane trafficking, organelle transport, and the cytoskeleton. *Curr Opin Cell Biol.* 12, 57-62.

Shi, S-R., Key, M.E., Kalra, K.L., 1991. Antigen retrieval in formalin-fixed, paraffin-

embedded tissues: an enhancement method for immunohistochemical staining based on microwave oven heating of tissue sections. *J Histochem and Cytochem.* 39, 741-748.

Sobhon, P., Upatham, E.S., 1990a. The tegument cytoskeleton. In: Snail hosts, life-

cycle, and tegumental structure of oriental schistosomes. UNDP/World Bank/WHO Special Programme for Research and Training in Tropical Diseases, pp. 204-232.

Sobhon, P., Upatham, E.S., 1990b. Effect of praziquantel on adult oriental schistosomes. In:

Snail hosts, life-cycle, and tegumental structure of oriental schistosomes. UNDP/World Bank/WHO Special Programme for Research and Training in Tropical Diseases, pp. 247-273

- Sobhon, P., Apinhasmit, W., 1995. *Opisthorchis viverrini*: The tegumental cytoskeleton. Int J Parasitol. 25, 787-796.
- Sobhon, P., Anantavara, S., Dangprasert, T., Meepool, A., Wanichanon, C., Viyanant, V., Upatham, S., Kusamran, T., Chompoochan, T., Thammasart, S., Prasittirat, P., 1996. *Fasciola gigantica*: Identification of adult antigens, their tissue sources and possible origins. J Sci Soc Thailand. 22, 143-162.
- Sobhon, P., Dangprasert, T., Chuanchaiyakul, S., Meepool, A., Khawsuk, W., Wanichanon, C., Viyanant, V., Upatham, E. S., 2000. *Fasciola gigantica*: Ultrastructure of the adult tegument. SciencAsia. 26, 137-148.
- Stitt, A.W., Fairweather, I., Trudgett, A.G., Johnston, C.F., Anderson, S.M.L., 1992a. Localization of actin in the liver fluke, *Fasciola hepatica*. Parasitol Res. 78, 96-102.
- Stitt, A.W., Fairweather, I., Trudgett, A.G., Johnston, C.F., 1992b. *Fasciola hepatica*: Localization and partial characterization of tubulin. Parasitol Res. 78, 103-107.
- Stitt, A.W., Fairweather, I., 1994. The effect of the sulfoxide metabolite of triclabendazole ('Fasinex') on the tegument of mature and immature stages of the liver fluke, *Fasciola hepatica*. Parasitology. 108, 555-567.
- Wilson, R.A., Barnes, P.E., 1974. The tegument of *Schistosoma mansoni*: observations on the formation, structure and composition of cytoplasmic inclusions in relation to tegument function. Parasitology. 68, 239-258.

Figure 1

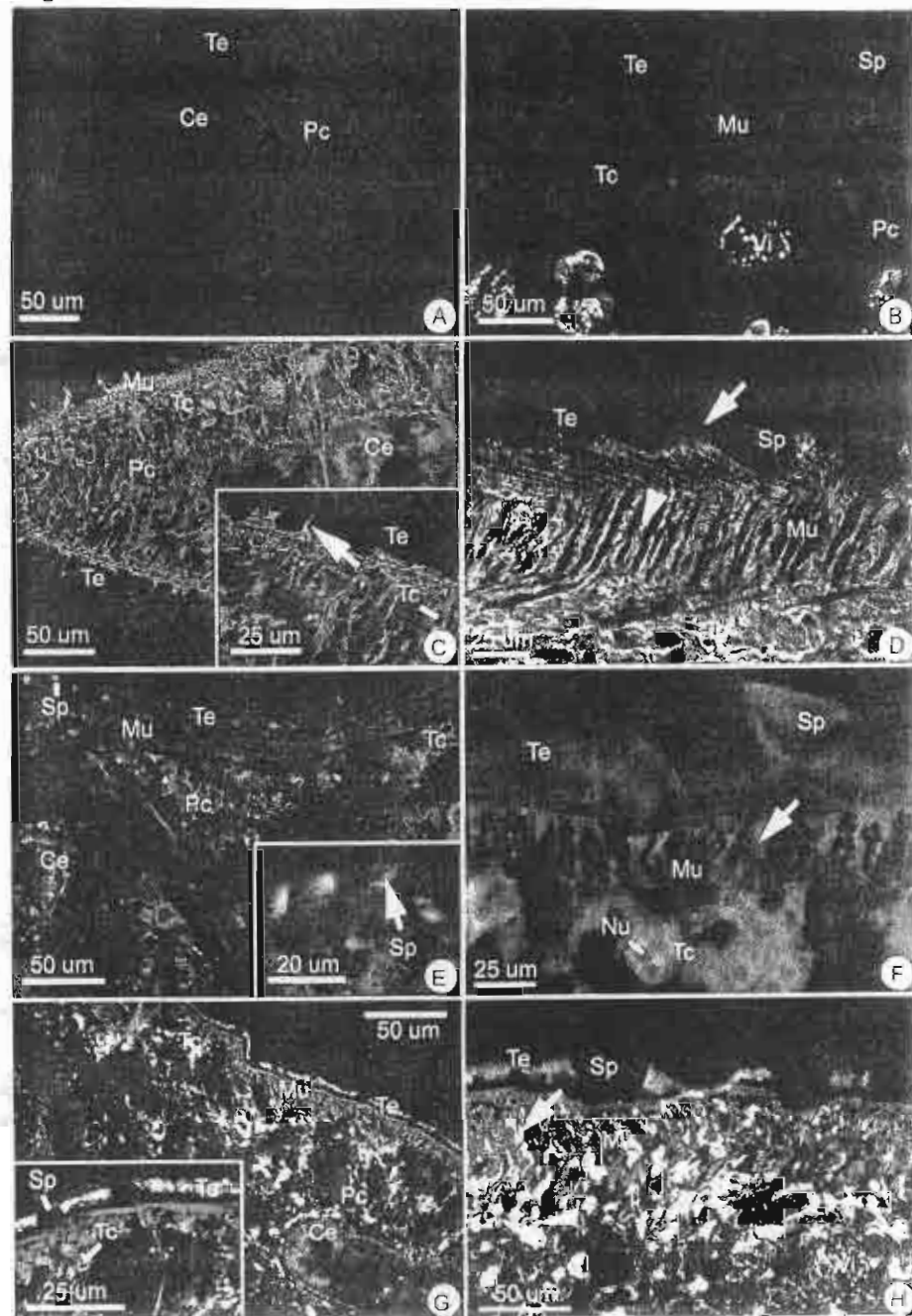
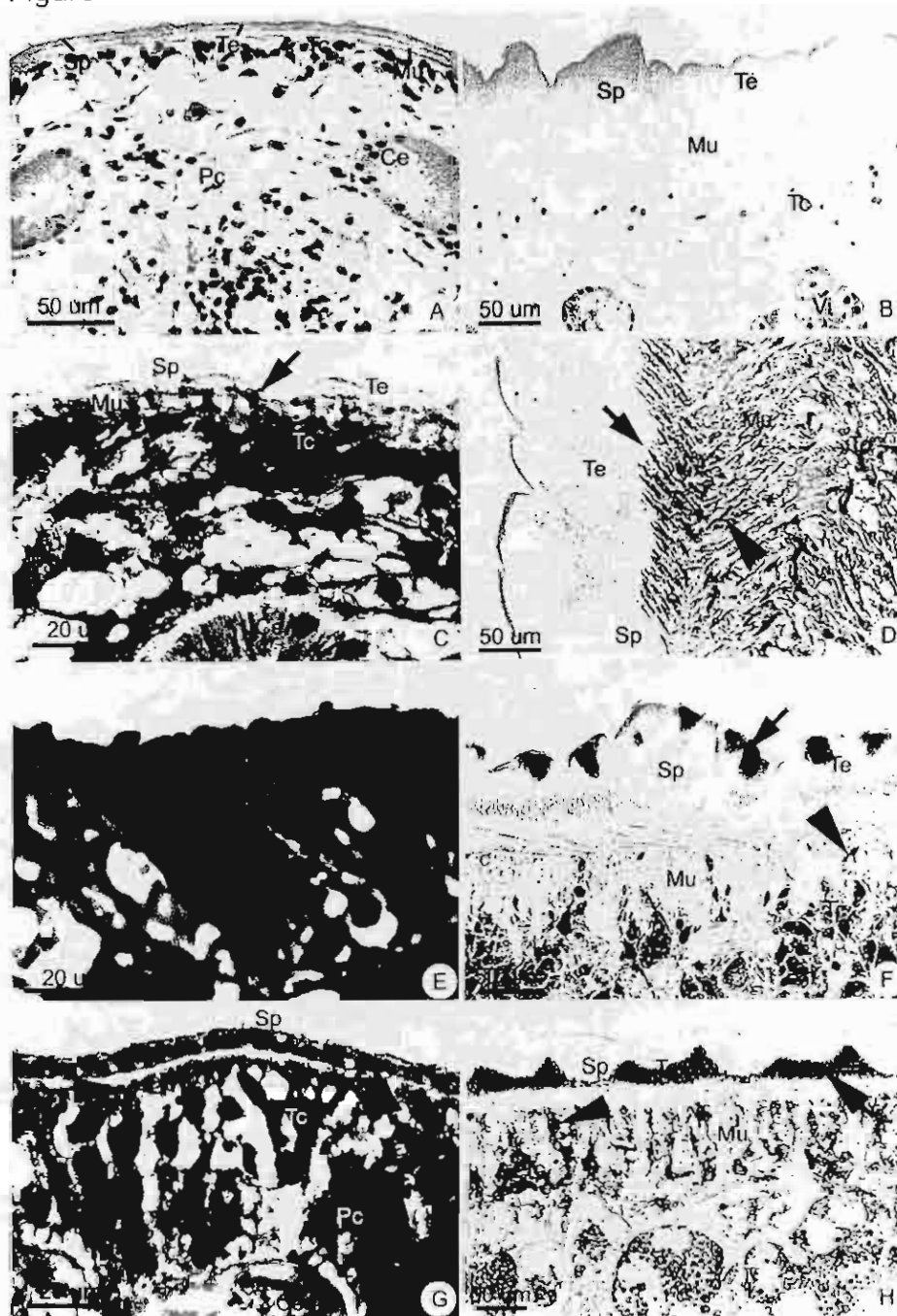


Figure 2



Legends to the figures

Fig. 1. Immunofluorescence micrographs of frozen sections of the 3-week-old juvenile (A, C, E, G) and adult *F. gigantica* (B, D, F, H). The negative controls of a cross-section of the 3-week-old juvenile (A) and the adult (B) fluke, showing tegumental syncytium (Te), spine (Sp), muscle (Mu), tegumental cell body (Tc), vitelline gland (Vi), caecum (Ce), parenchymal cells (Pc). (C) A section of 3-week-old juvenile showing intense staining of anti-tubulin at the basal layer (inset, arrow) of the tegumental syncytium (Te); the parenchymal cells (Pc) and caecal epithelium (Ce) are also strongly stained. (D) Strong staining with the same antibody in an adult section, appears in the tegumental cell bodies (Tc) and their cytoplasmic processes (arrow head) running between the muscle (Mu) to the basal layer (arrow) of tegumental syncytium. (E) A section of 3-week-old juvenile showing strong staining of anti-cytokeratin in tegumental cell bodies (Tc) and tegumental spines (inset, Sp), moderate staining in tegumental syncytium (Te), parenchymal cells (Pc) and caecal epithelium (Ce). (F) In an adult section, intense staining of anti-cytokeratin is also exhibited in the tegumental cell (Tc) cytoplasm around the nucleus (Nu) and the cells' processes (arrow) running between the muscle (Mu) to join with the syncytium (Te) which exhibits moderate staining. The spines (Sp) are strongly stained. (G) A section of 3-week-old juvenile showing intense staining of phalloidin in the tegumental cell bodies (Tc) and the syncytium (inset, Te), moderate staining in parenchymal cells (Pc) and caecal epithelium (Ce), while the spines are not stained (inset, Sp). (H) In an adult section, intense staining of phalloidin is also exhibited in the cell bodies (Tc) and their cytoplasmic processes (arrow) running between the muscle (Mu); tegumental syncytium (Te) exhibits intense staining in the middle two thirds of its thickness. The spines (Sp) and vitelline gland (Vi) are not stained.